CITY UNIVERSITY OF HONG KONG
香港城市大學

To Co-locate or to Distribute: A Comparative Study on the Asymptotic Downlink Performance of MIMO Cellular Networks with Massive Base-station Antennas

集中式還是分佈式: 採用不同基站天線佈局的大規模 MIMO蜂窩網絡的下行漸進性能的比較性研究

Submitted to
Department of Electronic Engineering
電子工程學系
in Partial Fulfillment of the Requirements
for the Degree of Doctor of Philosophy
哲學博士學位

by

Liu Zhiyang
劉之洋

October 2014
二零一四年十月

Abstract

The mobile Internet has experienced rapid development in recent years, leading to an unprecedentedly urgent demand for data rate in cellular networks. Thanks to the substantial capacity gains from implementing multiple antennas at both the base-station (BS) and the user sides, multiple-input-multiple-output (MIMO) technology has been widely adopted in current cellular standards such as Long Term Evolution (LTE). To provide a high data rate to support the vast amounts of mobile applications in the future, a large number of antennas are expected to be employed at BSs in the next-generation cellular network.

To evaluate the performance of MIMO cellular networks with massive BS antennas, significant efforts have been made in previous studies. Most of them, nevertheless, focus on the co-located BS antennas. If the BS antennas are grouped into geographically distributed clusters and connected to a central processing unit by fiber, substantial capacity gains can be expected. In the meantime, the implementation cost of distributed BS antennas is much higher than that of co-located ones. It is, therefore, of great practical importance to compare the rate performance of different BS antenna layouts to ascertain whether the increased cost is justified.

This thesis is devoted to a comparative study of the downlink performance of MIMO cellular networks with massive BS antennas which are either co-located at the center of each cell or grouped into uniformly distributed clusters in the inscribed circle of each cell. In the single-user case, the effect of the channel state information at the transmitter side (CSIT) on the scaling behavior of the average ergodic capacity is studied. By assuming that the number of BS antennas and the number of user antennas go to infinity with a fixed ratio, explicit expressions for the asymptotic average ergodic capacity with the co-located antenna (CA) layout and an asymptotic lower-bound of the average ergodic capacity with the distributed antenna (DA) layout are derived for the cases with and without CSIT. The analysis reveals that the average ergodic capacity with the DA layout has a higher scaling order than that with the CA layout regardless of whether CSIT is available or not.

The analysis is further extended to a multi-user MIMO cellular system with two representative linear precoding schemes: singular-value-decomposition (SVD)

and block diagonalization (BD). By assuming that the number of BS antennas and the number of user antennas go to infinity with a fixed ratio, the asymptotic average ergodic rate with the CA layout and an asymptotic bound of the average ergodic rate with the DA layout are derived for the SVD and BD cases. In the single-cell case, the analysis reveals that for both SVD and BD, the average ergodic rate with the DA layout has a higher scaling order than that with the CA layout, and the gains become more prominent when an orthogonal precoding scheme such as BD is adopted. In the multi-cell case, despite the fact that the average rate performance is degraded by the inter-cell interference, the scaling orders with the CA and DA layouts remain the same as the single-cell case.

Finally, the effect of power allocation on the ergodic rate is studied. With equal power allocation, the ergodic rates with the CA and DA layouts are shown to be sensitive to the user's position. Interference-aware power allocation schemes are then proposed to achieve a uniform ergodic rate in the CA and DA cases. Despite the better fairness, the average rates in both cases are degraded compared to that with equal power allocation, indicating a fundamental tradeoff between fairness and average rate performance. With the DA layout, the tradeoff is more evident, and becomes increasingly significant as the ratio of the number of BS antennas to the total number of user antennas increases, which highlights the importance of including fairness as an indispensable constraint in the design of distributed MIMO cellular systems.

Acknowledgements

I feel very fortunate to have pursued my Ph.D. degree in City University of Hong Kong where I learnt from so many excellent individuals. First of all, I would like to express my most sincere gratitude to my supervisor, Prof. Lin Dai, who guided me into this fantastic area and showed me the way to overcome successive challenges in research. I benefited tremendously from not only her profound technical insights, but also her critical yet creative way of solving problems. She can always find an effective path whenever I found no route to take. Besides, her patience with students, passion for work and enthusiasm in life always impress me and stimulate me to be better. I will always remember the beneficial technical discussions in meetings, the interesting talks over dinner and the joyful time shared while hiking. I believe that her attitude to conducting research and enjoying life will be my lifelong treasure. I will also strive to be a devoted teacher and pass her precious knowledge and experience on to my future students.

I would like to offer my special thanks to my qualifying panel members, Prof. Ping Li and Prof. Albert Sung, for their valuable comments on each of my annual progressive reports. I thank Prof. Moshe Zukerman, Prof. Guanrong Chen and Prof. Chee Wai Tan for their outstanding teaching in the amazing courses. I also thank my friends in this group, Xinghua Sun, Yayu Gao, Junyuan Wang and Yitong Li, with whom I have had the good fortune to collaborate and spend happy leisure time with during the past four years in Hong Kong. Moreover, I thank Yang Liu, Jie Zhao, Lidan Zhang, Yuelin Yang and Junping Tang, with whom I shared my happiness and bitterness in life.

Last but not least, I thank my family, my parents, my brother, my lover, and all my old friends. Without your care and support, I could never have finished my Ph.D. study.

Contents

List of Figures

List of Tables

Abbreviations

1G	1st-Generation
2G	2nd-Generation
3G	3rd-Generation
3GPP	3rd Generation Partnership Project
4G	4th-Generation
5G	5th-Generation
AMPS	Advanced Mobile Phone System
AWGN	Additive White Gaussian Noise
BD	Block Diagonalization
BS	Base-Station
CA	Co-located Antenna
cdf	Cumulative Distribution Function
CDMA	Code Division Multiple Access
CPU	Central Processing Unit
CSI	Channel State Information
CSIT	Channel State Information at the Transmitter side
DA	Distributed Antenna

DPC	Dirty Paper Coding
EDGE	Enhanced Data for GSM Evolution
FCC	Federal Communication Commission
FDMA	Frequency Division Multiple Access
GPRS	General Packet Radio Service
GSM	Global System for Mobile Communications
HSPA	High-Speed Packet Access
IEEE	Institute of Electrical and Electronics Engineers
i.i.d.	Independent and identically distributed
IS-95	Interim Standard 95
ITU	International Telecommunication Union
LTE	Long Term Evolution
MIMO	Multiple-Input-Multiple-Output
MISO	Multiple-Input-Single-Output
NMT	Nordic Mobile Telephone
OFDMA	Orthogonal Frequency Division Multiple Access
pdf	Probability Density Function
SINR	Signal-to-Interference-plus-Noise Ratio
SNR	Signal-to-Noise Ratio
SVD	Singular Value Decomposition
TACS	Total Access Communication System
TDMA	Time Division Multiple Access
TDS-CDMA	Time Division Synchronous Code Division Multiple Access

WCDMA	Wideband Code Division Multiple Access
WLAN	Wireless Local Area Network

Notations

$\circ$	Hadamard product
$\mathbb{E}[\cdot]$	Expectation operator
$\lceil \cdot \rceil$	Ceiling operator
$\lvert\mathcal{X}\rvert$	Cardinality of a set $\mathcal{X}$
$\lvert x\rvert$	Modulus of a scalar x
$\lVert\mathbf{x}\rVert$	Euclidean norm of a vector $\mathbf{x}$
$\mathbf{X}^T$	Transpose of a matrix $\mathbf{X}$
$\mathbf{X}^\dagger$	Conjugate transpose of a matrix $\mathbf{X}$
$\mathrm{Tr}(\mathbf{X})$	Trace of a matrix $\mathbf{X}$
$\det(\mathbf{X})$	Determinant of a matrix $\mathbf{X}$
$\mathbf{I}_N$	An $N \times N$ identity matrix
$\mathbf{1}_{N\times M}$	An $N \times M$ matrix with all entries one
$\mathbf{0}_{N\times M}$	An $N \times M$ matrix with all entries zero
$\mathrm{diag}\,(a_1, \cdots, a_N)$	An $N \times N$ matrix with diagonal entries $\{a_i\}$
$\mathcal{W}_n\,(m, \mathbf{\Sigma})$	An $n \times n$ Wishart matrix with m degrees of freedom and covariance matrix $\mathbf{\Sigma}$
$\mathcal{CN}(\mathbf{u}, \mathbf{\Sigma})$	A complex Gaussian random vector with mean $\mathbf{u}$

	and covariance matrix $\mathbf{\Sigma}$
$\mathbb{C}$	Set of complex numbers
$\mathbb{R}$	Set of real numbers
$\mathcal{B}_i$	Set of BS antennas of Cell i
$\mathcal{K}_i$	Set of users of Cell i
$\mathcal{L}_l^i$	Set of BS antennas at the l-th cluster in Cell i
α	Path-loss factor
β	Ratio of the number of user antennas to the number
	of BS antennas at each cluster
ξ	Ratio of the number of BS antennas to the total number of
	user antennas in each cell
ρ_k	Radial coordinate of user k
θ_k	Angular coordinate of user k
$\gamma_{k,m}$	Large-scale fading coefficient from user k to
	BS antenna m
$\gamma_{k,m}^C$	Large-scale fading coefficient from user k to
	BS antenna m with the CA layout
$\gamma_{k,m}^D$	Large-scale fading coefficient from user k to
	BS antenna m with the DA layout
$\beta_{k,m}$	Normalized large-scale fading coefficient from user k to
	BS antenna m
$\beta_{k,m}^C$	Normalized large-scale fading coefficient from user k to

	BS antenna m with the CA layout
$\beta_{k,m}^{D}$	Normalized large-scale fading coefficient from user k to BS antenna m with the DA layout
M	Number of BS antennas per cell
N	Number of user antennas
K	Number of users per cell
N_c	Number of BS antennas at each cluster
L	Number of BS antenna clusters per cell
P_t	Total transmit power at each BS
$\bar{P}_k$	Average transmit power for user k
N_0	Noise power
P_k^{int}	Normalized inter-cell interference power at user k
$P_k^{int,C}$	Normalized inter-cell interference power at user k with the CA layout
$P_k^{int,D}$	Normalized inter-cell interference power at user k with the DA layout
$d_{k,l,i}$	Distance from user k to BS antenna cluster l in Cell i
$d_{k,i}^{(l)}$	Distance from user k to the l-th closest BS antenna cluster in Cell i
$d_{k,\mathcal{K}_0}^{(1)}$	Distance from user k to the closest user among the other users in Cell 0
$\mathbf{x}_k$	Transmitted signal for user k

$\mathbf{y}_k$	Received signal of user k
$\mathbf{z}_k$	Noise at user k
$\mathbf{u}_k^{intra}$	Intra-cell interference at user k
$\mathbf{u}_k^{inter}$	Inter-cell interference at user k
$\mathbf{r}_k^U$	Position of user k
$\mathbf{r}_m^B$	Position of BS antenna m
$\boldsymbol{\gamma}_{k,\mathcal{B}_i}$	Large-scale fading vector between user k and BS antennas in Cell i
$\boldsymbol{\beta}_{k,\mathcal{B}_i}$	Normalized large-scale fading vector between user k and BS antennas in Cell i
$\mathbf{G}_{k,\mathcal{B}_i}$	Channel gain matrix between user k and the BS antennas in Cell i
$\tilde{\mathbf{G}}_{k,\mathcal{B}_i}$	Normalized channel gain matrix between user k and BS antennas in Cell i
$\mathbf{H}_{k,\mathcal{B}_i}$	Small-scale fading matrix between user k and BS antennas in Cell i
$\boldsymbol{\Gamma}_{k,\mathcal{B}_i}$	Large-scale fading matrix between user k and BS antennas in Cell i
$\mathbf{B}_{k,\mathcal{B}_i}$	Normalized large-scale fading matrix between user k and BS antennas in Cell i
$\mathbf{Q}_k^{intra}$	Covariance matrix of intra-cell interference at user k
$\mathbf{Q}_k^{inter}$	Covariance matrix of inter-cell interference at user k

$\mathbf{Q}_k^{inter,C}$	Covariance matrix of inter-cell interference at user k with the CA layout
$\mathbf{Q}_k^{inter,D}$	Covariance matrix of inter-cell interference at user k with the DA layout
$\mathbf{W}_k$	Precoding matrix for user k
$\mathbf{W}_k^{SVD}$	Precoding matrix with SVD for user k
$\mathbf{W}_k^{BD}$	Precoding matrix with BD for user k
R_k	Ergodic rate of user k
$\bar{R}$	Average ergodic rate
R_k^C	Ergodic rate of user k with the CA layout
R_k^D	Ergodic rate of user k with the DA layout
R_k^S	Ergodic capacity of user k in the single-user case
R_k^{S-o}	Ergodic capacity of user k without CSIT in the single-user case
R_k^{S-o-C}	Ergodic capacity of user k without CSIT with the CA layout in the single-user case
R_k^{S-o-D}	Ergodic capacity of user k without CSIT with the DA layout in the single-user case
R_k^{S-w}	Ergodic capacity of user k with CSIT in the single-user case
R_k^{S-w-C}	Ergodic capacity of user k with CSIT with the CA layout in the single-user case
R_k^{S-w-D}	Ergodic capacity of user k with CSIT with the DA layout

	in the single-user case
R_k^{MU}	Ergodic rate of user k in the multi-user single-cell case
R_k^{MU-SVD}	Ergodic rate of user k with SVD in the multi-user single-cell case
R_k^{MU-BD}	Ergodic rate of user k with BD in the multi-user single-cell case
$R_k^{MU-SVD-C}$	Ergodic rate of user k with SVD with the CA layout in the multi-user single-cell case
$R_k^{MU-BD-C}$	Ergodic rate of user k with BD with the CA layout in the multi-user single-cell case
$R_k^{MU-SVD-D}$	Ergodic rate of user k with SVD with the DA layout in the multi-user single-cell case
$R_k^{MU-BD-D}$	Ergodic rate of user k with BD with the DA layout in the multi-user single-cell case
R_k^{MC}	Ergodic rate of user k in the multi-user multi-cell case
R_k^{MC-D}	Ergodic rate of user k with the DA layout in the multi-user multi-cell case
R_k^{MC-SVD}	Ergodic rate of user k with SVD in the multi-user multi-cell case
R_k^{MC-BD}	Ergodic rate of user k with BD in the multi-user multi-cell case
$R_k^{MC-SVD-C}$	Ergodic rate of user k with SVD with the CA layout in the multi-user multi-cell case

$R_k^{MC-BD-C}$	Ergodic rate of user k with BD with the CA layout in the multi-user multi-cell case
$R_k^{MC-SVD-D}$	Ergodic rate of user k with SVD with the DA layout in the multi-user multi-cell case
$R_k^{MC-BD-D}$	Ergodic rate of user k with BD with the DA layout in the multi-user multi-cell case
$\mathcal{R}_k$	Asymptotic ergodic rate of user k
$\mathcal{R}_k^C$	Asymptotic ergodic rate of user k with the CA layout
$\mathcal{R}_k^D$	Asymptotic ergodic rate of user k with the DA layout
$\mathcal{R}_k^{S-o-C}$	Asymptotic ergodic capacity of user k without CSIT with the CA layout in the single-user case
$\mathcal{R}_k^{S-o-D}$	Asymptotic ergodic capacity of user k without CSIT with the DA layout in the single-user case
$\mathcal{R}_{k,lb}^{S-o-D}$	Asymptotic lower-bound of ergodic capacity of user k without CSIT with the DA layout in the single-user case
$\mathcal{R}_k^{S-w-C}$	Asymptotic ergodic capacity of user k with CSIT with the CA layout in the single-user case
$\mathcal{R}_k^{S-w-D}$	Asymptotic ergodic capacity of user k with CSIT with the DA layout in the single-user case
$\mathcal{R}_{k,lb}^{S-w-D}$	Asymptotic lower-bound of ergodic capacity of user k with CSIT with the DA layout in the single-user case
$\mathcal{R}_k^{MU-SVD-C}$	Asymptotic ergodic rate of user k with SVD with the CA layout in the multi-user single-cell case

$\mathcal{R}_k^{MU-SVD-D}$	Asymptotic ergodic rate of user k with SVD with the DA layout in the multi-user single-cell case
$\mathcal{R}_{k,ub}^{MU-SVD-D}$	Asymptotic upper-bound of ergodic rate of user k with SVD with the DA layout in the multi-user single-cell case
$\mathcal{R}_k^{MU-BD-C}$	Asymptotic ergodic rate of user k with BD with the CA layout in the multi-user single-cell case
$\mathcal{R}_k^{MU-BD-D}$	Asymptotic ergodic rate of user k with BD with the DA layout in the multi-user single-cell case
$\mathcal{R}_{k,lb}^{MU-BD-D}$	Asymptotic lower-bound of ergodic rate of user k with BD with the DA layout in the multi-user single-cell case
$\mathcal{R}_k^{MC-SVD-C}$	Asymptotic ergodic rate of user k with SVD with the CA layout in the multi-user multi-cell case
$\mathcal{R}_k^{MC-BD-C}$	Asymptotic ergodic rate of user k with BD with the CA layout in the multi-user multi-cell case
$\mathcal{R}_k^{MC-BD-D}$	Asymptotic ergodic rate of user k with BD with the DA layout in the multi-user multi-cell case
$\mathcal{R}_{k,lb}^{MC-BD-D}$	Asymptotic lower-bound of ergodic rate of user k with BD with the DA layout in the multi-user multi-cell case
$\mathcal{R}_{k,epa}^{MC-SVD-C}$	Asymptotic ergodic rate of user k with SVD and equal power allocation with the CA layout in the multi-user multi-cell case
$\mathcal{R}_{k,epa}^{MC-BD-C}$	Asymptotic ergodic rate of user k with BD and equal power allocation with the CA layout

	in the multi-user multi-cell case
$\mathcal{R}_{k,cpa}^{MC-SVD-C}$	Asymptotic ergodic rate of user k with SVD and channel-inversion power allocation with the CA layout in the multi-user multi-cell case
$\mathcal{R}_{k,cpa}^{MC-BD-C}$	Asymptotic ergodic rate of user k with BD and channel-inversion power allocation with the CA layout in the multi-user multi-cell case
$\mathcal{R}_{k,ipa}^{MC-SVD-C}$	Asymptotic ergodic rate of user k with SVD and interference-aware power allocation with the CA layout in the multi-user multi-cell case
$\mathcal{R}_{k,ipa}^{MC-BD-C}$	Asymptotic ergodic rate of user k with BD and interference-aware power allocation with the CA layout in the multi-user multi-cell case
$\bar{\mathcal{R}}$	Asymptotic average ergodic rate
$\bar{\mathcal{R}}^{C}$	Asymptotic average ergodic rate with the CA layout
$\bar{\mathcal{R}}^{S-o-C}$	Asymptotic average ergodic capacity without CSIT with the CA layout in the single-user case
$\bar{\mathcal{R}}_{lb}^{S-o-D}$	Asymptotic lower-bound of the average ergodic capacity without CSIT with the DA layout in the single-user case
$\bar{\mathcal{R}}^{S-w-C}$	Asymptotic average ergodic capacity with CSIT with the CA layout in the single-user case
$\bar{\mathcal{R}}_{lb}^{S-w-D}$	Asymptotic lower-bound of the average ergodic capacity with CSIT with the DA layout in the single-user case

$\bar{\mathcal{R}}^{MU-SVD-C}$	Asymptotic average ergodic rate with SVD with the CA layout in the multi-user single-cell case
$\bar{\mathcal{R}}_{ub}^{MU-SVD-D}$	Asymptotic upper-bound of the average ergodic rate with SVD with the DA layout in the multi-user single-cell case
$\bar{\mathcal{R}}^{MU-BD-C}$	Asymptotic average ergodic rate with BD with the CA layout in the multi-user single-cell case
$\bar{\mathcal{R}}_{lb}^{MU-BD-D}$	Asymptotic lower-bound of the average ergodic rate with BD with the DA layout in the multi-user single-cell case
$\bar{\mathcal{R}}^{MC-SVD-C}$	Asymptotic average ergodic rate with SVD with the CA layout in the multi-user multi-cell case
$\bar{\mathcal{R}}^{MC-BD-C}$	Asymptotic average ergodic rate with BD with the CA layout in the multi-user multi-cell case
$\bar{\mathcal{R}}_{lb}^{MC-BD-D}$	Asymptotic lower-bound of the average ergodic rate with BD with the DA layout in the multi-user multi-cell case
μ_k	Average received SINR of user k
μ_k^S	Average received SNR of user k in the single-user case
μ_k^{S-C}	Average received SNR of user k with the CA layout in the single-user case
μ_k^{MU-SVD}	Average received SINR of user k with SVD in the multi-user single-cell case
$\mu_k^{MU-SVD-C}$	Average received SINR of user k with SVD with the CA layout in the multi-user single-cell case

μ_k^{MU-BD}	Average received SINR of user k with BD in the multi-user single-cell case
$\mu_k^{MU-BD-C}$	Average received SINR of user k with BD with the CA layout in the multi-user single-cell case
μ_k^{MC-SVD}	Average received SINR of user k with SVD in the multi-user multi-cell case
$\mu_k^{MC-SVD-C}$	Average received SINR of user k with SVD with the CA layout in the multi-user multi-cell case
μ_k^{MC-BD}	Average received SINR of user k with BD in the multi-user multi-cell case
$\mu_k^{MC-BD-C}$	Average received SINR of user k with BD with the CA layout in the multi-user multi-cell case
$\bar{\mu}_k^{MU-SVD-D}$	Normalized average received SINR of user k with SVD with the DA layout in the multi-user single-cell case
$\bar{\mu}_{k,ub}^{MU-SVD-D}$	Upper-bound of the normalized average received SINR of user k with SVD with the DA layout in the multi-user single-cell case
$\bar{\mu}_k^{MC-BD-D}$	Normalized average received SINR of user k with BD with the DA layout in the multi-user multi-cell case
$\bar{\mu}_{k,epa}^{MC-SVD-C}$	Normalized average received SINR of user k with SVD and equal power allocation with the CA layout in the multi-user multi-cell case
$\bar{\mu}_{k,epa}^{MC-BD-C}$	Normalized average received SINR of user k with BD

	and equal power allocation with the CA layout in the multi-user multi-cell case
$\bar{\mu}_{k,cpa}^{MC-SVD-C}$	Normalized average received SINR of user k with SVD and channel-inversion power allocation with the CA layout in the multi-user multi-cell case
$\bar{\mu}_{k,cpa}^{MC-BD-C}$	Normalized average received SINR of user k with BD and channel-inversion power allocation with the CA layout in the multi-user multi-cell case
$\bar{\mu}_{k,ipa}^{MC-SVD-C}$	Normalized average received SINR of user k with SVD and interference-aware power allocation with the CA layout in the multi-user multi-cell case
$\bar{\mu}_{k,ipa}^{MC-BD-C}$	Normalized average received SINR of user k with BD and interference-aware power allocation with the CA layout in the multi-user multi-cell case
$\tilde{\mu}_{k}^{MC-D}$	Instantaneous received SINR of user k with the DA layout in the multi-user multi-cell case
$\tilde{\mu}_{k}^{MC-SVD-D}$	Instantaneous received SINR of user k with SVD with the DA layout in the multi-user multi-cell case
$\tilde{\mu}_{k}^{MC-BD-D}$	Instantaneous received SINR of user k with BD with the DA layout in the multi-user multi-cell case

To my Golden Age...

Chapter 1

Introduction

1.1 Next-Generation Mobile Communication System

1.1.1 Wireless Communication: An Indispensable Part of Modern Society

Initiated by the prediction of electromagnetic waves by James Clerk Maxwell in 1864, wireless communications have experienced giant steps in development over the past 150 years, and have become an indispensable part of our lives. Since the successful demonstration of the Trans-Atlantic telegraph by Guglielmo Marconi in 1895, wireless communications have attracted extensive public attention, and deeply affected society in the first half of the 20th Century thanks to the popularity of radio and television broadcast services.

Interpersonal communication has also been significantly changed by wireless technologies. Ever since the Federal Communication Commission (FCC)'s approval of the spectrum for cellular systems in 1971, the wireless cellular system has experienced exponential growth. By the end of 2013, the number of mobile phones in the world was as high as 6.7 billion according to the International Telecommunication Union (ITU), and the number is still growing. On the other hand, the wireless local area networks (WLANs) have also experienced a rapid expansion in the past decade. The WiFi networks based on the family of IEEE 802.11 standards have been widely employed in many homes, offices, and even

public transportation facilities such as buses and trains. Thanks to the advanced wireless communication technologies, people are able to communicate with each other and get access to the latest information rapidly regardless of where they are. It may be said without exaggeration that we cannot live without wireless communications in modern society.

1.1.2 Mobile Communication: From 1G to 5G

In sharp contrast to the huge amount of mobile phone users nowadays, the mobile communication systems in their early stages were designed for much fewer users. The first mobile communication system introduced in 1946 was an analog system, where each carrier could only be occupied by one single call. Without the concept of cellular, no handover technology was adopted, which meant that calls would be terminated once the user moved across the coverages of different transmitting towers. As a result, the first mobile communication system could only serve a small number of users, and the mobility of each user was severely restricted by the coverage of each transmitting tower.

To expand the service to more users, Bell Labs proposed the cellular system [3], which then became the basis of mobile communication systems. In a cellular system, the whole area is divided into a large number of cells with a base-station (BS) serving the users in each cell. When a user moves from one cell to another, the call is handed over between BSs. Compared to the earlier mobile communication systems, the coverage area and the number of available channels in cellular systems have been significantly enlarged by carefully planned frequency reuse. Since the commercialization of the 1st-generation (1G) cellular system, the cellular systems have undergone rapid development in the following decades, as summarized in Table 1.1.

The 1G cellular systems were typically only countrywide with a variety of incompatible standards, which mainly included Advanced Mobile Phone System (AMPS) in the United States, Total Access Communication System (TACS) in the United Kingdom and Nordic Mobile Telephone (NMT) in the Nordic countries[4]. The similarity is that they are all analog systems with a Frequency-Division-Multiple-Access (FDMA) scheme to avoid inter-user interference in each cell. Although the 1G cellular system can support more users than its predecessor thanks to the frequency reuse among cells, the number of users it can serve is still limited

TABLE 1.1: Physical Layer Specifications of the Downlink Channels of Representative Cellular Systems [2]

	Standard	Multiple Access Schemes	Bandwidth	Peak Data Rate
1G	AMPS	FDMA	30kHz	9.6kbps
	TACS	FDMA	25kHz	9.6kbps
	NMT	FDMA	25kHz	9.6kbps
2G	GSM	TDMA	200kHz	9.6kbps
	IS-95	CDMA	1.25MHz	9.6kbps
3G	WCDMA	CDMA	5MHz	2Mbps
	TDS-CDMA	CDMA	1.6MHz	2Mbps
	cdma2000	CDMA	1.25MHz	2Mbps
4G	LTE	OFDMA	20MHz	100Mbps

by the bandwidth as each carrier can only be occupied by one active user with analog modulation.

Driven by the extensive demand for mobile communications, digital transmission was employed in the 2nd-generation (2G) cellular system in the 1990s. By adopting a Time-Division-Multiple-Access (TDMA) scheme in the Global System for Mobile Communications (GSM) system or a Code-Division-Multiple-Access (CDMA) scheme in the Interim Standard 95 (IS-95) system, each carrier can be shared by multiple users using different time slots or spreading codes, and thus the system capacity is largely improved [4].

The soaring development of the Internet raises the demand for accessing the Internet through the cellular systems. As the 2G cellular systems were initially designed for voice communications over circuit-switched networks, they could only support a data rate of 9.6kbps which is far from enough for multi-media data transmission. To provide efficient data transmission, some enhancements of the 2G cellular systems were later proposed. For instance, the General Packet Radio Service (GPRS) and the Enhanced Data Rates for GSM Evolution (EDGE) were introduced in the late 1990s as enhancements of the GSM system. By adding packet-switched domain networks, the peak data rates of GPRS and EDGE were much higher than the original GSM system [5]. The data rate demand, nevertheless, grew faster than expected, and could hardly be satisfied by further enhancement of the existing 2G systems. Coordinated by the 3rd Generation Partnership Project (3GPP) and the 3GPP2, three CDMA-based standards, including Wideband Code Division Multiple Access (WCDMA), Time Division Synchronous Code

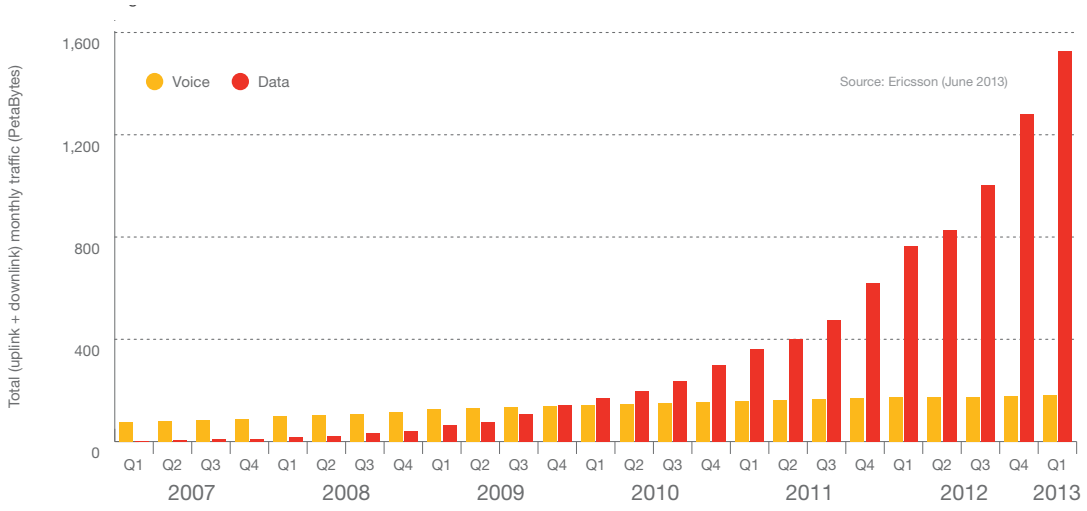

FIGURE 1.1: Global total voice and data traffics in mobile networks, 2007-2013 [1].

Division Multiple Access (TDS-CDMA) and cdma2000, were selected by the ITU as the 3rd-generation (3G) cellular system standards, and were commercialized by operators from the early 2000s [6]. The peak data rate of a 3G cellular system was originally around 2Mbps, and was later enhanced to 21Mbps with High-Speed Packet Access (HSPA) technology.

Since the announcement of the iPhone in 2007, the mobile Internet has experienced rapid growth in recent years, leading to an unprecedentedly increasing demand for data traffic on cellular systems. As Fig. 1.1 shows, data traffic has exceeded voice traffic and increased exponentially since the 4th quarter of 2009. To support such massive data traffic, a much higher data rate is expected from cellular systems. The 4th-generation (4G) cellular system, which is known as the Long Term Evolution (LTE) system, is therefore proposed and commercialized in 2010. In the LTE system, an Orthogonal-Frequency-Division-Multiple-Access (OFDMA) scheme is adopted to avoid inter-user interference, which also enables better utilization of the frequency resource and improves the peak data rate to 100Mbps in a 20MHz bandwidth channel [2].

Note that the data rates listed in Table 1.1 are peak data rates. In practical systems, as each BS typically serves a large number of users, the data rate of each user is usually much lower than the peak one. On the other hand, it is predicted that to meet the demand in 2020, the cellular system should be able to support 1,000 times more data traffic compared to 2010 [7]. To satisfy the massive data

rate demand in the future, the multiple-input-multiple-output (MIMO) technology should be adopted in the next-generation cellular system, or the 5th-generation (5G) cellular system. With multiple antennas at both the BS and the user sides, much better performance can be expected over the single-antenna system. In fact, MIMO has been included in the LTE standard, where a peak data rate of 300Mbps can be achieved when 4 antennas are employed at both the user and BS sides. Intuitively, the more antennas equipped, the higher the data rate that can be achieved. Yet due to the size limit of mobile devices, the number of antennas at the user side has to be small. Therefore, to support the intensive data traffic in the 5G cellular system, a large number of BS antennas should be employed. In the following section, we will take a closer look at a MIMO cellular system with massive BS antennas.

1.2 MIMO: Co-located Antennas (CA) versus Distributed Antennas (DA)

1.2.1 MIMO Cellular Systems

In a MIMO cellular system, how the BS antennas are placed may have significant impact on the system performance. Fig. 1.2 illustrates two possible BS antenna layouts: the co-located antenna (CA) layout and the distributed antenna (DA) layout.

Similar to the conventional cellular structure, with the CA layout, the antennas are co-located at the BS at the center of each cell. With the advanced antenna technologies nowadays, hundreds of antennas can be integrated into a large-scale antenna array[1] and deployed at the BS. By doing so, the transmit power of each antenna can be as low as tens of milliwatts, so that the cost of power amplifiers can be greatly reduced. With the CA layout, the current cellular systems can also be easily upgraded by installing large-scale antenna arrays on the existing BS sites.

With the DA layout, instead of a tower-mounted BS, the BS antennas are grouped into geographically distributed clusters in each cell and connected to a

[1]Recently, an experimental platform with a 96-antenna array has been built [8].

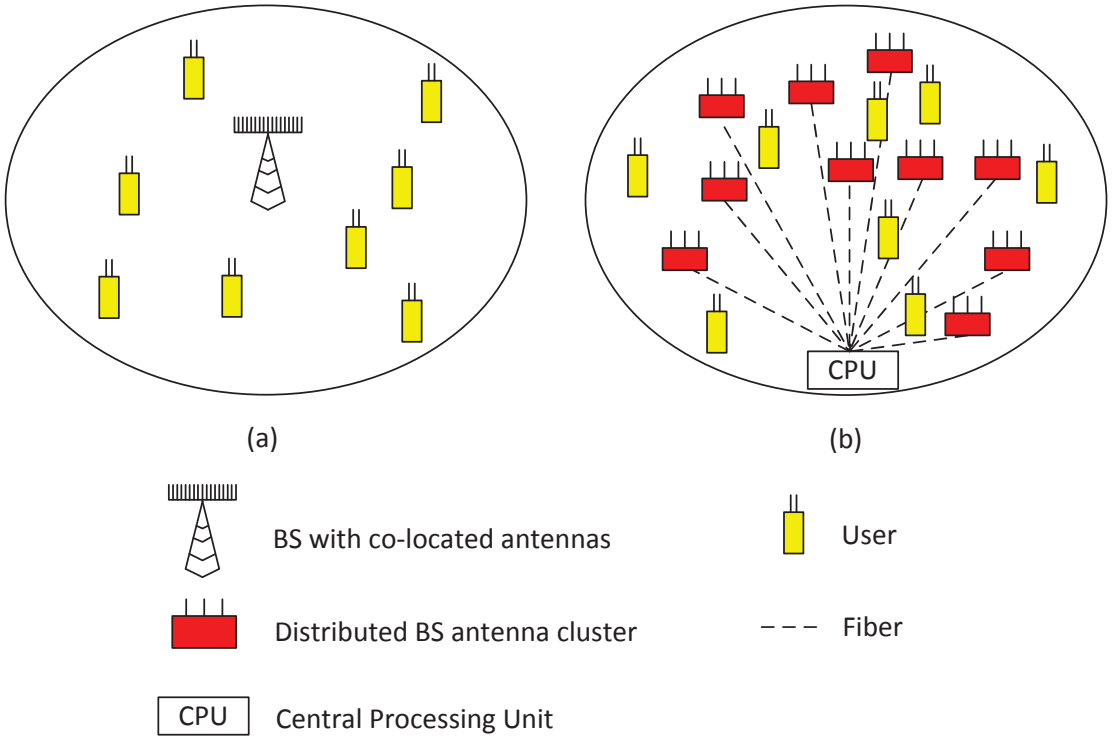

FIGURE 1.2: Graphic illustration of two BS antenna layouts. (a) Co-located antenna (CA) layout. (b) Distributed antenna (DA) layout. With the DA layout, the remote antenna ports are connected to a central processing unit (CPU) by fiber.

central processing unit (CPU) by fiber. As we can see from Fig. 1.2b, compared to the CA layout, here a much larger number of antenna sites should be built, and a significant amount of fiber should be laid to connect the distributed BS antennas to the CPU. Therefore, the DA layout is more complicated to implement in the real world. The implementation cost also sharply increases with the number of BS antenna clusters.

Nevertheless, by distributing the BS antennas, the minimum access distance from each user to the BS antennas can be significantly reduced on average. As we can see from Fig. 1.2, in contrast to the CA layout where the cell-edge users are far away from the BS, with the DA layout, the minimum access distance of a cell-edge user is greatly shortened, resulting in a much improved channel condition. Better rate performance can then be expected in the DA case.

In the 5G cellular system where massive BS antennas are intended to be employed, the rate gains achieved by the DA layout could be significant. In the meantime, the implementation cost of distributed BS antennas could also be much

higher than that of the co-located ones, especially when the number of distributed BS antenna clusters is large. It is, therefore, of great practical importance to compare the rate performance of cellular networks under different BS antenna layouts to ascertain whether the increased cost is justified.

1.2.2 Capacity Analysis of MIMO Systems

To address the above issue, let us start with a literature review of the capacity analysis of MIMO systems. In the single-user case, the ergodic capacity of a point-to-point MIMO channel has been extensively studied in the past decade. With co-located antennas at both sides, the signals from the transmit antennas to the receive antennas experience the same large-scale fading effect. In this case, the ergodic capacity can be characterized as a function of the average received signal-to-noise ratio (SNR), and grows linearly with $\min(M, N)$ in a rich-scattering environment, where M and N are the numbers of transmit and receive antennas, respectively [9, 10]. When the number of antennas is large, the random matrix theory [11, 12] is applied to characterize the ergodic capacity [13, 14]. By assuming that the number of antennas at both sides go to infinity with a fixed ratio, the asymptotic ergodic capacity of a co-located MIMO channel has been shown to be an explicit function of the average received signal-to-noise ratio (SNR) and the ratio of the number of transmit antennas to the number of receive antennas [13].

With the DA layout, as the signals from BS antennas to the user are subject to independent and different levels of large-scale fading, potential capacity gains can be expected over the CA layout [15–17]. To characterize the ergodic capacity, the random matrix theory can also be applied in the DA case. By assuming that the numbers of antennas at each cluster and each user both grow infinitely with a fixed ratio, the asymptotic ergodic capacity of a distributed MIMO channel was derived as an implicit function of the large-scale fading coefficients between the user and BS antenna clusters [18–21]. With the DA layout, as the ergodic capacity is further determined by the positions of BS antenna clusters, the average ergodic capacity was considered in [16, 22–24], where the ergodic capacity is averaged over the large-scale fading coefficients from distributed BS antenna clusters to the user. When the number of BS antenna clusters is large, it becomes increasingly difficult to obtain the average ergodic capacity due to high computational complexity.

Therefore, most studies have focused on a regular BS antenna layout with a small number of BS antenna clusters [18–24].

In the multi-user case, the uplink sum capacity with the CA layout has been intensively studied in [25–28]. With the channel state information at the transmitter side (CSIT), the sum capacity of a MIMO Gaussian uplink channel is shown to be achieved by an iterative waterfilling procedure, where the single-user waterfilling power allocation is applied to each user by regarding the other users' signals as noise at each iteration until equilibrium is reached [26]. With the DA layout, the uplink sum capacity has been characterized in [29], which shows that for given average received SNR, a higher sum capacity can be achieved with the DA layout only when CSIT is available. Under the same consumption of transmit power, on the other hand, regardless of whether CSIT is available or not, substantial capacity gains can always be achieved with the DA layout thanks to the reduction of the minimum access distance.

For the downlink channel, as the users are typically unable to coordinate with each other, precoding is usually required at the BS. The sum capacity of a MIMO Gaussian downlink channel has been extensively studied in [27, 28, 30, 31], and the capacity region was characterized in [32], which showed that the optimum precoding is a pre-interference-cancelation strategy known as dirty paper coding (DPC) [33]. Despite the information-theoretical optimality, it is difficult to implement the idea of DPC in practice. Therefore, a number of suboptimal precoding schemes were proposed to approach the sum capacity with manageable complexity [30, 34–50]. When an orthogonal precoding scheme such as block diagonalization (BD) [41] is adopted, for instance, near-capacity performance can be achieved with low complexity when the number of BS antennas is large [51]. Although the above mentioned precoding strategies were originally proposed for the CA layout, they can be applied to the DA layout in a straightforward manner. In the DA case, the downlink rate performance is crucially dependent on the positions of users and BS antenna clusters. For computational tractability, most studies have focused on a small group of users and BS antenna clusters [52–59].

In the 5G cellular system, a large number of BS antennas are expected to be employed. So far the majority of the literature on the MIMO cellular system with massive BS antennas has focused on the CA layout [60–63]. With the DA layout, how the downlink rate performance scales with the number of antennas remains largely unknown, which is mainly due to the high computational complexity when

the number of distributed BS antenna clusters is large. Moreover, most studies have focused on either the CA layout or the DA layout. To determine whether to employ the CA or DA layout in the 5G cellular system, a comprehensive comparison of the downlink rate performance of MIMO cellular systems with different BS antenna layouts would be highly desirable, which, unfortunately, has been largely missing.

1.3 Thesis Contributions and Outline

This thesis is devoted to a comparative study of the downlink rate performance of MIMO cellular networks with a massive number of BS antennas which are either co-located at the center of each cell or grouped into uniformly distributed clusters in the inscribed circle of each cell. We focus on the scaling behavior of the average ergodic rates with the CA and DA layouts in three cases, i.e., single-user, multi-user single-cell, and multi-user multi-cell. The effect of power allocation on the ergodic rate of each user in a MIMO cellular network is also discussed. The contributions of this thesis are summarized as follows.

First, in the single-user case, by assuming that the number of BS antennas M and the number of user antennas N go to infinity with $M/N \to \xi \gg 1$, the asymptotic average ergodic capacities with and without the channel state information at the transmitter side (CSIT) in the CA case are derived explicitly. With the DA layout, closed-form expressions of asymptotic lower-bounds of the average ergodic capacities with and without CSIT are developed. The analysis reveals that the scaling order of the average ergodic capacity with the DA layout is higher than that with the CA layout thanks to the reduced minimum access distance regardless of whether CSIT is available or not.

The asymptotic analysis is then extended to a multi-user MIMO system with K uniformly distributed users in the inscribed circle of each cell. By assuming that the number of BS antennas M and the number of user antennas N go to infinity with $M/N \to \xi K \gg 1$, the asymptotic average ergodic rates with two representative precoding schemes, singular-value-decomposition (SVD) [10] and block diagonalization (BD) [41], are characterized in the CA case. With the DA layout, asymptotic bounds are developed to characterize the scaling orders of the average ergodic rates with SVD and BD. In the single-cell case, the analysis reveals

that the average ergodic rate with the DA layout has a higher scaling order in both the SVD and BD cases, while the gain becomes more prominent when BD is adopted. In the multi-cell case, despite the fact that the average rate performance is degraded by the inter-cell interference, the scaling orders of the average ergodic rates with the CA and DA layouts remain the same as the single-cell case.

Finally, the effect of different power allocation schemes on the ergodic rate is studied. As the signals from the BS antennas to each user suffer from distinct large-scale fading effects, the ergodic rate of each user is shown to be sensitive to its position in both the CA and DA cases when equal power allocation is adopted. By maintaining a constant received SINR for each user, a uniform ergodic rate can be achieved with the proposed interference-aware power allocation, while the average rate performance is degraded compared to that with equal power allocation, which indicates a fundamental tradeoff between fairness and average rate performance. With the DA layout, the tradeoff becomes more significant, indicating that fairness should be included as an important constraint in the design of MIMO cellular networks with a massive number of distributed BS antennas.

The remainder of this thesis is organized as follows. Chapter 2 introduces the downlink signal model and basic assumptions of this thesis. Chapter 3 presents an asymptotic analysis on the scaling behavior of the average capacity of a single-user MIMO system. The analysis is extended to the multi-user single-cell MIMO systems with different precoding schemes in Chapter 4 and the multi-user multi-cell MIMO systems in Chapter 5. Chapter 6 studies the effect of different power allocation schemes on the ergodic rate. Finally, concluding remarks and suggestions for future work are summarized in Chapter 7.

Chapter 2

System Model and Preliminary Analysis

In this chapter, the signal model and basic assumptions of this thesis are presented, based on which the asymptotic average ergodic rate is further defined. This chapter provides the fundamental system model for the analysis in the following chapters.

2.1 Downlink Signal Model

Consider a 1-tier hexagonal cellular network with a total number of 7 cells that share the same frequency band as shown in Fig. 2.1. For illustration, we mark the central cell as Cell 0, and the surrounding ones as Cell $1-6$ clockwise. Each cell has a set of users, denoted by $\mathcal{K}_i$, and a set of base-station (BS) antennas, denoted by $\mathcal{B}_i$, with $|\mathcal{K}_i|=K$ and $|\mathcal{B}_i|=M$, $i=0,\ldots,6$. Suppose that each user is equipped with $N \ll M$ antennas.

Let us focus on the downlink transmission of the central cell, i.e., Cell 0. Specifically, the received signal of user $k \in \mathcal{K}_0$ can be written as

$$\mathbf{y}_k = \underbrace{\mathbf{G}_{k,\mathcal{B}_0}\mathbf{x}_k}_{\text{Desired Signal}} + \underbrace{\mathbf{G}_{k,\mathcal{B}_0}\sum_{j\neq k, j\in\mathcal{K}_0}\mathbf{x}_j}_{\text{Intra-cell Interference}} + \underbrace{\sum_{i=1}^{6}\mathbf{G}_{k,\mathcal{B}_i}\sum_{j\in\mathcal{K}_i}\mathbf{x}_j}_{\text{Inter-cell Interference}} + \mathbf{z}_k, \tag{2.1}$$

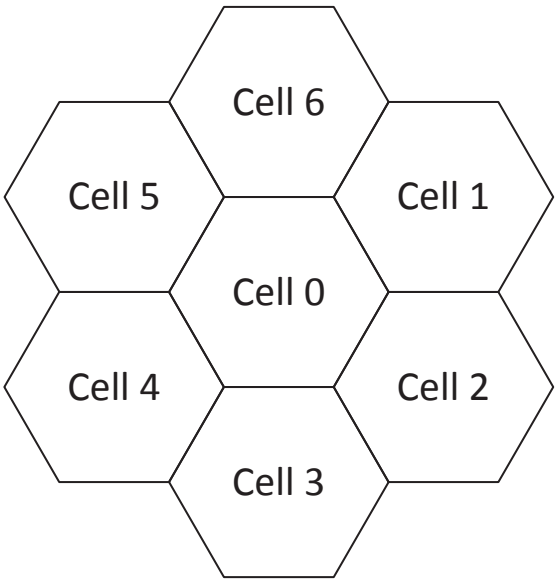

FIGURE 2.1: Graphic illustration of the 1-tier cellular network model with 7 hexagonal cells. The central cell is marked as Cell 0, and the surrounding ones are marked as Cell $1-6$ clockwise.

where $\mathbf{x}_j \in \mathbb{C}^{M\times 1}$ is the transmitted signal vector from BS i to user $j \in \mathcal{K}_i$, i=$0,\ldots,6$. $\mathbf{z}_k \in \mathbb{C}^{N\times 1}$ is the additive white Gaussian noise (AWGN) at user k, which has independent and identically distributed (i.i.d.) complex Gaussian entries with zero mean and variance N_0. $\mathbf{G}_{k,\mathcal{B}_i} \in \mathbb{C}^{N\times M}$ denotes the channel gain matrix between BS i and user k, i=$0,\ldots,6$, which is given by

$$\mathbf{G}_{k,\mathcal{B}_i} = \mathbf{\Gamma}_{k,\mathcal{B}_i} \circ \mathbf{H}_{k,\mathcal{B}_i}, \tag{2.2}$$

where $\circ$ denotes the Hadamard product. $\mathbf{H}_{k,\mathcal{B}_i} \in \mathbb{C}^{N\times M}$ denotes the small-scale fading matrix between BS i and user $k \in \mathcal{K}_0$ with entries modeled as i.i.d. complex Gaussian random variables with zero mean and unit variance. $\mathbf{\Gamma}_{k,\mathcal{B}_i} \in \mathbb{R}^{N\times M}$ denotes the corresponding large-scale fading matrix, which is composed of N identical M-dimension row vectors $\boldsymbol{\gamma}_{k,\mathcal{B}_i}$. The large-scale fading vector $\boldsymbol{\gamma}_{k,\mathcal{B}_i}$ characterizes the long-term channel effect such as path loss and shadowing. In this thesis, we ignore the shadowing effect and model the large-scale fading coefficient as

$$\gamma_{k,m} = \|\mathbf{r}_k^U - \mathbf{r}_m^B\|^{-\alpha/2}, \tag{2.3}$$

where $\mathbf{r}_k^U$ and $\mathbf{r}_m^B$ denote the positions of user $k \in \mathcal{K}_0$ and BS antenna $m \in \mathcal{B}_i$, $i = 1,\cdots,6$, respectively. $\alpha > 2$ is the path-loss factor.

We assume that each user $j \in \mathcal{K}_i$ has full channel state information (CSI) of the channel from its BS to itself, i.e., $\mathbf{G}_{j,\mathcal{B}_i}$, $i = 0, \cdots, 6$, and no cooperation is adopted among BSs. With linear precoding, the transmitted signal vector from BS i to user $j \in \mathcal{K}_i$ can be written as

$$\mathbf{x}_j = \mathbf{W}_j \mathbf{s}_j, \tag{2.4}$$

where $\mathbf{W}_j \in \mathbb{C}^{M \times N_s}$ denotes the normalized precoding matrix with $\mathrm{Tr}\{\mathbf{W}_j \mathbf{W}_j^\dagger\} = 1$. $\mathbf{s}_j \sim \mathcal{CN}(\mathbf{0}_{N_s \times 1}, \bar{P}_j \mathbf{I}_{N_s})$ is the information-bearing signal vector, with N_s denoting the number of data streams[1]. $\bar{P}_j$ is the average transmit power of the signal from BS i to user j, $j \in \mathcal{K}_i$ and $i = 0, \cdots, 6$. For each BS, the total transmit power is assumed to be fixed at P_t, i.e.,

$$\sum_{j \in \mathcal{K}_i} \bar{P}_j = P_t, \tag{2.5}$$

for $i = 0, \cdots, 6$.

The second and the third terms on the right-hand side of (2.1), i.e., $\mathbf{u}_k^{intra} = \sum_{j \in \mathcal{K}_0, j \neq k} \mathbf{G}_{k,\mathcal{B}_0} \mathbf{x}_j$ and $\mathbf{u}_k^{inter} = \sum_{i=1}^{6} \sum_{j \in \mathcal{K}_i} \mathbf{G}_{k,\mathcal{B}_i} \mathbf{x}_j$, denote the intra-cell interference and inter-cell interference received at user k, respectively. With a large number of BS antennas $M \gg 1$, $\mathbf{u}_k^{intra}$ and $\mathbf{u}_k^{inter}$ can be modeled as complex Gaussian random vectors with zero mean and covariance matrices $\mathbf{Q}_k^{intra}$ and $\mathbf{Q}_k^{inter}$, respectively.

In this thesis, we normalize the total system bandwidth to unity and focus on the spectral efficiency. According to (2.1) and (2.4), the maximum achievable ergodic rate of user k can be written as $\tilde{R}_k = NR_k$, where R_k is the ergodic rate of user k normalized by the number of user antennas N, which is given by

$$R_k = \frac{1}{N} \mathbb{E}_{\mathbf{H}_{k,\mathcal{B}_0}} \left[\log_2 \det \left(\mathbf{I}_N + \frac{\bar{P}_k \|\boldsymbol{\gamma}_{k,\mathcal{B}_0}\|^2 \tilde{\mathbf{G}}_{k,\mathcal{B}_0} \mathbf{W}_k \mathbf{W}_k^\dagger \tilde{\mathbf{G}}_{k,\mathcal{B}_0}^\dagger}{N_0 \mathbf{I}_N + \mathbf{Q}_k^{intra} + \mathbf{Q}_k^{inter}} \right) \right]. \tag{2.6}$$

$\tilde{\mathbf{G}}_{k,\mathcal{B}_0}$ is the normalized channel gain matrix, which is defined as

$$\tilde{\mathbf{G}}_{k,\mathcal{B}_0} = \mathbf{B}_{k,\mathcal{B}_0} \circ \mathbf{H}_{k,\mathcal{B}_0}, \tag{2.7}$$

[1]The number of data streams N_s depends on whether the channel state information at the transmitter side (CSIT) is available or not. Without CSIT, the data should be transmitted over M BS antennas, i.e., $N_s = M$. With CSIT, the data should be transmitted over $\min(M, N) = N$ sub-channels, i.e., $N_s = N$.

where $\mathbf{B}_{k,\mathcal{B}_0} \in \mathbb{R}^{N\times M}$ is the normalized large-scale fading matrix, which is composed of N identical row vectors $\boldsymbol{\beta}_{k,\mathcal{B}_0}$ with entries

$$\beta_{k,m} = \frac{\gamma_{k,m}}{\|\boldsymbol{\gamma}_{k,\mathcal{B}_0}\|}, \tag{2.8}$$

for $m \in \mathcal{B}_0$. It is clear from (2.8) that for any user $k \in \mathcal{K}_0$, $\|\boldsymbol{\beta}_{k,\mathcal{B}_0}\| = 1$.

2.2 Two Base-Station Antenna Layouts: CA and DA

We can clearly see from (2.6) that the ergodic rate R_k is closely dependent on the large-scale fading vector $\boldsymbol{\gamma}_{k,\mathcal{B}_0}$, which varies with the positions of users and BS antennas. In this thesis, we assume that K users are uniformly distributed in the inscribed circle of each hexagonal cell, and consider two BS antenna layouts as shown in Fig. 2.2: (a) the co-located antenna (CA) layout where M BS antennas are placed at the center of each cell, and (b) the distributed antenna (DA) layout where M BS antennas in each cell are grouped into L clusters with N_c BS antennas in each cluster. Denote the set of BS antennas at the l-th cluster in Cell i as $\mathcal{L}_l^i$. We have $|\mathcal{L}_l^i| = N_c$, $l = 1, \cdots, L$, $i = 0, \cdots, 6$. The clusters are supposed to be uniformly distributed in the inscribed circle of each hexagonal cell. Without loss of generality, the radius of the inscribed circle of each hexagonal cell is normalized to be 1.

It is clear from (2.3) that the large-scale fading coefficients of user k depend on the distances to BS antennas. With the CA layout, the positions of BS antennas are given by

$$\mathbf{r}_m^B = \begin{cases} (0,0) & m \in \mathcal{B}_0 \\ (2, i\cdot\frac{\pi}{3} - \frac{\pi}{6}) & m \in \mathcal{B}_i, i = 1, \cdots, 6. \end{cases} \tag{2.9}$$

(2.9) indicates that the large-scale fading vector with the CA layout $\boldsymbol{\gamma}_{k,\mathcal{B}_i}^C$ is composed of identical entries. For user $k \in \mathcal{K}_0$ at (ρ_k, θ_k), its large-scale fading coefficient $\gamma_{k,m}^C$ can be obtained by combining (2.3) and (2.9) as

$$\gamma_{k,m}^C = \begin{cases} \rho_k^{-\alpha/2} & m \in \mathcal{B}_0 \\ \left(\rho_k^2 + 4 - 4\rho_k \cos\left(\theta_k - \left(i\cdot\frac{\pi}{3} - \frac{\pi}{6}\right)\right)\right)^{-\alpha/4} & m \in \mathcal{B}_i, i = 1, \cdots, 6. \end{cases} \tag{2.10}$$

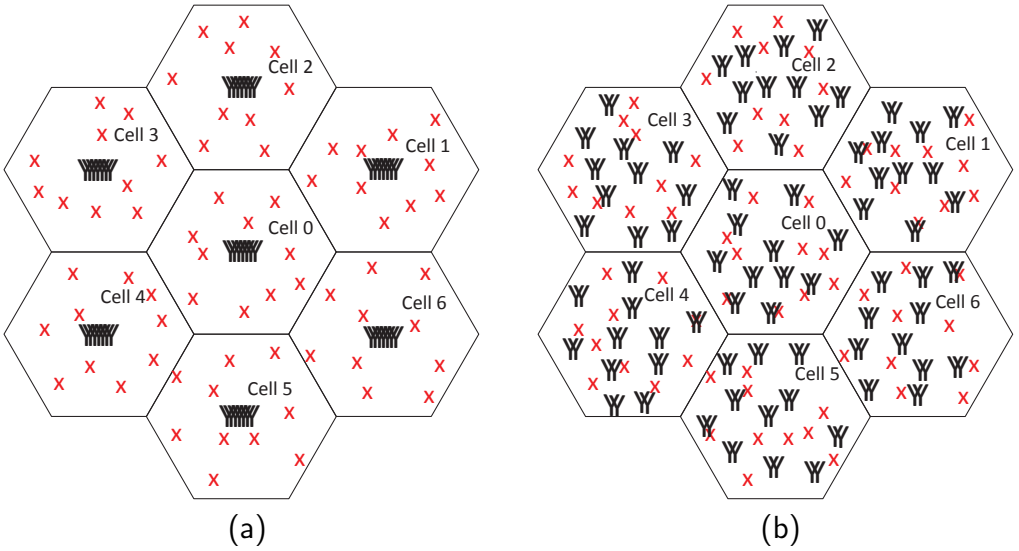

FIGURE 2.2: A 1-tier hexagonal cellular network with K uniformly distributed users in each cell and M BS antennas with two antenna layouts: (a) with the CA layout, BS antennas are co-located at the center of each cell, and (b) with the DA layout, BS antennas are grouped as a set of antenna clusters that are uniformly distributed in the inscribed circle of each cell. "Y" represents a BS antenna and "X" represents a user.

With the DA layout, the BS antennas are grouped into clusters in each cell. The large-scale fading coefficient of user $k \in \mathcal{K}_0$ to BS antenna m can be then written as

$$\gamma_{k,m}^{D} = d_{k,l,i}^{-\alpha/2}, \tag{2.11}$$

for $m \in \mathcal{L}_l^i$, where $d_{k,l,i}$ denotes the distance from user k to BS antenna cluster l in Cell i, $l = 1, \cdots, L$, $i = 0, \cdots, 6$. With BS antenna clusters uniformly distributed in the inscribed circle of each cell, [29] shows that the access distance $d_{k,l,0}$ given the position of user $k \in \mathcal{K}_0$ at (ρ_k, θ_k) has the following conditional cumulative distribution function (cdf) and probability density function (pdf) as

$$F_{d_{k,l,0}|\rho_k}(x|y) = \begin{cases} x^2 & 0 \le x \le 1-y \\ x^2\left(1 - \frac{1}{\pi}\arccos\frac{1-x^2-y^2}{2xy}\right) + \frac{1}{\pi}\arccos\frac{1-x^2+y^2}{2y} - \frac{2}{\pi}S_\Delta & 1-y < x \le 1+y \end{cases} \tag{2.12}$$

with

$$S_\Delta = \sqrt{\tfrac{1+x+y}{2}\left(\tfrac{1+x+y}{2}-1\right)\left(\tfrac{1+x+y}{2}-x\right)\left(\tfrac{1+x+y}{2}-y\right)}, \tag{2.13}$$

and

$$f_{d_{k,l,0}|\rho_k}(x|y) = \begin{cases} 2x & 0 \le x \le 1-y \\ \frac{2x}{\pi}\arccos\frac{x^2+y^2-1}{2xy} & 1-y < x \le 1+y, \end{cases} \tag{2.14}$$

respectively. For the distance $d_{k,l,i}$ from user $k \in \mathcal{K}_0$ to BS antenna cluster l in Cell i, $i = 1 \cdots, 6$, Appendix A shows that its conditional pdf given the position of user k at (ρ_k, θ_k) is given by

$$f_{d_{k,l,i}|\rho_k,\theta_k}(x|y,z) = \frac{2x}{\pi} \arccos \frac{x^2 + y^2 + 3 - 4y\cos\left(z - \left(i \cdot \frac{\pi}{3} - \frac{\pi}{6}\right)\right)}{2x\sqrt{y^2 + 4 - 4y\cos\left(z - \left(i \cdot \frac{\pi}{3} - \frac{\pi}{6}\right)\right)}}, \tag{2.15}$$

if

$$\sqrt{y^2 + 4 - 4y\cos\left(z - \left(i \cdot \frac{\pi}{3} - \frac{\pi}{6}\right)\right)} - 1 \leq x \leq \sqrt{y^2 + 4 - 4y\cos\left(z - \left(i \cdot \frac{\pi}{3} - \frac{\pi}{6}\right)\right)} + 1. \tag{2.16}$$

Otherwise $f_{d_{k,l,i}|\rho_k,\theta_k}(x|y,z) = 0$, $i = 1, \cdots, 6$. In contrast to $d_{k,l,0}$ which only depends on user k's radial coordinate ρ_k, $d_{k,l,i}$ is further determined by its angular coordinate θ_k, $i = 1, \cdots, 6$.

2.3 Asymptotic Average Ergodic Rate

In this thesis, we focus on the downlink rate performance of MIMO cellular networks with a massive number of BS antennas. An asymptotic analysis on the ergodic rate will be presented. By assuming that the number of BS antennas M and the number of user antennas N go to infinity with $M/N \to \xi K$, the asymptotic ergodic rate of user k is defined as

$$\mathcal{R}_k \triangleq \lim_{M,N\to\infty, M/N\to\xi K} R_k. \tag{2.17}$$

Note that with the DA layout, M BS antennas of each cell are grouped into L clusters with N_c antennas at each cluster, i.e., $M = N_c L$. With a finite number of BS antenna clusters L, the asymptotic assumption is then reduced to $N, N_c \to \infty$ and $N/N_c \to \beta$, and the asymptotic ergodic rate with the DA layout is given by

$$\mathcal{R}_k^D \triangleq \lim_{N,N_c\to\infty, N/N_c\to\beta} R_k^D, \tag{2.18}$$

with $\beta = \frac{L}{K\xi}$.

As the ergodic rate varies with the positions of users and BS antennas, we define the average ergodic rate as

$$\bar{R} \triangleq \mathbb{E}_{\mathbf{r}_k^U, \{\mathbf{r}_m^B\}_{m\in\mathcal{B}_i, i=0,\cdots,6}} \left[R_k\right], \tag{2.19}$$

where the ergodic rate R_k is averaged over all possible positions of user k and BS antennas. By combining (2.17) and (2.19), the asymptotic average ergodic rate can be further defined as

$$\bar{\mathcal{R}} \triangleq \mathbb{E}_{\mathbf{r}_k^U, \{\mathbf{r}_m^B\}_{m\in\mathcal{B}_i, i=0,\cdots,6}} \left[\mathcal{R}_k\right]. \tag{2.20}$$

Note that with the CA layout, the positions of BS antennas are given in (2.9). The asymptotic average ergodic rate with the CA layout is then reduced to

$$\bar{\mathcal{R}}^C \triangleq \mathbb{E}_{\mathbf{r}_k^U} \left[\mathcal{R}_k^C\right]. \tag{2.21}$$

In this thesis, we aim to compare the downlink average rate performance of MIMO cellular networks with either co-located or distributed BS antennas. We are interested at the scaling behavior of the average ergodic rate, i.e., how it scales with the ratio ξ of the number of BS antennas M to the total number of user antennas KN. With the DA layout, as $\xi = \frac{L}{K\beta}$, the scaling order with ξ can be also interpreted as how the average ergodic rate increases with the number of BS antenna clusters L. For illustration, our analysis starts from the single-user case in Chapter 3, and is then extend to the multi-user single-cell case in Chapter 4 and the multi-user multi-cell case in Chapter 5. Finally, the effect of power allocation on the ergodic rate will be discussed in Chapter 6.

Chapter 3

Asymptotic Average Ergodic Capacity of Single-User MIMO

In this chapter, an asymptotic analysis on the downlink capacity of a single-user MIMO system is presented, based on which the scaling behavior of the average ergodic capacity is characterized. This chapter is organized as follows. Section 3.1 presents a literature review on previous related work. The asymptotic average ergodic capacity is characterized in Section 3.2. The scaling behavior is discussed in Section 3.3 and verified by simulation results presented in Section 3.4. Section 3.5 summarizes this chapter.

3.1 Literature Review

Originated from the pioneering work of Telatar [10], the ergodic capacity of a single-user MIMO channel has been extensively studied in the past decade. With co-located antennas at the transmitter and receiver sides, as all the transmit signals experience the same large-scale fading, its ergodic capacity can be fully described as a function of the average received signal-to-noise ratio (SNR)[10]. Asymptotic results from random matrix theory [11, 12] were also successfully applied to characterize the ergodic capacity when the number of antennas is large [13, 14]. By assuming that the number of antennas on both sides grow infinitely with a fixed ratio, the asymptotic ergodic capacity of a single-user MIMO channel has been shown to be solely determined by the average received SNR and the ratio of the number of transmit antennas to the number of receive antennas [13].

With distributed BS antennas, in contrast, the ergodic capacity is further determined by the positions of the user and BS antennas [16, 18–24]. By assuming that BS antennas are grouped into L geographically distributed antenna clusters, and the number of antennas at each cluster and the number of user antennas grow infinitely with a fixed ratio, the asymptotic ergodic capacity of a distributed MIMO channel was derived in [18–21] as an implicit function of L large-scale fading coefficients. As the positions of BS antennas and the user may vary under different scenarios, the *average ergodic capacity* was considered in [16, 22–24], where the ergodic capacity is averaged over the large-scale fading coefficients from distributed BS antenna clusters to the user. When the number of BS antenna clusters L is large, nevertheless, it becomes increasingly difficult to obtain the average ergodic capacity due to high computational complexity. Therefore, how the average ergodic capacity scales with L has remained largely unknown. As we will show in this chapter, asymptotic bounds would be helpful for us to characterize the scaling behavior of the average ergodic capacity of distributed MIMO channels.

In this chapter, an asymptotic analysis on the average ergodic capacities of single-user MIMO systems with the CA and DA layouts will be presented. Specifically, by assuming that the number of BS antennas M and the number of user antennas N grow infinitely with $M/N \to \xi \gg 1$, the asymptotic average ergodic capacity with the CA layout and an asymptotic lower-bound of the average ergodic capacity with the DA layout are derived. Simulation results verify that as

the number of BS antennas increases, the average ergodic capacity with the DA layout has a higher scaling order than that with the CA layout.

3.2 Asymptotic Average Capacity Analysis

In this chapter, we assume that a single user is located in the central cell, i.e., Cell 0. (2.6) is then reduced to

$$R_k^S = \frac{1}{N}\mathbb{E}_{\mathbf{H}_{k,\mathcal{B}_0}}\left[\log_2 \det\left(\mathbf{I}_N + \mu_k^S \tilde{\mathbf{G}}_{k,\mathcal{B}_0}\mathbf{W}_k\mathbf{W}_k^\dagger\tilde{\mathbf{G}}_{k,\mathcal{B}_0}^\dagger\right)\right], \tag{3.1}$$

where μ_k^S denotes the average received SNR of user k, which is given by

$$\mu_k^S = \frac{\bar{P}_k\|\boldsymbol{\gamma}_{k,\mathcal{B}_0}\|^2}{N_0}. \tag{3.2}$$

To achieve the single-user capacity, the precoding matrix $\mathbf{W}_k$ should be properly selected, which is further dependent on whether CSIT is available or not.

In this chapter, we assume that the user's position follows the uniform distribution in the inscribed circle of Cell 0, and present an asymptotic analysis on the average ergodic capacity by assuming that the number of BS antennas M and the number of user antennas N go to infinity with $M/N \to \xi \gg 1$. Note that with the DA layout, the BS antennas are grouped into L clusters with N_c antennas at each cluster. The asymptotic assumption is then reduced to $N, N_c \to \infty$ and $N/N_c \to \beta$.

3.2.1 Without CSIT

Without CSIT, the transmit power $\bar{P}_k$ should be equally divided over M transmit antennas, i.e.,

$$\mathbf{W}_k = \sqrt{\frac{1}{M}}\mathbf{I}_M. \tag{3.3}$$

By combining (3.3) and (3.1), the ergodic capacity without CSIT R^{S-o} can be then written as

$$R_k^{S-o} = \frac{1}{N}\mathbb{E}_{\mathbf{H}_{k,\mathcal{B}_0}}\left[\log_2 \det\left(\mathbf{I}_N + \frac{\mu_k^S}{M}\tilde{\mathbf{G}}_{k,\mathcal{B}_0}\tilde{\mathbf{G}}_{k,\mathcal{B}_0}^\dagger\right)\right], \tag{3.4}$$

where the average received SNR μ_k^S is given in (3.2).

3.2.1.1 CA Layout

With the CA layout, M BS antennas are placed at the center of Cell 0. By combining (2.10) and (3.2), the average received SNR with the CA layout μ_k^{S-C} can be obtained as

$$\mu_k^{S-C} = \frac{M\bar{P}_k\rho_k^{-\alpha}}{N_0}. \tag{3.5}$$

Moreover, according to (2.10), the normalized channel gain matrix can be obtained as $\tilde{\mathbf{G}}_{k,\mathcal{B}_0}^C = \sqrt{\frac{1}{M}}\mathbf{H}_{k,\mathcal{B}_0}$. According to the Marcenko-Pastur law [64], as $M, N \to \infty$ and $M/N \to \xi \geq 1$, the empirical eigenvalue distribution of $\tilde{\mathbf{G}}_{k,\mathcal{B}_0}^C \left(\tilde{\mathbf{G}}_{k,\mathcal{B}_0}^C\right)^\dagger \sim \mathcal{W}_N(M, \frac{1}{M}\mathbf{I}_N)$ converges almost surely to the following distribution:

$$f_\lambda(x) = \begin{cases} \frac{1}{2\pi x}\sqrt{(x_+ - \xi x)(\xi x - x_-)} & \text{if } \frac{1}{\xi}x_- \leq x \leq \frac{1}{\xi}x_+ \\ 0 & \text{otherwise,} \end{cases} \tag{3.6}$$

where $x_+ = \left(\sqrt{\xi}+1\right)^2$ and $x_- = \left(\sqrt{\xi}-1\right)^2$. As we can see from Fig. 3.1, as ξ grows, the eigenvalues of $\tilde{\mathbf{G}}_{k,\mathcal{B}_0}^C \left(\tilde{\mathbf{G}}_{k,\mathcal{B}_0}^C\right)^\dagger$ become increasingly deterministic, and eventually converge to $\mathbb{E}[\lambda] = 1$. As a result, we have

$$\mathbf{\Lambda}_{k,\mathcal{B}_0} \approx \left[\mathbf{I}_N, \mathbf{0}_{N\times(M-N)}\right], \tag{3.7}$$

for large $\xi \gg 1$. By combining (3.4-3.5) and (3.7), the asymptotic ergodic capacity of user k with the CA layout as $M, N \to \infty$ with $M, N \to \xi \gg 1$ can be obtained as

$$\mathcal{R}_k^{S-o-C} \approx \log_2\left(1 + \frac{\bar{P}_k}{N_0}\rho_k^{-\alpha}\right). \tag{3.8}$$

As we can see from (3.8), the asymptotic ergodic capacity without CSIT $\mathcal{R}_k^{S-o-C}$ varies with the radial coordinate of the user ρ_k. By combining (3.8) and (2.21), the asymptotic average ergodic capacity with the CA layout can be then obtained as

$$\bar{\mathcal{R}}^{S-o-C} \approx \int_0^1 \log_2\left(1 + \frac{\bar{P}_k}{N_0}x^{-\alpha}\right) f_{\rho_k}(x)dx, \tag{3.9}$$

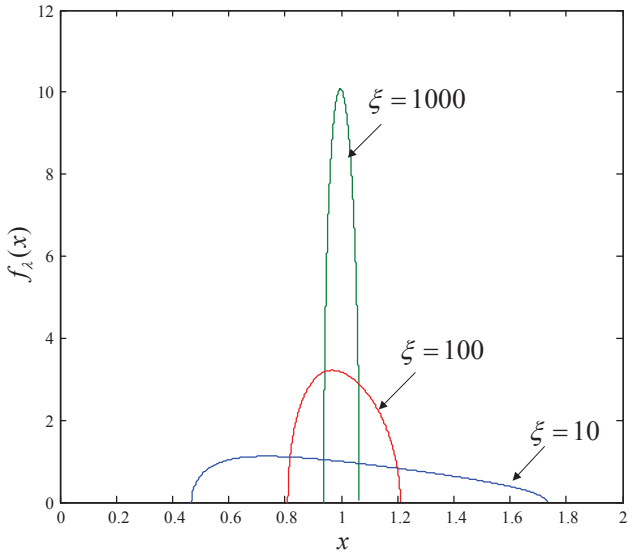

FIGURE 3.1: Empirical eigenvalue distribution (3.6) of $\tilde{\mathbf{G}}^C_{k,\mathcal{B}_0}\left(\tilde{\mathbf{G}}^C_{k,\mathcal{B}_0}\right)^\dagger \sim \mathcal{W}_N(M, \frac{1}{M}\mathbf{I}_N)$ as $M, N \to \infty$ with $M/N \to \xi \geq 1$.

where $f_{\rho_k}(x) = 2x$ is the pdf of its radial coordinate，as the user's position follows the uniform distribution in the inscribed circle of the central cell. For large $\frac{\bar{P}_k}{N_0} \gg 1$, we have

$$\bar{\mathcal{R}}^{S-o-C} \approx \log_2 \frac{\bar{P}_k}{N_0} + \frac{\alpha}{\ln 4}. \tag{3.10}$$

3.2.1.2 DA Layout

With the DA layout, [19] shows that as the number of user antennas N and the number of antennas at each cluster N_c go to infinity with $N/N_c \to \beta$, the asymptotic ergodic capacity $\mathcal{R}_k^{S-o-D}$ can be obtained as

$$\begin{aligned}\mathcal{R}_k^{S-o-D} = &\frac{1}{\beta}\sum_{l=1}^{L}\log_2 U_k^{(l)} + \log_2\left(1 + \frac{1}{L}\frac{\bar{P}_k}{N_0}\sum_{l=1}^{L}\left(d_{k,0}^{(l)}\right)^{-\alpha}\left(U_k^{(l)}\right)^{-1}\right)\\ &- \frac{\frac{1}{L}\frac{\bar{P}_k}{N_0}\sum_{l=1}^{L}\left(d_{k,0}^{(l)}\right)^{-\alpha}\left(U_k^{(l)}\right)^{-1}}{1 + \frac{1}{L}\frac{\bar{P}_k}{N_0}\sum_{l=1}^{L}\left(d_{k,0}^{(l)}\right)^{-\alpha}\left(U_k^{(l)}\right)^{-1}}\log_2 e,\end{aligned} \tag{3.11}$$

where $\{U_k^{(l)}\}$ are the roots of following equations:

$$U_k^{(l)} = 1 + \frac{\frac{\beta}{L}\frac{\bar{P}_k}{N_0}\left(d_{k,0}^{(l)}\right)^{-\alpha}}{1+\frac{1}{L}\frac{\bar{P}_k}{N_0}\sum_{j=1}^{L}\left(d_{k,0}^{(j)}\right)^{-\alpha}\left(U_k^{(j)}\right)^{-1}}, \tag{3.12}$$

$l = 1, \cdots, L$. $d_{k,0}^{(l)}$ denotes the access distance from user k to the l-th closest BS antenna cluster in Cell 0.

We can see from (3.11) that the asymptotic ergodic capacity with the DA layout $\mathcal{R}_k^{S-o-D}$ depends on the access distances $\{d_{k,0}^{(l)}\}$, which varies with the positions of distributed BS antenna clusters. As it is difficult to derive a closed-form expression for the asymptotic average ergodic capacity from (3.11-3.12), we develop an asymptotic lower-bound to study its scaling behavior. Specifically, by noting that the number of BS antennas clusters $L \gg \beta$ as the total number of BS antennas M is assumed to be much larger than the number of user antennas N, and that the last item on the right-hand side of (3.11) is larger than $-\log_2 e$, we can obtain from (3.11) that

$$\mathcal{R}_k^{S-o-D} > \frac{1}{\beta}\sum_{l=1}^{\lceil\beta\rceil}\log_2(U_k^{(l)}) + \log_2\left(\frac{1}{L}\frac{\bar{P}_k}{N_0}\sum_{l=1}^{\lceil\beta\rceil}\left(d_{k,0}^{(l)}\right)^{-\alpha}\left(U_k^{(l)}\right)^{-1}\right) - \log_2 e. \tag{3.13}$$

According to the inequality of arithmetic and geometric means,

$$\frac{1}{\lceil\beta\rceil}\sum_{l=1}^{\lceil\beta\rceil}\left(d_{k,0}^{(l)}\right)^{-\alpha}\left(U_k^{(l)}\right)^{-1} \geq \prod_{l=1}^{\lceil\beta\rceil}\left(\left(d_{k,0}^{(l)}\right)^{-\alpha}\left(U_k^{(l)}\right)^{-1}\right)^{\frac{1}{\lceil\beta\rceil}}. \tag{3.14}$$

By combining (3.13-3.14), we have

$$\mathcal{R}_k^{S-o-D} > \left(\frac{1}{\beta}-\frac{1}{\lceil\beta\rceil}\right)\sum_{l=1}^{\lceil\beta\rceil}\log_2 U_k^{(l)} - \frac{\alpha}{\lceil\beta\rceil}\sum_{l=1}^{\lceil\beta\rceil}\log_2 d_{k,0}^{(l)} + \log_2\left(\frac{\lceil\beta\rceil}{L}\frac{\bar{P}_k}{N_0}\right) - \log_2 e. \tag{3.15}$$

Note that $\beta \leq \lceil\beta\rceil$. We further have

$$\mathcal{R}_k^{S-o-D} > \mathcal{R}_{k,lb}^{S-o-D} = -\frac{\alpha}{\lceil\beta\rceil}\sum_{l=1}^{\lceil\beta\rceil}\log_2 d_{k,0}^{(l)} + \log_2\left(\frac{\lceil\beta\rceil}{L}\frac{\bar{P}_k}{N_0}\right) - \log_2 e. \tag{3.16}$$

An asymptotic lower-bound of the average ergodic capacity can be then obtained from (3.16) and (2.20) as

$$\bar{\mathcal{R}}_{lb}^{S-o-D} = -\frac{\alpha}{\lceil\beta\rceil}\sum_{l=1}^{\lceil\beta\rceil}\int_0^1\int_0^{1+y}\log_2 x\cdot f_{d_{k,0}^{(l)}|\rho_k}(x|y)f_{\rho_k}(y)dxdy + \log_2\left(\frac{\lceil\beta\rceil}{L}\frac{\bar{P}_k}{N_0}\right) - \log_2 e, \tag{3.17}$$

where $f_{\rho_k}(y) = 2y$ denotes the pdf of its radial coordinate. $f_{d_{k,0}^{(l)}|\rho_k}(x|y)$ is the pdf of the access distance $d_{k,0}^{(l)}$ from the user to its l-th closest BS antenna cluster, $l = 1, \cdots, L$, which is given by

$$f_{d_{k,0}^{(l)}|\rho_k}(x|y) = \frac{L!}{(l-1)!(L-l)!}\left(F_{d_{k,l,0}|\rho_k}(x|y)\right)^{l-1}\left(1 - F_{d_{k,l,0}|\rho_k}(x|y)\right)^{L-l} f_{d_{k,l,0}|\rho_k}(x|y), \tag{3.18}$$

where $F_{d_{k,l,0}|\rho_k}(x|y)$ and $f_{d_{k,l,0}|\rho_k}(x|y)$ denote the cdf and pdf of the access distance $d_{k,l,0}$ from user k to BS antenna cluster l in Cell 0 given its radial coordinate ρ_k, respectively, $l = 1, \cdots, L$, which are given in (2.12-2.13) and (2.14), respectively.

3.2.2 With CSIT

With CSIT, according to [10], the capacity can be achieved by the singular-value-decomposition (SVD) transmission, and the corresponding precoding matrix $\mathbf{W}_k^{SVD}$ is given by

$$\mathbf{W}_k^{SVD} = \mathbf{V}_{k,\mathcal{B}_0}\mathbf{\Omega}_k. \tag{3.19}$$

$\mathbf{V}_{k,\mathcal{B}_0}$ is a unitary matrix obtained from the SVD of the normalized channel gain matrix $\tilde{\mathbf{G}}_{k,\mathcal{B}_0}$:

$$\tilde{\mathbf{G}}_{k,\mathcal{B}_0} = \mathbf{U}_{k,\mathcal{B}_0}\mathbf{\Lambda}_{k,\mathcal{B}_0}\mathbf{V}_{k,\mathcal{B}_0}^{\dagger}, \tag{3.20}$$

where $\mathbf{\Lambda}_{k,\mathcal{B}_0} = \left[\text{diag}\left(\sqrt{\lambda_1}, \sqrt{\lambda_2}, \ldots, \sqrt{\lambda_N}\right), \mathbf{0}_{N\times(M-N)}\right]$ is composed by eigenvalues $\{\lambda_n\}$ of $\tilde{\mathbf{G}}_{k,\mathcal{B}_0}\tilde{\mathbf{G}}_{k,\mathcal{B}_0}^{\dagger}$. $\mathbf{\Omega}_k$ denotes the power distribution over N parallel sub-channels, which is given by

$$\mathbf{\Omega}_k = \left[\text{diag}\left(\sqrt{\frac{P_k(\lambda_1)}{\bar{P}_k\|\boldsymbol{\gamma}_{k,\mathcal{B}_0}\|^2}}, \sqrt{\frac{P_k(\lambda_2)}{\bar{P}_k\|\boldsymbol{\gamma}_{k,\mathcal{B}_0}\|^2}}, \ldots, \sqrt{\frac{P_k(\lambda_N)}{\bar{P}_k\|\boldsymbol{\gamma}_{k,\mathcal{B}_0}\|^2}}\right), \mathbf{0}_{N\times(M-N)}\right]^T, \tag{3.21}$$

with $\{P_k(\lambda_n)\}$ denoting the water-filling power allocation, i.e.,

$$P_k(\lambda_n) = \left(\zeta - \frac{N_0}{\lambda_n}\right)^+, \tag{3.22}$$

where $(x)^+ = \max(x, 0)$, and ζ is chosen to satisfy

$$\sum_{n=1}^{N} P_k(\lambda_n) = \bar{P}_k \|\boldsymbol{\gamma}_{k,\mathcal{B}_0}\|^2. \tag{3.23}$$

By combining (3.19-3.23) with (3.1), the ergodic capacity with CSIT R_k^{S-w} can be obtained as

$$R_k^{S-w} = \frac{1}{N}\mathbb{E}_{\mathbf{H}_{k,\mathcal{B}_0}}\left[\log_2 \det\left(\mathbf{I}_N + \mu_k^S \boldsymbol{\Lambda}_{k,\mathcal{B}_0}\boldsymbol{\Omega}_k\boldsymbol{\Omega}_k^\dagger\boldsymbol{\Lambda}_{k,\mathcal{B}_0}^\dagger\right)\right], \tag{3.24}$$

where the average received SNR μ_k^S is given in (3.2).

3.2.2.1 CA Layout

With the CA layout, the empirical eigenvalue distribution of $\tilde{\mathbf{G}}_{k,\mathcal{B}_0}^C\left(\tilde{\mathbf{G}}_{k,\mathcal{B}_0}^C\right)^\dagger \sim \mathcal{W}_N(M, \frac{1}{M}\mathbf{I}_N)$ with $M, N \to \infty$ and $M/N \to \xi \geq 1$ is given in (3.6). As the ratio ξ of the number of BS antennas M to the number of user antennas N increases, the eigenvalues $\{\lambda_n\}$ of $\tilde{\mathbf{G}}_{k,\mathcal{B}_0}^C\left(\tilde{\mathbf{G}}_{k,\mathcal{B}_0}^C\right)^\dagger \sim \mathcal{W}_N(M, \frac{1}{M}\mathbf{I}_N)$ become increasingly deterministic and eventually converge to $\mathbb{E}[\lambda] = 1$. By combining (3.5), (3.7) and (3.19-3.24), the asymptotic ergodic capacity of user k with the CA layout $\mathcal{R}_k^{S-w-C}$ as $M, N \to \infty$ and $M/N \to \xi \gg 1$ can be obtained as

$$\mathcal{R}_k^{S-w-C} \approx \log_2\left(1 + \frac{\bar{P}_k}{N_0}\xi\rho_k^{-\alpha}\right). \tag{3.25}$$

As we can see from (3.25), the asymptotic ergodic rate with the CA layout varies with the radial coordinate ρ_k of the user. By combining (3.25) and (2.21), the asymptotic average ergodic capacity with the CA layout can be then obtained as

$$\bar{\mathcal{R}}^{S-w-C} \approx \int_0^1 \log_2\left(1 + \frac{\bar{P}_k}{N_0}\xi x^{-\alpha}\right) f_{\rho_k}(x)dx, \tag{3.26}$$

where $f_{\rho_k}(x) = 2x$ is the pdf of its radial coordinate. For large $\frac{\bar{P}_k}{N_0} \gg 1$, we have

$$\bar{\mathcal{R}}^{S-w-C} \approx \log_2\frac{\bar{P}_k}{N_0} + \frac{\alpha}{\ln 4} + \log_2\xi. \tag{3.27}$$

3.2.2.2 DA Layout

With the DA layout, there is no closed-form expression for the average ergodic capacity with CSIT. Similar to the no-CSIT case, we resort to a lower-bound to characterize the scaling behavior of the average ergodic capacity with CSIT. Specifically, if the transmit power is equally distributed over N sub-channels, i.e., $\mathbf{\Omega}_k = \sqrt{\frac{1}{N}}\left[\mathbf{I}_N, \mathbf{0}_{N\times(M-N)}\right]^T$, we can obtain a lower-bound of R_k^{S-w-D} as

$$R_k^{S-w-D} > \frac{1}{N}\mathbb{E}_{\mathbf{H}_{k,\mathcal{B}_0}}\left[\log_2 \det\left(\mathbf{I}_N + \frac{\mu_k^S}{N}\mathbf{\Lambda}_{k,\mathcal{B}_0}\mathbf{\Lambda}_{k,\mathcal{B}_0}^{\dagger}\right)\right]. \tag{3.28}$$

As $N, N_c \to \infty$ with $N/N_c \to \beta$, the limit of the right-hand side of (3.28) can be obtained as

$$\begin{aligned}\mathcal{R}_k^{S-w-D} > & \frac{1}{\beta}\sum_{l=1}^{L}\log_2(V_k^{(l)}) + \log_2\left(1 + \frac{1}{\beta}\frac{\bar{P}_k}{N_0}\sum_{l=1}^{L}\left(d_{k,0}^{(l)}\right)^{-\alpha}\left(V_k^{(l)}\right)^{-1}\right) \\ & - \frac{\frac{1}{\beta}\frac{\bar{P}_k}{N_0}\sum_{l=1}^{L}\left(d_{k,0}^{(l)}\right)^{-\alpha}\left(V_k^{(l)}\right)^{-1}}{1 + \frac{1}{\beta}\frac{\bar{P}_k}{N_0}\sum_{l=1}^{L}\left(d_{k,0}^{(l)}\right)^{-\alpha}\left(V_k^{(l)}\right)^{-1}}\log_2 e,\end{aligned} \tag{3.29}$$

where $\{V_k^{(l)}\}$ are the roots of following equations:

$$V_k^{(l)} = 1 + \frac{\frac{\bar{P}_k}{N_0}\left(d_{k,0}^{(l)}\right)^{-\alpha}}{1 + \frac{1}{\beta}\frac{\bar{P}_k}{N_0}\sum_{j=1}^{L}\left(d_{k,0}^{(j)}\right)^{-\alpha}\left(V_k^{(j)}\right)^{-1}}, \tag{3.30}$$

$l = 1, \cdots, L$.

Similar to that without CSIT, the asymptotic ergodic capacity with CSIT $\mathcal{R}_k^{S-w-D}$ is dependent on the access distances $\{d_{k,0}^{(l)}\}$, which varies with the positions of distributed BS antenna clusters. Due to the lack of a closed-form expression for the asymptotic average ergodic capacity, we resort to an asymptotic lower-bound to study the scaling behavior of the average ergodic capacity. By noting that the number of BS antennas clusters $L \gg \beta$ as the total number of BS antennas M is assumed to be much larger than the number of user antennas N, and that the last item on the right-hand side of (3.29) is larger than $-\log_2 e$, we

can obtain from (3.29) as

$$\mathcal{R}_k^{S-w-D} > \frac{1}{\beta}\sum_{l=1}^{\lceil\beta\rceil}\log_2 V_k^{(l)} + \log_2\left(\frac{1}{\beta}\frac{\bar{P}_k}{N_0}\sum_{l=1}^{\lceil\beta\rceil}\left(d_{k,0}^{(l)}\right)^{-\alpha}\left(V_k^{(l)}\right)^{-1}\right) - \log_2 e. \quad (3.31)$$

According to the inequality of arithmetic and geometric means,

$$\frac{1}{\lceil\beta\rceil}\sum_{l=1}^{\lceil\beta\rceil}\left(d_{k,0}^{(l)}\right)^{-\alpha}\left(V_k^{(l)}\right)^{-1} \geq \prod_{l=1}^{\lceil\beta\rceil}\left(\left(d_{k,0}^{(l)}\right)^{-\alpha}\left(V_k^{(l)}\right)^{-1}\right)^{\frac{1}{\lceil\beta\rceil}}. \quad (3.32)$$

By combining (3.31-3.32), we have

$$\mathcal{R}_k^{S-w-D} > \left(\frac{1}{\beta}-\frac{1}{\lceil\beta\rceil}\right)\sum_{l=1}^{\lceil\beta\rceil}\log_2 V_k^{(l)} - \frac{\alpha}{\lceil\beta\rceil}\sum_{l=1}^{\lceil\beta\rceil}\log_2 d_{k,0}^{(l)} + \log_2\left(\frac{\lceil\beta\rceil}{\beta}\frac{\bar{P}_k}{N_0}\right) - \log_2 e. \quad (3.33)$$

Note that $\beta \leq \lceil\beta\rceil$. We further have

$$\mathcal{R}_k^{S-w-D} > \mathcal{R}_{k,lb}^{S-w-D} = -\frac{\alpha}{\lceil\beta\rceil}\sum_{l=1}^{\lceil\beta\rceil}\log_2 d_{k,0}^{(l)} + \log_2\left(\frac{\lceil\beta\rceil}{\beta}\frac{\bar{P}_k}{N_0}\right) - \log_2 e. \quad (3.34)$$

An asymptotic lower-bound of the average ergodic capacity with CSIT can be then obtained by combining (3.34) and (2.20) as

$$\bar{\mathcal{R}}_{lb}^{S-w-D} = -\frac{\alpha}{\lceil\beta\rceil}\sum_{l=1}^{\lceil\beta\rceil}\int_0^1\int_0^{1+y}\log_2 x\cdot f_{d_{k,0}^{(l)}|\rho_k}(x|y)f_{\rho_k}(y)dxdy + \log_2\left(\frac{\lceil\beta\rceil}{\beta}\frac{\bar{P}_k}{N_0}\right) - \log_2 e, \quad (3.35)$$

where $f_{\rho_k}(y) = 2y$ denotes the pdf of the radial coordinate of the user. $f_{d_{k,0}^{(l)}|\rho_k}(x|y)$ is the pdf of the access distance $d_{k,0}^{(l)}$ from the user to its l-th closest BS antenna cluster, $l = 1, \cdots, L$, which is given in (3.18).

3.3 Scaling Behavior

3.3.1 CA Layout

With the CA layout, (3.10) and (3.27) indicate that the asymptotic ergodic capacities without and with CSIT have different scaling orders. Specifically, as

the ratio ξ of the number of BS antennas M to the number of user antennas N increases, the asymptotic average ergodic capacity without CSIT $\bar{\mathcal{R}}^{S-o-C}$ remains constant. Yet the asymptotic average ergodic capacity with CSIT $\bar{\mathcal{R}}^{S-w-C}$ logarithmically increases with ξ. More specifically, we have $\bar{\mathcal{R}}^{S-o-C} = \Theta(1)$ and $\bar{\mathcal{R}}^{S-w-C} = \Theta(\log_2 \xi)$.

3.3.2 DA Layout

With the DA layout, it is difficult to see how the asymptotic lower-bounds $\bar{\mathcal{R}}_{lb}^{S-o-D}$ and $\bar{\mathcal{R}}_{lb}^{S-w-D}$ scale with the number of BS antenna clusters L from (3.17) and (3.35). To characterize the scaling behavior, let us first assume that the user is located at (0,0). Numerical results will show that the asymptotic lower-bounds of the average ergodic capacities with and without CSIT given the user's position at (0,0) have the same scaling orders as that with a randomly placed user.

In particular, with the user located at $(0,0)$ and L BS antenna clusters uniformly distributed in the inscribed circle of Cell 0, the asymptotic lower-bounds of the average ergodic capacity without and with CSIT can be written from (3.17) and (3.35) as

$$\bar{\mathcal{R}}_{lb}^{S-o-D}|_{(0,0)} = -\frac{\alpha}{\lceil\beta\rceil}\sum_{l=1}^{\lceil\beta\rceil}\int_0^1 \log_2 x \cdot f_{d_{k,0}^{(l)}|\rho_k}(x|0)dx + \log_2\left(\frac{\lceil\beta\rceil}{L}\frac{\bar{P}_k}{N_0}\right) - \log_2 e, \tag{3.36}$$

and

$$\bar{\mathcal{R}}_{lb}^{S-w-D}|_{(0,0)} = -\frac{\alpha}{\lceil\beta\rceil}\sum_{l=1}^{\lceil\beta\rceil}\int_0^1 \log_2 x \cdot f_{d_{k,0}^{(l)}|\rho_k}(x|0)dx + \log_2\left(\frac{\lceil\beta\rceil}{\beta}\frac{\bar{P}_k}{N_0}\right) - \log_2 e, \tag{3.37}$$

respectively, where $f_{d_{k,0}^{(l)}|\rho_k}(x|0)$ is the pdf of the access distance from the user at (0,0) to its l-th closest BS antenna cluster, which is given by

$$f_{d_{k,0}^{(l)}|\rho_k}(x|0) = \frac{2L!}{(l-1)!(L-l)!}x^{2l-1}\left(1-x^2\right)^{L-l}, \tag{3.38}$$

by substituting (2.14) into (3.18).

We can then obtain the asymptotic lower-bounds without and with CSIT from (3.36) and (3.37) as

$$\bar{\mathcal{R}}_{lb}^{S-o-D}|_{(0,0)} = \frac{\alpha \log_2 e}{2}\left(1 + \mathbb{H}(L) - \mathbb{H}(\lceil \beta \rceil)\right) + \log_2\left(\frac{\lceil \beta \rceil}{L}\frac{\bar{P}_k}{N_0}\right) - \log_2 e, \quad (3.39)$$

and

$$\bar{\mathcal{R}}_{lb}^{S-w-D}|_{(0,0)} = \frac{\alpha \log_2 e}{2}\left(1 + \mathbb{H}(L) - \mathbb{H}(\lceil \beta \rceil)\right) + \log_2\left(\frac{\lceil \beta \rceil}{\beta}\frac{\bar{P}_k}{N_0}\right) - \log_2 e, \quad (3.40)$$

respectively, where $\mathbb{H}(k)=\sum_{l=1}^{k}\frac{1}{l}$ is the k-th harmonic number. The detailed derivation of (3.39-3.40) is presented in Appendix B. Note that the k-th harmonic number $\mathbb{H}(k)$ can be further written as

$$\mathbb{H}(k) = \ln k + \sigma + \epsilon_k, \quad (3.41)$$

where $\sigma \approx 0.5772$ is the Euler-Mascheroni constant, and $\epsilon_k{=}O\left(\frac{1}{2k}\right)$. By substituting (3.41) into (3.39) and (3.40), the asymptotic lower-bounds without and with CSIT can be written as

$$\bar{\mathcal{R}}_{lb}^{S-o-D}|_{(0,0)} = \left(\frac{\alpha}{2} - 1\right)\log_2\frac{L}{\lceil \beta \rceil} + \log_2\frac{\bar{P}_k}{N_0} + \left(\frac{\alpha}{2} - 1 + \frac{\alpha}{2}(\epsilon_L - \epsilon_{\lceil \beta \rceil})\right)\log_2 e, \quad (3.42)$$

and

$$\bar{\mathcal{R}}_{lb}^{S-w-D}|_{(0,0)} = \frac{\alpha}{2}\log_2\frac{L}{\lceil \beta \rceil} + \log_2\frac{\lceil \beta \rceil}{\beta} + \log_2\frac{\bar{P}_k}{N_0} + \left(\frac{\alpha}{2} - 1 + \frac{\alpha}{2}(\epsilon_L - \epsilon_{\lceil \beta \rceil})\right)\log_2 e, \quad (3.43)$$

respectively.

3.3.2.1 Fixed β

Let us first see how the asymptotic lower-bounds of the average ergodic capacity with and without CSIT scale with the number of BS antenna clusters L when the ratio β of the number of user antennas N to the number of BS antennas at each cluster N_c is constant. It can be easily obtained from (3.42) and (3.43)

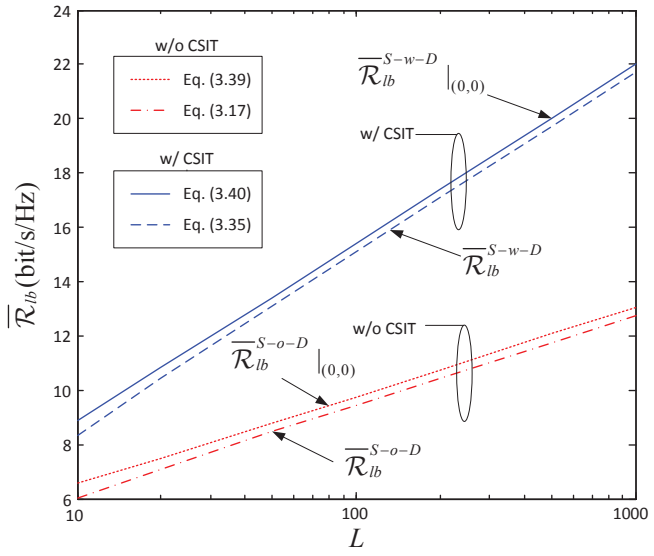

FIGURE 3.2: Asymptotic lower-bounds of the average ergodic capacity without and with CSIT with the DA layout in the single-user case. $\bar{\mathcal{R}}_{lb}^{S-w-D}|_{(0,0)}$ and $\bar{\mathcal{R}}_{lb}^{S-w-D}|_{(0,0)}$ are obtained by assuming that the user is fixed at (0,0). $\bar{\mathcal{R}}_{lb}^{S-w-D}$ and $\bar{\mathcal{R}}_{lb}^{S-w-D}$ are obtained by assuming that the user's position follows the uniform distribution in the inscribed circle of Cell 0. $\bar{P}_k/N_0 = 10$dB. $\beta = 2$. $\alpha = 4$.

that with a fixed β, the asymptotic lower-bounds $\bar{\mathcal{R}}_{lb}^{S-o-D}|_{(0,0)}$ and $\bar{\mathcal{R}}_{lb}^{S-w-D}|_{(0,0)}$ increase logarithmically with L in the orders of $\Theta\left(\left(\frac{\alpha}{2}-1\right)\log_2 L\right)$ and $\Theta\left(\frac{\alpha}{2}\log_2 L\right)$, respectively, where $\alpha > 2$ is the path-loss factor.

Fig. 3.2 plots the asymptotic lower-bounds of the average ergodic capacity without and with CSIT when the ratio β is fixed to be 2. We can see from Fig. 3.2 that both $\bar{\mathcal{R}}_{lb}^{S-o-D}|_{(0,0)}$ and $\bar{\mathcal{R}}_{lb}^{S-w-D}|_{(0,0)}$ increase logarithmically with the number of BS antenna clusters L, but a higher scaling order is achieved with CSIT. The numerical results of the asymptotic lower-bounds of the average ergodic capacity of a randomly located user, i.e., $\bar{\mathcal{R}}_{lb}^{S-o-D}$ and $\bar{\mathcal{R}}_{lb}^{S-w-D}$, are also plotted in Fig. 3.2. We can see from Fig. 3.2 that the asymptotic lower-bounds of a randomly placed user have the same scaling orders as that of a fixed user at $(0,0)$.

3.3.2.2 Fixed $\xi = \frac{L}{\beta}$

When the ratio $\xi = \frac{L}{\beta}$ of the number of BS antennas to the number of user antennas is fixed, we can see from (3.42) and (3.43) that the asymptotic lower-bound without CSIT $\bar{\mathcal{R}}_{lb}^{S-o-D}|_{(0,0)}$ and that with CSIT $\bar{\mathcal{R}}_{lb}^{S-w-D}|_{(0,0)}$ have the same

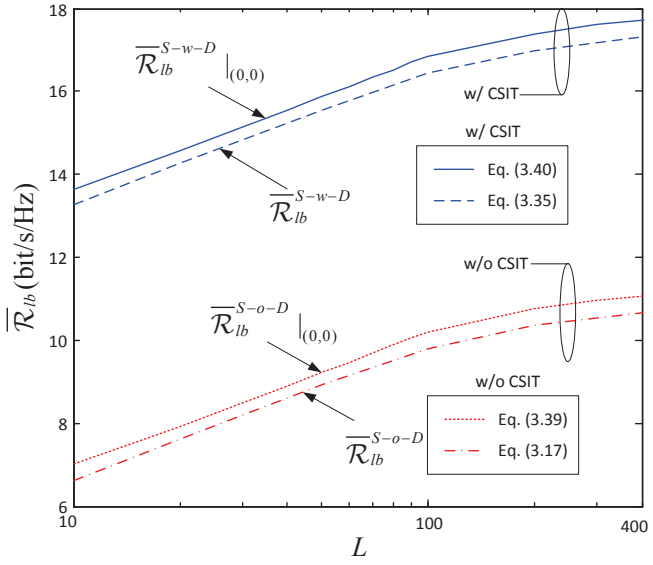

FIGURE 3.3: Asymptotic lower-bounds of the average ergodic capacity without and with CSIT with the DA layout in the single-user case. $\bar{\mathcal{R}}_{lb}^{S-w-D}|_{(0,0)}$ and $\bar{\mathcal{R}}_{lb}^{S-w-D}|_{(0,0)}$ are obtained by assuming that the user is fixed at (0,0). $\bar{\mathcal{R}}_{lb}^{S-w-D}$ and $\bar{\mathcal{R}}_{lb}^{S-w-D}$ are obtained by assuming that the user's position follows the uniform distribution in the inscribed circle of Cell 0. $\bar{P}_k/N_0 = 10$dB. $\xi = 100$. $\alpha = 4$.

scaling order, which is found to be $\Theta\left(\left(\frac{\alpha}{2}-1\right)\log_2 L\right)$ for $L \geq \xi$. When $L > \xi$, the scaling order is reduced to $\Theta\left(\left(\frac{\alpha}{2}-1\right)\log_2 \frac{L}{\lceil \frac{L}{\xi} \rceil} + \frac{\alpha}{2}(\epsilon_L - \epsilon_{\lceil \frac{L}{\xi} \rceil})\log_2 e\right)$.

Fig. 3.3 demonstrates the asymptotic lower-bounds of the average ergodic capacity without and with CSIT when the ratio ξ is fixed to be 100. As we can see from Fig. 3.3, both $\bar{\mathcal{R}}_{lb}^{S-o-D}|_{(0,0)}$ and $\bar{\mathcal{R}}_{lb}^{S-w-D}|_{(0,0)}$ increase logarithmically with L when $L \leq \xi$. For $L > \xi$, the scaling order decreases and gradually approaches $\Theta(1)$ as L increases. The numerical results of the asymptotic lower-bounds of the average ergodic capacity of a randomly located user with and without CSIT are also plotted in Fig. 3.3. We can see from Fig. 3.3 that the asymptotic lower-bounds of the average ergodic capacity of a randomly placed user with and without CSIT have the same scaling orders as that of a fixed user at (0,0).

3.4 Simulation Results and Discussions

In this section, simulation results are presented to verify the asymptotic analysis. With the CA layout, the average ergodic capacity is obtained by averaging

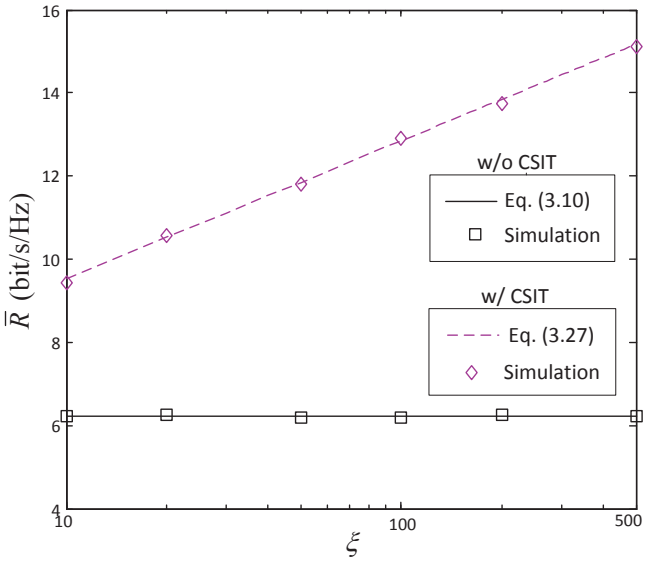

FIGURE 3.4: Average ergodic capacities without and with CSIT with the CA layout versus the ratio ξ of the number of BS antennas M to the number of user antennas N in the single-user case. $N = 4$. $\bar{P}_k/N_0 = 10$dB. $\alpha = 4$.

over 100 realizations of the user's position. With the DA layout, it is further averaged over 100 realizations of BS antennas' positions. Let us first focus on the average ergodic capacity with the CA layout.

3.4.1 CA Layout

Fig. 3.4 plots the average ergodic capacity with the CA layout. As we can see from Fig. 3.4, the asymptotic results are accurate even when N is small, i.e., $N = 4$. As the ratio ξ of the number of BS antennas to the number of user antennas N increases, the average ergodic capacities without and with CSIT have the scaling orders of $\Theta(1)$ and $\Theta\left(\log_2 \xi\right)$, respectively. Substantial capacity gains can be achieved with CSIT when the number of BS antennas M is large thanks to the $\frac{M}{N}$-fold power gain.

3.4.2 DA Layout

Fig. 3.5 plots the average ergodic capacity with the DA layout. As we can see from Fig. 3.5, the average ergodic capacities without and with CSIT have the same scaling orders as their asymptotic lower-bounds.

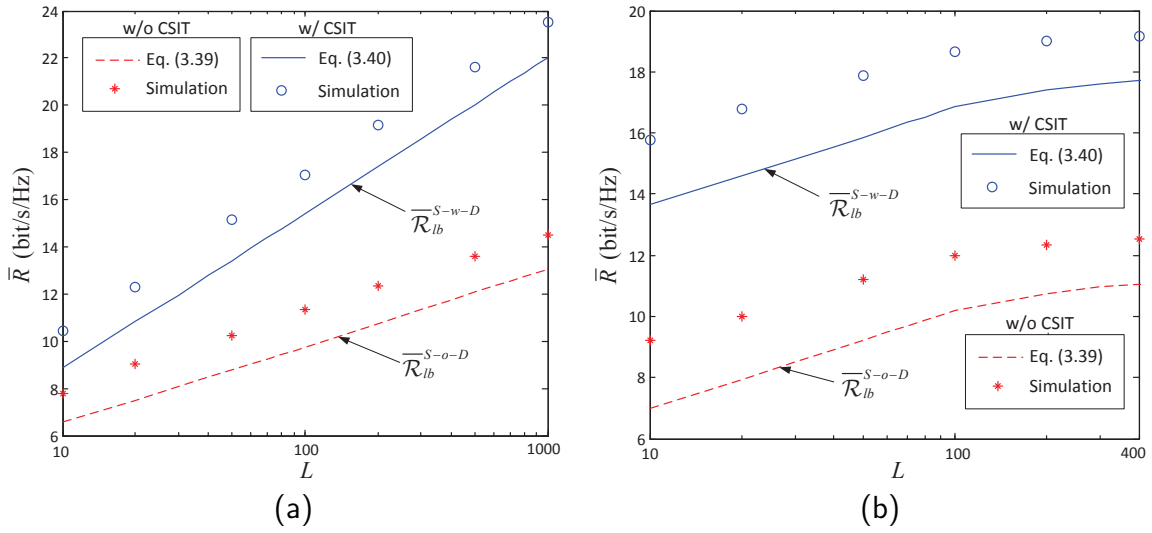

FIGURE 3.5: Average ergodic capacities without and with CSIT with the DA layout versus the number of BS antenna clusters L in the single-user case. $N = 4$. $\bar{P}_k/N_0 = 10$dB. $\alpha = 4$. (a)$\beta = 2$. (b)$\xi = 100$.

Specifically, we can see from Fig. 3.5a that when the ratio β of the number of user antennas N to the number of BS antennas at each cluster N_c is fixed, the average ergodic capacities without and with CSIT scale with the number of BS antenna clusters L in the orders of $\Theta\left(\left(\frac{\alpha}{2}-1\right)\log_2 L\right)$ and $\Theta\left(\frac{\alpha}{2}\log_2 L\right)$, respectively. Intuitively, with L uniformly distributed BS antenna clusters, the minimum access distance decreases in the order of $\Theta\left(L^{-1/2}\right)$ as L increases. As a result, the average ergodic capacities without and with CSIT both increase logarithmically with the number of BS antenna clusters L. Moreover, as the power gain achieved with CSIT is determined by the ratio of the number of BS antennas M to the number of user antennas N, or $\frac{L}{\beta}$ in the asymptotic case, the gap between the average ergodic capacity with CSIT and that without CSIT is enlarged when the ratio β is constant and the number of BS antenna clusters L increases, as we can observe from Fig. 3.5a.

In Fig. 3.5b, the ratio ξ of the number of BS antennas M to the number of user antennas N is fixed to be 100. We can see from Fig. 3.5b that the scaling orders of the average ergodic capacities without and with CSIT are the same as their asymptotic lower-bounds, which are found to be $\Theta\left(\left(\frac{\alpha}{2}-1\right)\log_2 L\right)$ for $L \leq \xi$, and $\Theta\left(\left(\frac{\alpha}{2}-1\right)\log_2 \frac{L}{\lceil \frac{L}{\xi} \rceil}+\frac{\alpha}{2}(\epsilon_L - \epsilon_{\lceil \frac{L}{\xi} \rceil})\log_2 e\right)$ for $L > \xi$.

With distributed BS antennas, the cluster size N_c is a crucial parameter that determines the system performance. For given total number of BS antennas M, an

increase in N_c leads to fewer BS antenna clusters, and thus a larger minimum access distance. Fig. 3.5b shows that for given ξ, or $\frac{M}{N}$ in the finite case, the average ergodic capacities monotonically increase with the number of BS antenna clusters L, indicating that a smaller cluster size leads to a higher capacity regardless of whether CSIT is available or not. We can then conclude from Fig. 3.5b that to maximize the average ergodic capacity, the BS antennas should be fully distributed in the cell, i.e., with the cluster size $N_c = 1$.

3.4.3 Comparison of CA and DA Layouts

For the sake of comparison, Fig. 3.6 further presents the average ergodic capacities with both the CA and the DA layouts. For the DA layout, with a fixed ratio β, (3.42) and (3.43) indicate that the asymptotic lower-bounds of the average ergodic capacity without and with CSIT have the scaling orders of $\Theta\left(\left(\frac{\alpha}{2}-1\right)\log_2\xi\right)$ and $\Theta\left(\frac{\alpha}{2}\log_2\xi\right)$, respectively, which are higher than that with the CA layout, i.e., $\bar{\mathcal{R}}^{S-o-C} = \Theta(1)$ and $\bar{\mathcal{R}}^{S-w-C} = \Theta(\log_2\xi)$. Simulation results verify the analysis. As we can see from Fig. 3.6, a higher scaling order can always be achieved with the DA layout regardless of whether CSIT is available or not. Thanks to the reduced minimum access distance, substantial capacity gains can be achieved with the DA layout when the number of BS antennas is large.

3.5 Summary

In this chapter, we present an asymptotic analysis on the average ergodic capacity of downlink single-user MIMO systems with the CA and DA layouts. By assuming that the user's position follows the uniform distribution in the inscribed circle of Cell 0, and the number of BS antennas M and the number of user antennas N go to infinity with $M/N \to \xi \gg 1$, explicit expressions for the asymptotic average ergodic capacities with and without CSIT with the CA layout are derived, and shown to be accurate. With the DA layout, asymptotic lower-bounds of the average ergodic capacities with and without CSIT are developed as functions of the number of BS antenna clusters L and the ratio β of the number of user antennas N to the number of BS antennas at each cluster N_c. Simulation results verify that the average ergodic capacities with and without CSIT in the DA case have the same scaling orders as their asymptotic lower-bounds.

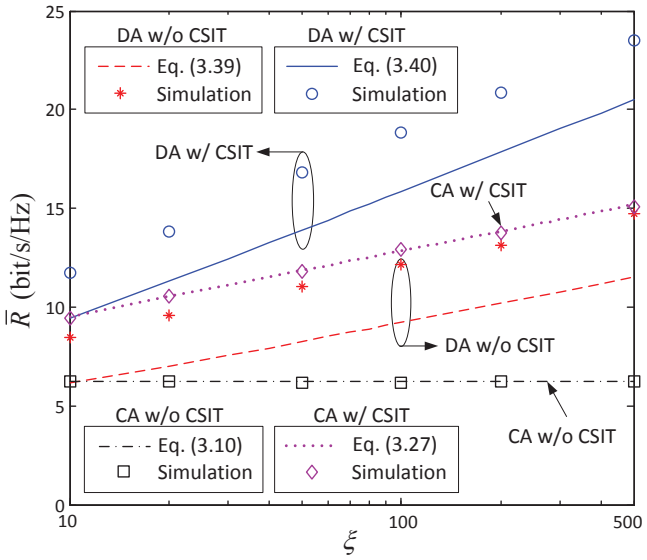

FIGURE 3.6: Average ergodic capacities without and with CSIT versus the ratio ξ of the number of BS antennas M to the number of user antennas N with the CA and DA layouts in the single-user case. $\beta = 2$. $N = 4$. $\bar{P}_k/N_0 = 10$dB. $\alpha = 4$.

The analysis reveals that when the ratio β of the number of user antennas N to the number of BS antennas at each cluster N_c is fixed, the average ergodic capacities without and with CSIT in the DA case scale with the ratio ξ of the number of BS antennas M to the number of user antennas N in the orders of $\Theta\left(\left(\frac{\alpha}{2}-1\right)\log_2\xi\right)$ and $\Theta\left(\frac{\alpha}{2}\log_2\xi\right)$, respectively, where $\alpha > 2$ is the path-loss factor. Both of them are shown to be higher than the scaling orders of the average ergodic capacities with the CA layout, which are found to be $\Theta(1)$ and $\Theta\left(\log_2\xi\right)$ for the cases without and with CSIT, respectively. Substantial capacity gains can be achieved with the DA layout when the number of BS antennas is large.

If the ratio ξ is fixed, the average ergodic capacities without and with CSIT in the DA case monotonically increase with the number of BS antenna clusters L at a decreasing rate, which indicates that for given amount of BS antennas, a fully distributed BS antenna layout, i.e., with the cluster size $N_c = 1$, achieves the highest average ergodic capacity regardless of whether CSIT is available or not.

Chapter 4

Asymptotic Average Ergodic Rate of Multi-User Single-Cell MIMO

In this chapter, the asymptotic analysis is extended to a multi-user single-cell MIMO system, and the effect of different precoding schemes on the scaling behavior of the average ergodic rate is further discussed. This chapter is organized as follows. Section 4.1 presents a literature review on previous related work. The ergodic rates with two representative linear precoding schemes, singular-value-decomposition (SVD) and block-diagonalization (BD), are analyzed in Section 4.2. The asymptotic average ergodic rates with SVD and BD are characterized in Section 4.3 and Section 4.4, respectively. The scaling behavior is discussed in Section 4.5 and verified by simulation results presented in Section 4.6. Section 4.7 summarizes this chapter.

4.1 Literature Review

In a multi-user MIMO system, precoding is usually adopted at the BS side as the users are typically unable to coordinate with each other. The downlink rate performance of each user is thus crucially determined by the precoding strategy.

For MIMO Gaussian downlink channels, the sum capacity has been extensively studied in [27, 28, 30, 31], and the capacity region was characterized in [32], which showed that the optimum precoding is a pre-interference-cancelation strategy known as dirty-paper coding (DPC)[33]. Despite the information-theoretical optimality, it is difficult to implement the idea of DPC in practice. A number of linear [30, 34–46] and non-linear precoding schemes [47–49] were, therefore, proposed to approach the sum capacity with manageable complexity (see [50] for a comprehensive overview). Among them, the singular-value-decomposition (SVD) [10] and block-diagonalization (BD) [41] are two representative non-orthogonal and orthogonal linear precoding schemes, respectively.

Although these precoding schemes are originally proposed for conventional multi-user MIMO systems with co-located BS antennas, they can be applied to that with distributed BS antennas in a straightforward manner. With BS antennas grouped into geographically distributed clusters, however, the downlink rate performance becomes closely dependent on the positions of BS antenna clusters. When the numbers of BS antennas and users are large, it is increasingly difficult to characterize the average rate performance. Therefore, most studies have focused on a regular BS antenna layout with a small number of BS antenna clusters for computational tractability [52–56]. In this chapter, asymptotic bounds will be developed to study the scaling behavior of the average ergodic rate when the number of BS antenna clusters and the number of users are large.

Specifically, we focus on a K-user single-cell MIMO system with two representative linear precoding schemes: SVD and BD. By assuming that the number of BS antennas M and the number of user antennas N go to infinity with $M/N \to \xi K \gg 1$, explicit expressions for the asymptotic average ergodic rates with the CA layout are derived. For the DA layout, asymptotic bounds are developed to characterize the scaling behavior of the average ergodic rate.

4.2 Ergodic Rate

In this chapter, we assume that K users are uniformly distributed in the inscribed circle of Cell 0, and the BS has full CSI of all K users. (2.6) is then reduced to

$$R_k^{MU}=\frac{1}{N}\mathbb{E}_{\mathbf{H}_{k,\mathcal{B}_0}}\left[\log_2\det\left(\mathbf{I}_N+\frac{\bar{P}_k\|\boldsymbol{\gamma}_{k,\mathcal{B}_0}\|^2\tilde{\mathbf{G}}_{k,\mathcal{B}_0}\mathbf{W}_k\mathbf{W}_k^\dagger\tilde{\mathbf{G}}_{k,\mathcal{B}_0}^\dagger}{N_0\mathbf{I}_N+\mathbf{Q}_k^{intra}}\right)\right], \tag{4.1}$$

where $\mathbf{Q}_k^{intra}$ is the covariance matrix of the intra-cell interference. If the precoding matrix $\mathbf{W}_j$ is independent of the normalized channel gain matrix $\tilde{\mathbf{G}}_{k,\mathcal{B}_0}$ from BS 0 to user k, for $j\in\mathcal{K}_0$ and $j\neq k$, Appendix C shows that the covariance matrix of the intra-cell interference can be obtained as

$$\mathbf{Q}_k^{intra}=\sum_{m\in\mathcal{B}_0}\sum_{j\in\mathcal{K}_0,j\neq k}|\gamma_{k,m}|^2\sum_{n=1}^{N}\mathbb{E}\left[|w_{m,n}^j|^2\right]\bar{P}_j\mathbf{I}_N, \tag{4.2}$$

where $w_{m,n}^j$ denotes the entry at the m-th row and n-th column of $\mathbf{W}_j$.

In this chapter, we assume that the number of BS antennas at each cluster N_c equals the number of user antennas N. As the ergodic rate is closely dependent on the precoding matrix $\mathbf{W}_k$, we first derive the ergodic rates with two representative precoding schemes: SVD and BD.

4.2.1 SVD

SVD is a classic capacity-achieving method in single-user MIMO systems with CSIT [10]. In particular, for user $k\in\mathcal{K}_0$, the precoding matrix $\mathbf{W}_k^{SVD}$ can be obtained from (3.19-3.23). It is clear that for user $j\in\mathcal{K}_0$, its precoding matrix $\mathbf{W}_j^{SVD}$ is only determined by its own normalized channel gain matrix $\tilde{\mathbf{G}}_{j,\mathcal{K}_0}$. By combining (4.1-4.2) and (3.19-3.23), the ergodic rate of user k with SVD in a multi-user single-cell MIMO system can be obtained as

$$R_k^{MU-SVD}=\frac{1}{N}\mathbb{E}_{\mathbf{H}_{k,\mathcal{B}_0}}\left[\log_2\det\left(\mathbf{I}_N+\mu_k^{MU-SVD}\boldsymbol{\Lambda}_{k,\mathcal{B}_0}\boldsymbol{\Omega}_k\boldsymbol{\Omega}_k^\dagger\boldsymbol{\Lambda}_{k,\mathcal{B}_0}^\dagger\right)\right], \tag{4.3}$$

where the average received signal-to-interference-plus-noise ratio (SINR) μ_k^{MU-SVD} is given by

$$\mu_k^{MU-SVD} = \frac{\bar{P}_k \|\boldsymbol{\gamma}_{k,\mathcal{B}_0}\|^2}{N_0 + \sum_{j\in\mathcal{K}_0, j\neq k} \sum_{m=1}^{M} |\gamma_{k,m}|^2 \sum_{n=1}^{N} \mathbb{E}\left[|w_{m,n}^j|^2\right] \bar{P}_j}. \tag{4.4}$$

4.2.2 BD

BD is a representative orthogonal linear precoding scheme. With BD, an intra-cell-interference-free block channel is obtained by projecting the desired signal to the null space of the channel gain matrices of the intra-cell users, and then decomposed to several parallel sub-channels. It requires that the number of BS antennas M is no smaller than the total number of user antennas KN. [41] shows that for user $k \in \mathcal{K}_0$, its precoding matrix $\mathbf{W}_k^{BD}$ can be obtained by an SVD-based method. In particular, for user $k \in \mathcal{K}_0$, define $\mathbf{X}_{k,\mathcal{B}_0}$ as

$$\mathbf{X}_{k,\mathcal{B}_0} = \left[\tilde{\mathbf{G}}_{1,\mathcal{B}_0}^T, \cdots, \tilde{\mathbf{G}}_{k-1,\mathcal{B}_0}^T, \tilde{\mathbf{G}}_{k+1,\mathcal{B}_0}^T, \cdots, \tilde{\mathbf{G}}_{K,\mathcal{B}_0}^T\right]^T, \tag{4.5}$$

and denote its SVD as

$$\mathbf{X}_{k,\mathcal{B}_0} = \hat{\mathbf{U}}_{k,\mathcal{B}_0} \hat{\mathbf{\Lambda}}_{k,\mathcal{B}_0} \left[\hat{\mathbf{V}}_{k,\mathcal{B}_0}^{(1)}, \hat{\mathbf{V}}_{k,\mathcal{B}_0}^{(0)}\right]^\dagger, \tag{4.6}$$

where $\hat{\mathbf{V}}_{k,\mathcal{B}_0}^{(1)}$ holds the first $(K-1)N$ right singular vectors and $\hat{\mathbf{V}}_{k,\mathcal{B}_0}^{(0)}$ holds the rest. $\hat{\mathbf{V}}_{k,\mathcal{B}_0}^{(0)}$ corresponds to zero singular values and forms an orthogonal basis for the null space of $\mathbf{X}_{k,\mathcal{B}_0}$. Let $\tilde{\mathbf{X}}_{k,\mathcal{B}_0} = \tilde{\mathbf{G}}_{k,\mathcal{B}_0} \hat{\mathbf{V}}_{k,\mathcal{B}_0}^{(0)}$, and denote its SVD as

$$\tilde{\mathbf{X}}_{k,\mathcal{B}_0} = \tilde{\mathbf{U}}_{k,\mathcal{B}_0} \tilde{\mathbf{\Lambda}}_{k,\mathcal{B}_0} \tilde{\mathbf{V}}_{k,\mathcal{B}_0}^\dagger, \tag{4.7}$$

where $\tilde{\mathbf{\Lambda}}_{k,\mathcal{B}_0} = \left[\text{diag}\left(\sqrt{\tilde{\lambda}_1}, \sqrt{\tilde{\lambda}_2}, \ldots, \sqrt{\tilde{\lambda}_N}\right), \mathbf{0}_{N\times(M-KN)}\right]$ is composed by eigenvalues $\{\tilde{\lambda}_n\}$ of $\tilde{\mathbf{X}}_{k,\mathcal{B}_0} \tilde{\mathbf{X}}_{k,\mathcal{B}_0}^\dagger$. The precoding matrix of user k with BD can be written as

$$\mathbf{W}_k^{BD} = \hat{\mathbf{V}}_{k,\mathcal{B}_0}^{(0)} \tilde{\mathbf{V}}_{k,\mathcal{B}_0} \tilde{\mathbf{\Omega}}_k, \tag{4.8}$$

where $\tilde{\mathbf{\Omega}}_k$ denotes the power distribution of the N parallel sub-channels, which is given by

$$\tilde{\mathbf{\Omega}}_k = \left[\text{diag}\left(\sqrt{\frac{P_k(\tilde{\lambda}_1)}{\bar{P}_k \|\boldsymbol{\gamma}_{k,\mathcal{B}_0}\|^2}}, \sqrt{\frac{P_k(\tilde{\lambda}_2)}{\bar{P}_k \|\boldsymbol{\gamma}_{k,\mathcal{B}_0}\|^2}}, \cdots, \sqrt{\frac{P_k(\tilde{\lambda}_N)}{\bar{P}_k \|\boldsymbol{\gamma}_{k,\mathcal{B}_0}\|^2}} \right), \mathbf{0}_{N \times M-KN} \right]^T, \tag{4.9}$$

with $\{P_k(\tilde{\lambda}_n)\}$ denoting the water-filling power allocation, i.e.,

$$P_k(\tilde{\lambda}_n) = \left(\tilde{\zeta} - \frac{N_0}{\tilde{\lambda}_n} \right)^+, \tag{4.10}$$

where $\tilde{\zeta}$ is chosen to satisfy

$$\sum_{n=1}^{N} P_k(\tilde{\lambda}_n) = \bar{P}_k \|\boldsymbol{\gamma}_{k,\mathcal{B}_0}\|^2. \tag{4.11}$$

With BD, the intra-cell interference $\mathbf{u}_k^{intra} = \mathbf{0}$ as $\tilde{\mathbf{G}}_{k,\mathcal{B}_0} \mathbf{W}_j^{BD} = \mathbf{0}$ for all $j \in \mathcal{K}_0$ and $j \neq k$. By combining (4.1) and (4.7-4.11), the ergodic rate with BD in a multi-user single-cell MIMO system can be obtained as

$$R_k^{MU-BD} = \frac{1}{N} \mathbb{E}_{\mathbf{H}_{k,\mathcal{B}_0}} \left[\log_2 \det \left(\mathbf{I}_N + \mu_k^{MU-BD} \tilde{\mathbf{\Lambda}}_{k,\mathcal{B}_0} \tilde{\mathbf{\Omega}}_k \tilde{\mathbf{\Omega}}_k^\dagger \tilde{\mathbf{\Lambda}}_{k,\mathcal{B}_0}^\dagger \right) \right], \tag{4.12}$$

where the average received SNR μ_k^{MU-BD} is given by

$$\mu_k^{MU-BD} = \frac{\bar{P}_k \|\boldsymbol{\gamma}_{k,\mathcal{B}_0}\|^2}{N_0}. \tag{4.13}$$

Note from (4.3) and (4.12) that the ergodic rates with SVD and BD are both dependent on $\bar{P}_k$. In this chapter, we assume that the total transmit power P_t is equally divided over K users, i.e.,

$$\bar{P}_k = \frac{1}{K} P_t. \tag{4.14}$$

With equal power allocation, the average received SINR with SVD μ_k^{MU-SVD} and the average received SNR with BD μ_k^{MU-BD} can be then obtained by substituting

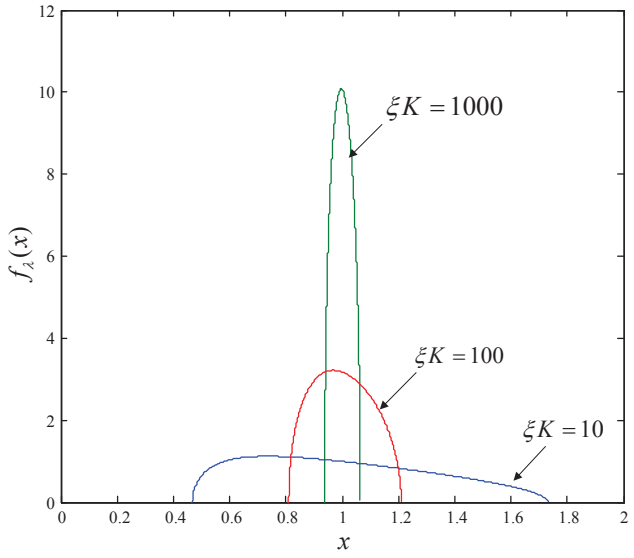

FIGURE 4.1: Empirical eigenvalue distribution (4.18) of $\tilde{\mathbf{G}}^C_{k,\mathcal{B}_0}\left(\tilde{\mathbf{G}}^C_{k,\mathcal{B}_0}\right)^\dagger \sim \mathcal{W}_N(M, \frac{1}{M}\mathbf{I}_N)$ as $M, N \to \infty$ with $M/N \to \xi K \geq 1$.

(4.14) into (4.4) and (4.13) as

$$\mu_k^{MU-SVD} = \frac{\|\boldsymbol{\gamma}_{k,\mathcal{B}_0}\|^2}{\frac{KN_0}{P_t} + \sum_{j\in\mathcal{K}_0, j\neq k}\sum_{m=1}^{M}|\gamma_{k,m}|^2\sum_{n=1}^{N}\mathbb{E}\left[|w_{m,n}^j|^2\right]}, \tag{4.15}$$

and

$$\mu_k^{MU-BD} = \frac{P_t\|\boldsymbol{\gamma}_{k,\mathcal{B}_0}\|^2}{KN_0}, \tag{4.16}$$

respectively.

In the following of this chapter, an asymptotic analysis on the average ergodic rates with SVD and BD will be presented by assuming that the number of BS antennas M and the number of user antennas N go to infinity with $M/N \to \xi K \gg 1$. With the DA layout, as the BS antennas are grouped into L clusters with N antennas at each cluster, the asymptotic assumption reduces to $N \to \infty$. In the next section, we will first focus on the asymptotic average ergodic rate with SVD.

4.3 Asymptotic Average Rate with SVD

4.3.1 CA Layout

With the CA layout, the average received SINR of user k can be obtained by combining (4.15) and (2.10) as

$$\mu_k^{MU-SVD-C} = \frac{M\rho_k^{-\alpha}}{\frac{KN_0}{P_t} + (K-1)\rho_k^{-\alpha}} \approx \frac{M}{K-1}, \tag{4.17}$$

for large $\frac{P_t}{N_0} \gg 1$.

Moreover, with the CA layout, the normalized channel gain matrix $\tilde{\mathbf{G}}_{k,\mathcal{B}_0}^C = \sqrt{\frac{1}{M}}\mathbf{H}_{k,\mathcal{B}_0}$. According to the Marcenko-Pastur law [64], as $M, N \to \infty$ and $M/N \to \xi K \geq 1$, the empirical eigenvalue distribution of $\tilde{\mathbf{G}}_{k,\mathcal{B}_0}^C \left(\tilde{\mathbf{G}}_{k,\mathcal{B}_0}^C\right)^\dagger \sim \mathcal{W}_N(M, \frac{1}{M}\mathbf{I}_N)$ converges almost surely to the following distribution:

$$f_\lambda(x) = \begin{cases} \frac{1}{2\pi x}\sqrt{(x_+ - \xi K x)(\xi K x - x_-)} & \text{if } \frac{1}{\xi K}x_- \leq x \leq \frac{1}{\xi K}x_+ \\ 0 & \text{otherwise,} \end{cases} \tag{4.18}$$

where $x_+ = \left(\sqrt{\xi K}+1\right)^2$ and $x_- = \left(\sqrt{\xi K}-1\right)^2$. As we can see from Fig. 4.1, as ξK grows, the eigenvalues of $\tilde{\mathbf{G}}_{k,\mathcal{B}_0}^C \left(\tilde{\mathbf{G}}_{k,\mathcal{B}_0}^C\right)^\dagger$ become increasingly deterministic, and eventually converge to $\mathbb{E}[\lambda] = 1$. As a result, we have

$$\mathbf{\Lambda}_{k,\mathcal{B}_0}^C \approx \left[\mathbf{I}_N, \mathbf{0}_{N\times(M-N)}\right], \tag{4.19}$$

for large $\xi K \gg 1$. By combining (3.21-3.23), (4.3), (4.17), and (4.19), the asymptotic ergodic rate of user k with SVD in the CA layout as $M, N \to \infty$ and $M/N \to \xi K \gg 1$ can be obtained as

$$\mathcal{R}_k^{MU-SVD-C} \approx \log_2(1+\xi), \tag{4.20}$$

for large $\frac{P_t}{N_0} \gg 1$ and $K \gg 1$. (4.20) indicates that the asymptotic ergodic rate with the CA layout does not vary with the position of user k. As a result, the asymptotic average ergodic rate can be then written as

$$\bar{\mathcal{R}}^{MU-SVD-C} = \mathcal{R}_k^{MU-SVD-C} \approx \log_2(1+\xi). \tag{4.21}$$

4.3.2 DA Layout

With the DA layout, as both the eigenvalue distribution of $\tilde{\mathbf{G}}^D_{k,\mathcal{B}_0}\left(\tilde{\mathbf{G}}^D_{k,\mathcal{B}_0}\right)^\dagger$ and the average received SINR $\mu_k^{MU-SVD-D}$ vary with the positions of users and BS antenna clusters, it is difficult to characterize the average ergodic rate. As a result, we resort to an asymptotic bound to study its scaling behavior.

In particular, with a large number of BS antenna clusters $L \gg 1$, each user $k \in \mathcal{K}_0$ is close to some antenna cluster l_k^*, such that the large-scale fading coefficient $d_{k,l_k^*,0}^{-\alpha} \gg d_{k,l,0}^{-\alpha}$ if $l \neq l_k^*$. In this case, $\|\gamma_{k,\mathcal{B}_0}\|^2 \approx d_{k,l_k^*,0}^{-\alpha} \gg 1$. According to (3.21-3.23), with $\frac{\bar{P}_k}{N_0}\|\gamma_{k,\mathcal{B}_0}\|^2 \gg 1$, the waterfilling power allocation can be approximated by equal power allocation over N sub-channels, i.e.,

$$\mathbf{\Omega}_k^D \approx \sqrt{\frac{1}{N}}\left[\mathbf{I}_N, \mathbf{0}_{N\times M-KN}\right]^T, \tag{4.22}$$

On the other hand, with $\|\gamma_{k,\mathcal{B}_0}\|^2 \approx d_{k,l_k^*,0}^{-\alpha}$, the normalized large-scale fading matrix can be approximated by

$$\mathbf{B}^D_{k,\mathcal{B}_0} \approx \sqrt{\frac{1}{N}}\left[\mathbf{0}_{N\times N(l_k^*-1)}, \mathbf{1}_{N\times N}, \mathbf{0}_{N\times N(L-l_k^*)}\right], \tag{4.23}$$

according to (2.8). The normalized channel gain matrix with the DA layout $\tilde{\mathbf{G}}^D_{k,\mathcal{B}_0}$ can be then written as

$$\tilde{\mathbf{G}}^D_{k,\mathcal{B}_0} \approx \sqrt{\frac{1}{N}}\left[\mathbf{0}_{N\times N(l_k^*-1)}, \mathbf{H}^{(1)}_{k,0}, \mathbf{0}_{N\times N(L-l_k^*)}\right], \tag{4.24}$$

where $\mathbf{H}^{(1)}_{k,0} \in \mathbb{C}^{N\times N}$ denotes the small-scale fading matrix between user k and its closest BS antenna cluster, i.e., $\mathcal{L}^0_{l_k^*}$. As $N \to \infty$, the empirical distribution of the eigenvalues of $\tilde{\mathbf{G}}^D_{k,\mathcal{B}_0}\left(\tilde{\mathbf{G}}^D_{k,\mathcal{B}_0}\right)^\dagger \approx \frac{1}{N}\mathbf{H}^{(1)}_{k,0}\left(\mathbf{H}^{(1)}_{k,0}\right)^\dagger \sim \mathcal{W}_N\left(N, \frac{1}{N}\mathbf{I}_N\right)$ converges to the following distribution [64]:

$$f_\lambda(x) = \begin{cases} \frac{1}{2\pi x}\sqrt{4x-x^2} & \text{if } 0 \leq x \leq 4 \\ 0 & \text{otherwise.} \end{cases} \tag{4.25}$$

By combining (4.22-4.25) and (4.3), the asymptotic ergodic rate with SVD in the DA layout as $N \to \infty$ can be then obtained as

$$\mathcal{R}_k^{MU-SVD-D} \approx \Phi\left(\bar{\mu}_k^{MU-SVD-D}\right), \tag{4.26}$$

with

$$\Phi(x) = 2\log_2\left(\frac{1+\sqrt{1+4x}}{2}\right) - \frac{\log_2 e}{4x}\left(\sqrt{1+4x}-1\right)^2, \tag{4.27}$$

where the normalized average received SINR $\bar{\mu}_k^{MU-SVD-D}$ is given by

$$\begin{aligned}\bar{\mu}_k^{MU-SVD-D} &= \frac{1}{N}\mu_k^{MU-SVD-D} \\ &\overset{L\gg 1}{\approx} \frac{d_{k,l_k^*,0}^{-\alpha}}{\frac{KN_0}{P_t} + \sum_{j\in\mathcal{K}_0, j\neq k} d_{j,l_j^*,0}^{-\alpha}} \\ &\overset{\frac{P_t}{N_0}\gg 1}{\approx} \frac{d_{k,l_k^*,0}^{-\alpha}}{\sum_{j\in\mathcal{K}_0, j\neq k} d_{j,l_j^*,0}^{-\alpha}},\end{aligned} \tag{4.28}$$

by substituting $\|\gamma_{j,\mathcal{B}_0}\|^2 \approx d_{j,l_j^*,0}^{-\alpha}$ into (4.15), for $j \in \mathcal{K}_0$. Let us write $\bar{\mu}_k^{MU-SVD-D}$ as

$$\begin{aligned}\bar{\mu}_k^{MU-SVD-D} &= \frac{d_{k,l_k^*,0}^{-\alpha}}{\sum_{j\neq k, l_j^*=l_k^*} d_{k,l_j^*,0}^{-\alpha} + \sum_{j\neq k, l_j^*\neq l_k^*} d_{k,l_j^*,0}^{-\alpha}} \\ &= \frac{1}{m_k + \sum_{j\neq k, l_j^*\neq l_k^*}\left(\frac{d_{k,l_j^*,0}}{d_{k,l_k^*,0}}\right)^{-\alpha}},\end{aligned} \tag{4.29}$$

where m_k denotes the number of interfering users whose closest BS antenna cluster is the same as user k's, i.e., $l_j^* = l_k^*$ for $j,k \in \mathcal{K}_0$ and $j \neq k$. With a large number of BS antenna clusters, the distance from each user $j \in \mathcal{K}_0$ to its closest BS antenna cluster l_j^* is very small such that $d_{k,l_j^*,0} \approx d_{k,j,\mathcal{K}_0}$, where $d_{k,j,\mathcal{K}_0}$ denotes the distance between user k and user $j \in \mathcal{K}_0$. We can then obtain an upper-bound of $\bar{\mu}_k^{MU-SVD-D}$ as

$$\bar{\mu}_k^{MU-SVD-D} \leq \bar{\mu}_{k,ub}^{MU-SVD-D} = \begin{cases} \frac{1}{m_k} & \text{if } m_k \neq 0 \\ Y^\alpha & \text{otherwise,}\end{cases} \tag{4.30}$$

where $Y = \frac{d_{k,\mathcal{K}_0}^{(1)}}{d_{k,0}^{(1)}}$, with $d_{k,0}^{(1)}$ and $d_{k,\mathcal{K}_0}^{(1)}$ denoting the distances from user k to the closest BS antenna cluster in Cell 0 and to the closest user among the other $K-1$ users in Cell 0, respectively. An asymptotic upper-bound of the average ergodic rate with the DA layout can be then obtained by combining (4.26) and (4.30) as

$$\mathcal{R}_k^{MU-SVD-D} \leq \mathcal{R}_{k,ub}^{MU-SVD-D} = \begin{cases} \Phi\left(\frac{1}{m_k}\right) & \text{if } m_k \neq 0 \\ \Phi\left(Y^\alpha\right) & \text{otherwise.}\end{cases} \tag{4.31}$$

It is clear from (4.31) that the asymptotic upper-bound of the ergodic rate $\mathcal{R}_{k,ub}^{M-SVD-D}$ is dependent on m_k and Y, which varies with the positions of users and BS antenna clusters. By combining (2.20) and (4.31), an asymptotic upper-bound of the average ergodic rate with the DA layout can be obtained as

$$\bar{\mathcal{R}}_{ub}^{MU-SVD-D} = \int_0^\infty \Phi(y^\alpha) f_Y(y) dy \cdot \Pr\{m_k = 0\} + \sum_{n=1}^{K-1} \Phi\left(\frac{1}{n}\right) \Pr\{m_k = n\}. \tag{4.32}$$

[65] shows that the pdf of $Y = \frac{d_{k,\mathcal{K}_0}^{(1)}}{d_{k,0}^{(1)}}$ can be obtained as

$$f_Y(y) \approx \frac{2\xi y}{(\xi + y^2)^2}, \tag{4.33}$$

for $L, K \gg 1$, where ξ equals the ratio of the number of BS antenna clusters L to the number of users K. With L uniformly distributed BS antennas, m_k follows the binomial distribution with parameters $K-1$ and $1/L$. For large $L, K \gg 1$, by noting that $\xi = \frac{L}{K}$, the distribution of m_k can be approximated as a Poisson distribution with parameter $\frac{1}{\xi}$:

$$\Pr\{m_k = n\} \approx \frac{\xi^{-n} e^{-1/\xi}}{n!}, \tag{4.34}$$

$n = 1, 2, \cdots, K-1$. By combining (4.32-4.34), the asymptotic upper-bound of the average ergodic rate with the DA layout can be then obtained as

$$\bar{\mathcal{R}}_{ub}^{MU-SVD-D} \approx \sum_{n=1}^{K-1} \Phi\left(\frac{1}{n}\right) \cdot \frac{\xi^{-n} e^{-\xi}}{n!} + e^{-1/\xi} \cdot \int_0^\infty \Phi(y^\alpha) \cdot \frac{2\xi y}{(\xi + y^2)^2} dy. \tag{4.35}$$

4.4 Asymptotic Average Rate with BD

4.4.1 CA Layout

With the CA layout, as the BS antennas are co-located at the center of the cell, by combining (4.16) and (2.10), we have

$$\mu_k^{MU-BD-C} = \frac{M P_t \rho_k^{-\alpha}}{K N_0}. \tag{4.36}$$

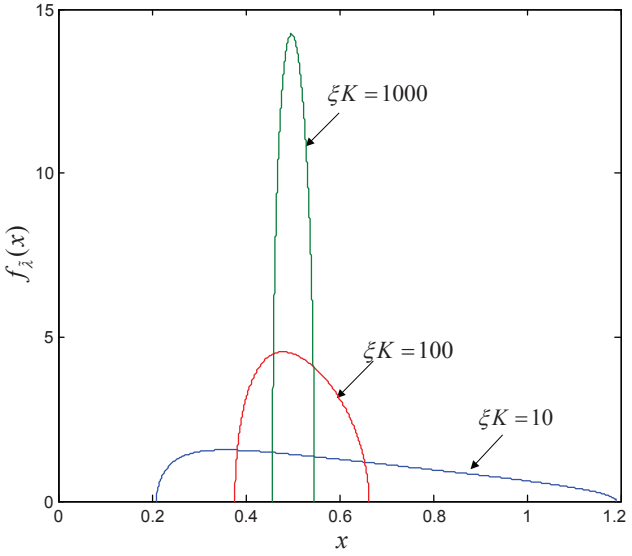

FIGURE 4.2: Empirical eigenvalue distribution (4.37) of $\tilde{\mathbf{X}}^C_{k,\mathcal{B}_0}\left(\tilde{\mathbf{X}}^C_{k,\mathcal{B}_0}\right)^\dagger \sim \mathcal{W}_N\left(M-(K-1)N, \frac{1}{M}\mathbf{I}_N\right)$ as $M, N \to \infty$ with $M/N \to \xi K \geq 1$.

As $M, N \to \infty$ and $M/N \to \xi K \geq 1$, the empirical eigenvalue distribution of $\tilde{\mathbf{X}}^C_{k,\mathcal{B}_0}\left(\tilde{\mathbf{X}}^C_{k,\mathcal{B}_0}\right)^\dagger \sim \mathcal{W}_N\left(M-(K-1)N, \frac{1}{M}\mathbf{I}_N\right)$ converges almost surely to the following distribution [64]:

$$f_{\tilde{\lambda}}(x) = \begin{cases} \frac{1}{2\pi x}\sqrt{(\tilde{x}_+ - \xi K x)(\xi K x - \tilde{x}_-)} & \text{if } \frac{1}{\xi K}\tilde{x}_- \leq x \leq \frac{1}{\xi K}\tilde{x}_+ \\ 0 & \text{otherwise,} \end{cases} \tag{4.37}$$

where $\tilde{x}_+ = \left(\sqrt{\xi K - K + 1} + 1\right)^2$ and $\tilde{x}_- = \left(\sqrt{\xi K - K + 1} - 1\right)^2$. As Fig. 4.2 shows, as ξK grows, the eigenvalues of $\tilde{\mathbf{X}}^C_{k,\mathcal{B}_0}\left(\tilde{\mathbf{X}}^C_{k,\mathcal{B}_0}\right)^\dagger$ become increasingly deterministic, and eventually converge to $\mathbb{E}[\tilde{\lambda}] = 1 - \frac{K-1}{\xi K}$. As a result, we have

$$\tilde{\mathbf{\Lambda}}^C_{k,\mathcal{B}_0} \approx \left[\sqrt{1 - \tfrac{K-1}{\xi K}}\mathbf{I}_N, \mathbf{0}_{N\times(M-KN)}\right], \tag{4.38}$$

for large $\xi K \gg 1$. By combining (4.9-4.12), (4.36), and (4.38), the asymptotic ergodic rate of user k with the CA layout can be obtained as

$$\mathcal{R}_k^{MU-BD-C} \approx \log_2\left(1 + \left(\xi - 1 + \frac{1}{K}\right)\cdot\frac{P_t}{N_0}\rho_k^{-\alpha}\right). \tag{4.39}$$

As $\mathcal{R}_k^{MU-BD-C}$ varies with the radial coordinate ρ_k of user k, by combining (4.39) and (2.21), the asymptotic average ergodic rate with the CA layout can be

further obtained as

$$\bar{\mathcal{R}}^{MU-BD-C} \approx \int_0^1 \log_2\left(1+\left(\xi-1+\frac{1}{K}\right)\cdot\frac{P_t}{N_0}x^{-\alpha}\right) f_{\rho_k}(x)dx, \tag{4.40}$$

where $f_{\rho_k}(x) = 2x$ is the pdf of the radial coordinate of user k. For large $\frac{\bar{P}_k}{N_0} \gg 1$ and $K \gg 1$, we have

$$\bar{\mathcal{R}}^{MU-BD-C} \approx \log_2\frac{P_t}{N_0} + \frac{\alpha}{\ln 4} + \log_2(\xi-1). \tag{4.41}$$

4.4.2 DA Layout

With the DA layout, the BS antennas are grouped into uniformly distributed clusters with N antennas at each cluster. As it is difficult to characterize the asymptotic average ergodic rate, similar to the single-user case, we resort to a lower-bound to study its scaling behavior.

Specifically, Appendix D shows that with $L \gg K$, the ergodic rate with the DA layout $R_k^{MU-BD-D}$ is lower-bounded by

$$R_{k,lb}^{MU-BD-D} = \frac{1}{N}\mathbb{E}_{\tilde{\mathbf{H}}_{k,0}^{(1)}}\left[\log_2\det\left(\mathbf{I}_N + \frac{1}{N}\frac{\bar{P}_k}{N_0}\left(\tilde{d}_{k,0}^{(1)}\right)^{-\alpha}\tilde{\mathbf{H}}_{k,0}^{(1)}\left(\tilde{\mathbf{H}}_{k,0}^{(1)}\right)^{\dagger}\right)\right], \tag{4.42}$$

where $\tilde{d}_{k,0}^{(1)}$ denotes the minimum access distance from user $k \in \mathcal{K}_0$ to $L-K+1$ BS antenna clusters which are uniformly distributed in the inscribed circle of Cell 0. $\tilde{\mathbf{H}}_{k,0}^{(1)} \in \mathbb{C}^{N\times N}$ denotes the corresponding small-scale fading matrix. As $N \to \infty$, the empirical eigenvalue distribution of $\frac{1}{N}\tilde{\mathbf{H}}_{k,0}^{(1)}\left(\tilde{\mathbf{H}}_{k,0}^{(1)}\right)^{\dagger} \sim \mathcal{W}_N\left(N, \frac{1}{N}\mathbf{I}_N\right)$ converges almost surely to the distribution given in (4.25). By combining (4.14), (4.25), and (4.42), the asymptotic lower-bound of the ergodic rate with the DA layout as $N \to \infty$ can be obtained as

$$\mathcal{R}_{k,lb}^{MU-BD-D} = \Phi\left(\frac{P_t}{N_0}\cdot\frac{\left(\tilde{d}_{k,0}^{(1)}\right)^{-\alpha}}{K}\right), \tag{4.43}$$

where $\Phi(x)$ is given in (4.27), which can be approximated as

$$\Phi(x) \approx \log_2 x - \log_2 e, \tag{4.44}$$

for large $x \gg 1$. With $L \gg K$, the minimum access distance $\tilde{d}_{k,0}^{(1)} \ll 1$. The asymptotic lower-bound of the average ergodic rate with the DA layout can be then obtained by combining (4.43-4.44) as

$$\mathcal{R}_{k,lb}^{MU-BD-D} \approx \log_2 \left(\frac{P_t}{N_0} \cdot \frac{\left(\tilde{d}_{k,0}^{(1)}\right)^{-\alpha}}{K} \right) - \log_2 e. \tag{4.45}$$

By combining (4.45) and (2.19), the asymptotic lower-bound of the average ergodic rate with the DA layout can be then obtain as

$$\bar{\mathcal{R}}_{lb}^{MU-BD-D} \approx \int_0^1 \int_0^{1+y} \log_2 \left(\frac{x^{-\alpha}}{K} \right) f_{\tilde{d}_{k,0}^{(1)}|\rho_k}(x|y) f_{\rho_k}(y) dx dy + \log_2 \left(\frac{P_t}{N_0} \right) - \log_2 e, \tag{4.46}$$

where $f_{\rho_k}(y) = 2y$ is the pdf of the radial coordinate of user k. $f_{\tilde{d}_{k,0}^{(1)}|\rho_k}(x|y)$ denotes the conditional pdf of $\tilde{d}_{k,0}^{(1)}$ given user k's position at (ρ_k, θ_k). Recall that $\tilde{d}_{k,0}^{(1)}$ is the minimum access distance from user k to $L-K+1$ uniformly distributed BS antenna clusters in Cell 0. It can be easily obtained that

$$f_{\tilde{d}_{k,0}^{(1)}|\rho_k}(x|y) = (L-K+1)(1 - F_{d_{k,l,0}|\rho_k}(x|y))^{L-K} f_{d_{k,l,0}|\rho_k}(x|y), \tag{4.47}$$

where $F_{d_{k,l,0}|\rho_k}(x|y)$ and $f_{d_{k,l,0}|\rho_k}(x|y)$ are given in (2.12-2.13) and (2.14), respectively.

4.5 Scaling Behavior

4.5.1 SVD

With SVD, the asymptotic average ergodic rate with the CA layout $\bar{\mathcal{R}}^{MU-SVD-C}$ and the asymptotic upper-bound of the average ergodic rate with the DA layout $\bar{\mathcal{R}}_{ub}^{MU-SVD-D}$ have been characterized in (4.21) and (4.35), respectively. As a non-orthogonal linear precoding scheme, the rate performance with SVD is limited by the intra-cell interference.

With the CA layout, it is clear from (4.21) that $\bar{\mathcal{R}}^{MU-SVD-C}$ has the scaling order of $\Theta(\log_2 \xi)$ as the ratio ξ of the number of BS antennas M to the total

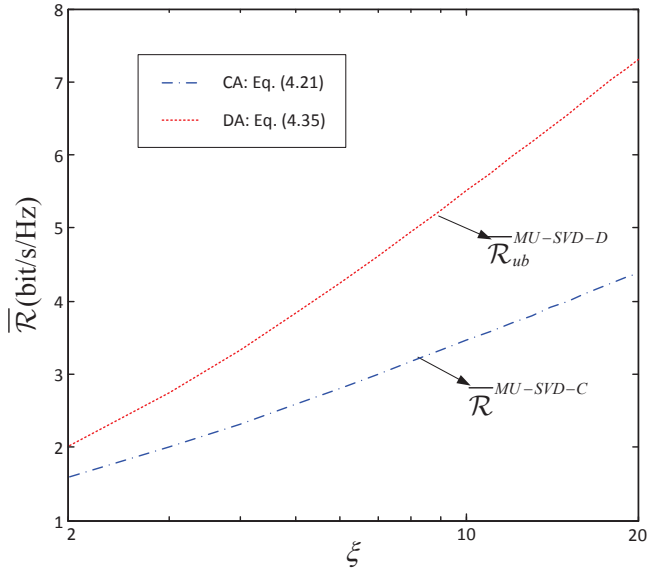

FIGURE 4.3: Asymptotic average ergodic rate with SVD versus the ratio ξ of the number of BS antennas M to the total number of user antennas KN in the single-cell case. $K = 20$. $\alpha = 4$.

number of user antennas KN increases. With the DA layout, (4.35) indicates that the scaling order of the asymptotic upper-bound $\bar{\mathcal{R}}_{ub}^{MU-SVD-D}$ is determined by the number m_k of interfering users whose closest BS antenna cluster is the same as user k's, and the ratio Y of the distance $d_{k,0}^{(1)}$ from user k to the closest BS antenna cluster to the distance $d_{k,\mathcal{K}_0}^{(1)}$ from user k to the closest user among the other $K-1$ users.

When $\xi \gg 1$, i.e., $L \gg K$, the probability that user k and user j are close to the same BS antenna cluster is low, i.e., $\Pr\{l_j^* = l_k^* | j \neq k\} \approx 0$. We then have $\Pr\{m_k = 0\} \approx 1$. Moreover, as L and K increase, the distances from the user to the closest BS antenna cluster $d_{k,0}^{(1)}$ and to the closest user among the other $K-1$ users $d_{k,\mathcal{K}_0}^{(1)}$ decrease in the orders of $\Theta\left(L^{-1/2}\right)$ and $\Theta\left(K^{-1/2}\right)$, respectively. As a result, we can see from (4.32) that with $L \gg K \gg 1$, the asymptotic upper-bound of the average ergodic capacity $\bar{\mathcal{R}}_{ub}^{MU-SVD-D}$ has the scaling order of $\Theta\left(\frac{\alpha}{2}\log_2\frac{L}{K}\right)$, or equivalently, $\Theta\left(\frac{\alpha}{2}\log_2\xi\right)$, where $\alpha > 2$ is the path-loss factor.

Fig. 4.3 demonstrates the asymptotic average ergodic rate with the CA layout $\bar{\mathcal{R}}^{MU-SVD-C}$ and the asymptotic upper-bound of the average ergodic rate with the DA layout $\bar{\mathcal{R}}_{ub}^{MU-SVD-D}$. As we can see from Fig. 4.3, both $\bar{\mathcal{R}}^{MU-SVD-C}$ and $\bar{\mathcal{R}}_{ub}^{MU-SVD-D}$ increase logarithmically with ξ, but a higher scaling order is achieved in the DA case.

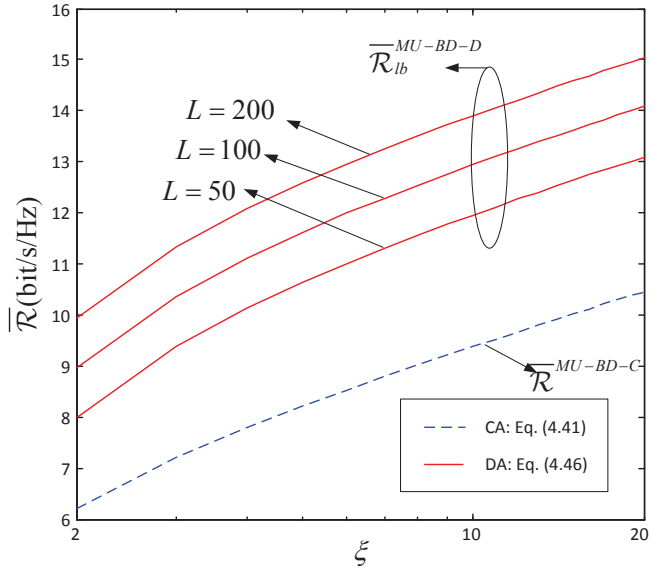

FIGURE 4.4: Asymptotic average ergodic rate with BD versus the ratio ξ of the number of BS antennas M to the total number of user antennas KN in the single-cell case. $P_t/N_0 = 10$dB. $\alpha = 4$.

4.5.2 BD

With BD, the asymptotic average ergodic rate with the CA layout and the asymptotic lower-bound of the average ergodic rate with the DA layout are characterized in (4.41) and (4.46), respectively. In contrast to SVD where the rate performance is intra-cell-interference limited, the rate performance with BD can be improved by increasing $\frac{P_t}{N_0}$.

With the CA layout, (4.41) indicates that the asymptotic average ergodic rate $\bar{\mathcal{R}}^{MU-BD-C}$ has the scaling order of $\Theta(\log_2 \xi)$. With the DA layout, we can see from (4.46) that the scaling behavior of the asymptotic lower-bound of the average ergodic rate $\bar{\mathcal{R}}_{lb}^{MU-BD-D}$ is determined by the minimum access distance $\tilde{d}_{k,0}^{(1)}$ from user k to $L-K+1$ uniformly distributed BS antenna clusters, which decreases in the order of $\Theta\left((L-K+1)^{-1/2}\right)$ as L and K increase. As a result, the asymptotic lower-bound $\bar{\mathcal{R}}_{lb}^{MU-BD-D}$ scales in the order of $\Theta\left(\log_2 \frac{(L-K+1)^{\alpha/2}}{K}\right)$. For $L \gg K$, we further have $\bar{\mathcal{R}}_{lb}^{MU-BD-D} = \Theta\left(\log_2\left(\xi L^{\frac{\alpha}{2}-1}\right)\right)$.

Fig. 4.4 illustrates how the asymptotic average ergodic rate with the CA layout $\bar{\mathcal{R}}^{MU-BD-C}$ and the asymptotic lower-bound of the average ergodic rate with the DA layout $\bar{\mathcal{R}}_{lb}^{MU-BD-D}$ vary with the ratio ξ of the number of BS antennas M to the total number of users KN. We can see from Fig. 4.4 that both $\bar{\mathcal{R}}^{MU-BD-C}$

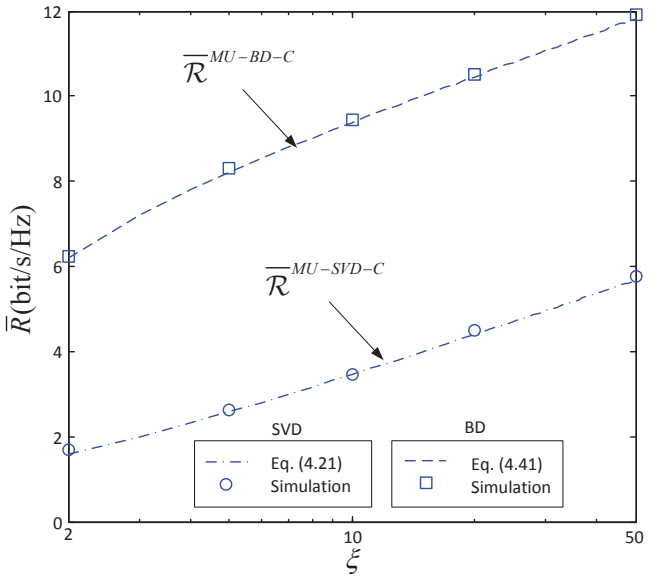

FIGURE 4.5: Average ergodic rate with the CA layout versus the ratio ξ of the number of BS antennas M to the total number of user antennas KN in the single-cell case. $N = 2$. $K = 20$. $P_t/N_0 = 10$dB. $\alpha = 4$.

and $\bar{\mathcal{R}}_{lb}^{MU-BD-D}$ logarithmically increase with ξ in the order of $\Theta(\log_2 \xi)$. In contrast to $\bar{\mathcal{R}}^{MU-BD-C}$ which is only determined by the ratio ξ, with the DA layout, $\bar{\mathcal{R}}_{lb}^{MU-BD-D}$ further increases with the number of BS antenna clusters L, indicating that substantial gains can be obtained when L is large.

4.6 Simulation Results and Discussions

In this section, simulation results are presented to verify the analysis. With the CA layout, the average ergodic rate is obtained by averaging over 100 realizations of the positions of the users. With the DA layout, it is further averaged over 100 realizations of BS antenna topologies.

4.6.1 CA Layout

Fig. 4.5 plots how the average ergodic rate with the CA layout varies with the ratio ξ of the number of BS antennas M to the total number of user antennas KN. As we can see from Fig. 4.5, the asymptotic results are accurate even when N is small, i.e., $N = 2$. The average ergodic rates with SVD and BD both scale with the ratio ξ in the same order, which is found to be $\Theta(\log_2 \xi)$. Nevertheless,

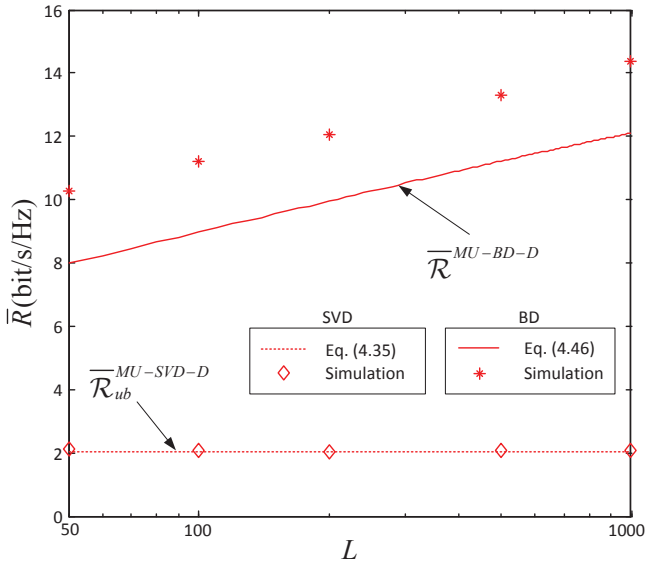

FIGURE 4.6: Average ergodic rate with the DA layout versus the number of BS antenna clusters L in the single-cell case. $\xi = 2$. $N = 2$. $P_t/N_0 = 10$dB. $\alpha = 4$.

because of the severe intra-cell interference, the rate performance with SVD is significantly inferior to that with BD.

4.6.2 DA Layout

Fig. 4.6 demonstrates how the average ergodic rate with the DA layout varies with the number of BS antenna clusters L when the ratio ξ of the number of BS antennas M to the total number of user antennas KN is fixed to be 2. As we can see from Fig. 4.6, the average ergodic rates with SVD and BD show the same scaling orders as their asymptotic bounds, which are found to be $\Theta\left(\frac{\alpha}{2}\log_2\frac{L}{K}\right)$ and $\Theta\left(\log_2\frac{(L-K+1)^{\alpha/2}}{K}\right)$, respectively. The average ergodic rate with SVD is significantly lower than that with BD due to the severe intra-cell interference, and the rate gap is enlarged as the number of BS antenna clusters L increases.

4.6.3 Comparison of CA and DA Layouts

For the sake of comparison, Fig. 4.7 further presents the average ergodic rates with both the CA and the DA layouts. Although a higher scaling order can always be observed with the DA layout, the gains are more prominent when BD is adopted. With the DA layout, the minimum access distance decreases with

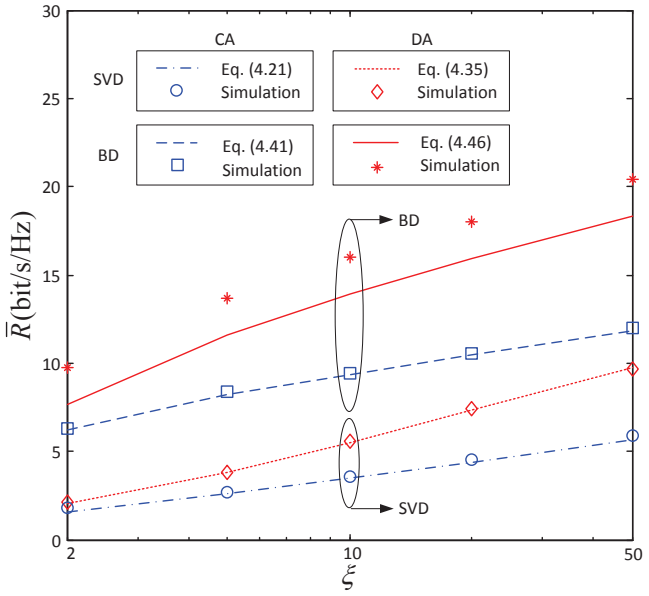

FIGURE 4.7: Average ergodic rates with SVD and BD versus the ratio ξ of the number of BS antennas M to the total number of user antennas KN with CA and DA layouts in the single-cell case. $K = 20$. $N = 2$. $P_t/N_0 = 10$dB. $\alpha = 4$.

the number of BS antenna clusters L. With SVD, both the desired signal and the interference signal become stronger as L increases, leading to marginal rate gains over that with the CA layout. With BD, as the intra-cell interference has been eliminated, more prominent rate gains can be achieved thanks to the reduced minimum access distance.

4.7 Summary

In this chapter, the asymptotic analysis is extended to a K-user single-cell MIMO system with two representative linear precoding schemes: SVD and BD. By assuming that the number of BS antennas M and the number of user antennas N go to infinity with $M/N \to \xi K \gg 1$, the asymptotic average ergodic rates with both SVD and BD are derived explicitly for the CA layout, which are shown to be accurate even for small N. With the DA layout, an asymptotic upper-bound of the average ergodic rate with SVD and an asymptotic lower-bound of the average ergodic rate with BD are developed. Simulation results verify that the average ergodic rates have the same scaling orders as their asymptotic bounds.

The analysis reveals that the scaling orders are dependent on the precoding schemes. With SVD, the average ergodic rates with the CA and DA layouts scale with the ratio ξ of the number of BS antennas to the number of total user antennas in the orders of $\Theta\left(\log_2 \xi\right)$ and $\Theta\left(\frac{\alpha}{2} \log_2 \xi\right)$, respectively, where $\alpha > 2$ is the path-loss factor. With BD, the scaling orders with the CA and DA layouts are found to be $\Theta\left(\log_2 \xi\right)$ and $\Theta\left(\log_2\left(\xi L^{\frac{\alpha}{2}-1}\right)\right)$, respectively.

Compared to the CA layout, a higher scaling order can be always observed in the DA case, and substantial gains can be achieved with both SVD and BD due to the reduction of the minimum access distance. The rate gains become more prominent when an orthogonal precoding scheme such as BD is adopted.

Chapter 5

Asymptotic Average Ergodic Rate of Multi-User Multi-Cell MIMO

In this chapter, the asymptotic analysis is further extended to a multi-user multi-cell MIMO system, and the scaling behavior of the average ergodic rates in the presence of inter-cell interference is studied. This chapter is organized as follows. Section 5.1 presents a literature review on previous related work. The inter-cell interference is discussed in Section 5.2. The scaling orders of the average ergodic rates in MIMO cellular networks with the CA and DA layouts are characterized and verified by simulation results in Section 5.3. Section 5.4 summarizes this chapter.

5.1 Literature Review

In a multi-user multi-cell MIMO system with universal frequency reuse, the inter-cell interference becomes a severe limiting factor to system performance and renders tremendous difficulties in modeling and performance evaluation [66]. A great deal of effort has been made to address this issue by introducing different levels of BS cooperation (see [67] for a comprehensive overview). In many cases, however, the problem becomes intractable when fading and interference are both taken into consideration. Various simplified models are therefore proposed [68–71], and a small group of users and BS antennas is usually assumed for computational tractability [72–76].

If the BS antennas are geographically distributed, the rate performance is further dependent on the BS antennas' positions. For computational tractability, most studies have focused on a regular BS antenna layout with a small number of BS antennas [57–59]. In this chapter, asymptotic bounds will be developed to characterize the scaling behavior of the average rate performance with SVD and BD when the number of BS antennas and the number of users are large.

Specifically, we focus on a multi-user multi-cell MIMO system with 7 cells and K uniformly distributed users in the inscribed circle of each cell. We assume that each BS has full CSI of all users in its own cell, and no cooperation is adopted among BSs. By assuming that the number of BS antennas M and the number of user antennas N go to infinity with $M/N \to \xi K \gg 1$, the asymptotic average ergodic rates with the CA layout are derived for the SVD and BD cases. With the DA layout, asymptotic bounds are developed to characterize the scaling orders of the average ergodic rates. Simulation results verify that with both the CA and DA layouts, the average ergodic rates in the multi-cell case have the same scaling orders as that in the single-cell case.

5.2 Inter-cell Interference

According to (2.6), the ergodic rate is crucially determined by the covariance matrix of the inter-cell interference $\mathbf{Q}_k^{inter}$. Appendix E shows that with equal

power allocation, $\mathbf{Q}_k^{inter}$ can be obtained as

$$\mathbf{Q}_k^{inter} = \frac{1}{M}\sum_{i=1}^{6}\sum_{m\in\mathcal{B}_i}|\gamma_{k,m}|^2 P_t \mathbf{I}_N. \tag{5.1}$$

It is clear from (5.1) that the inter-cell interference is determined by the large-scale fading coefficients between user k and BS antennas in Cell i, $i = 1, \cdots, 6$. In the following of this section, we will examine how the inter-cell interference varies with different BS antenna layouts. For illustration, we normalize the inter-cell interference by the total transmit power P_t, and denote the normalized inter-cell interference power as P_k^{int}. The covariance matrix of the inter-cell interference can be then rewritten as

$$\mathbf{Q}_k^{inter} = P_k^{int} P_t \mathbf{I}_N. \tag{5.2}$$

By combining (5.1-5.2), the normalized inter-cell interference power with equal power allocation is given by

$$P_k^{int} = \frac{1}{M}\sum_{i=1}^{6}\sum_{m\in\mathcal{B}_i}|\gamma_{k,m}|^2. \tag{5.3}$$

5.2.1 CA Layout

With the CA layout, the normalized inter-cell interference power at user $k \in \mathcal{K}_0$ can be obtained by combining (5.3) and (2.10) as

$$P_k^{int,C} = \sum_{i=1}^{6}\left(\rho_k^2 + 4 - 4\rho_k \cos\left(\theta_k - \left(i\cdot\frac{\pi}{3} - \frac{\pi}{6}\right)\right)\right)^{-\alpha/2}. \tag{5.4}$$

(5.4) indicates that the normalized inter-cell interference power with the CA layout $P_k^{int,C}$ is solely determined by the position of user k. Due to the symmetric nature of the positions of BS antennas shown in (2.9), $P_k^{int,C}$ is a periodic function of period $\pi/3$ for any $\rho_k \in [0, 1]$. It is maximized when $\theta_k = i\cdot\frac{\pi}{3} - \frac{\pi}{6}$, and minimized when $\theta_k = i\cdot\frac{\pi}{3}$, $i = 1, \cdots, 6$. For given θ_k, the normalized inter-cell interference $P_k^{int,C}$ is a monotonic increasing function of ρ_k. With the path-loss factor $\alpha = 4$, for instance, $P_k^{int,C}$ is minimized at $(0, 0)$ with $P_k^{int,C}|(0, 0) = 0.375$, and maximized at $(1, i\cdot\frac{\pi}{3} - \frac{\pi}{6})$ with $P_k^{int,C}|(1, i\cdot\frac{\pi}{3} - \frac{\pi}{6}) \approx 1.275$, $i = 1, \cdots, 6$.

5.2.2 DA Layout

With the DA layout, the normalized inter-cell interference power at user $k \in \mathcal{K}_0$ can be obtained by combining (5.3) and (2.11) as

$$P_k^{int,D} = \frac{1}{L} \sum_{i=1}^{6} \sum_{l=1}^{L} d_{k,l,i}^{-\alpha}, \tag{5.5}$$

with the n-th moment

$$\mathbb{E}\left[\left(P_k^{int,D}\right)^n\right] = \frac{1}{L^n} \sum_{\sum_{l=1}^{L} t_l = n} \frac{n!}{\prod_{l=1}^{L} t_l!} \prod_{l=1}^{L} \mathbb{E}\left[\left(\sum_{i=1}^{6} d_{k,l,i}^{-\alpha}\right)^{t_l}\right], \tag{5.6}$$

where the sum is taken over all possible combinations of nonnegative integers t_l given $\sum_{l=1}^{L} t_l = n$. It is clear from (5.6) that the n-th moment of the normalized inter-cell interference $\mathbb{E}\left[\left(P_k^{int,D}\right)^n\right]$ crucially depends on the distribution of the distance $d_{k,l,i}$ from user $k \in \mathcal{K}_0$ to BS antenna cluster l in Cell i, $l = 1, \cdots, L$, $i = 1, \cdots, 6$, which varies with user k's position as shown in (2.15-2.16).

If user k is at the cell center $(0, 0)$, for instance, the conditional pdf of $d_{k,l,i}$ can be obtained from (2.15-2.16) as

$$f_{d_{k,l,i}|\rho_k,\theta_k}(x|0,0) = \begin{cases} \frac{2x}{\pi} \arccos \frac{x^2+3}{4x} & \text{if } 1 \le x \le 3 \\ 0 & \text{otherwise,} \end{cases} \tag{5.7}$$

$i = 1, \cdots, 6$. We can see from (5.7) that $f_{d_{k,l,i}|\rho_k,\theta_k}(x|0,0)$ is independent of i, indicating an isotropic normalized inter-cell interference power. With $\alpha = 4$, the mean normalized inter-cell interference power for a cell-center user can be obtained by combining (5.6) and (5.7) as $\mathbb{E}\left[P_k^{int,D}|(0,0)\right] = \frac{2}{3}$, which is slightly higher than the normalized inter-cell interference power in the CA layout, i.e., $P_k^{int,C}|(0,0) = 0.375$.

On the other hand, for a cell-edge user located at $(1, \frac{\pi}{6})$, the conditional pdf of $d_{k,l,i}$ can be obtained from (2.15-2.16) as

$$f_{d_{k,l,i}|\rho_k,\theta_k}\left(x|1,\frac{\pi}{6}\right) = \frac{2x}{\pi} \arccos \frac{4 - 4\cos\frac{(1-i)\pi}{3} + x^2}{2x\sqrt{5 - 4\cos\frac{(1-i)\pi}{3}}}, \tag{5.8}$$

if $\sqrt{5-4\cos\frac{(1-i)\pi}{3}}-1 \leq x \leq \sqrt{5-4\cos\frac{(1-i)\pi}{3}}+1$, $i=1,\cdots,6$. Otherwise, $f_{d_{k,l,i}|\rho_k,\theta_k}\left(x|1,\frac{\pi}{6}\right)=0$. In this case, $f_{d_{k,l,i}|\rho_k,\theta_k}(x|1,\frac{\pi}{6})$ varies with i, indicating that the BS antenna clusters in different cells have distinct contributions to the normalized inter-cell interference power $P_k^{int,D}$. Specifically, as user k is close to the neighboring Cell 1, we have $d_{k,l,1} \ll d_{k,l,i}$, for $i=2,\cdots,6$. As a result, $\sum_{i=1}^{6} d_{k,l,i}^{-\alpha} \approx d_{k,l,1}^{-\alpha}$, and (5.6) reduces to

$$\mathbb{E}\left[\left(P_k^{int,D}\right)^n|(1,\tfrac{\pi}{6})\right] \approx \frac{1}{L^n}\sum_{\sum_{l=1}^{L} t_l=n}\frac{n!}{\prod_{l=1}^{L} t_l!}\prod_{l=1}^{L}\mathbb{E}\left[d_{k,l,1}^{-t_l\alpha}|(1,\pi/6)\right]. \tag{5.9}$$

With $t_l \geq 1$ and the path-loss factor $\alpha > 2$, we have $t_l\alpha > 2$. $\mathbb{E}\left[d_{k,l,1}^{-t_l\alpha}|(1,\pi/6)\right]$ can be then obtained from (5.8) as

$$\begin{aligned}
&\mathbb{E}\left[d_{k,l,1}^{-t_l\alpha}|(1,\pi/6)\right] = \frac{2}{\pi}\int_0^2 x^{-t_l\alpha+1}\arccos\frac{x}{2}dx \\
&= \begin{cases} \frac{1}{\pi(t_l\alpha-2)(t_l\alpha-3)}\left(\frac{2^{3-t_l\alpha}\sqrt{\pi}\Gamma(\frac{5-t_l\alpha}{2})}{\Gamma(\frac{4-t_l\alpha}{2})}+\lim\limits_{x\to 0^+}\frac{2(t_l\alpha-3)\arccos\frac{x}{2}-{}_2F_1\left(\frac{1}{2},\frac{3-t_l\alpha}{2};\frac{5-t_l\alpha}{2};\frac{x^2}{4}\right)x}{x^{t_l\alpha-2}}\right) & t_l\alpha\neq 3 \\ \frac{2}{\pi}\lim\limits_{x\to 0^+}\frac{1}{x}\arccos\frac{x}{2}-\frac{1}{2}\ln x & t_l\alpha=3 \end{cases} \\
&= \infty,
\end{aligned} \tag{5.10}$$

where ${}_2F_1(a,b;c;z)$ denotes the hypergeometric function. We can conclude from (5.9-5.10) that for the cell-edge user at $(1,\frac{\pi}{6})$, the n-th moment of the normalized inter-cell interference power with the DA layout $\mathbb{E}\left[\left(P_k^{int,D}\right)^n|(1,\frac{\pi}{6})\right]=\infty$. Intuitively, the inter-cell interference power becomes extremely strong if the user is close to some BS antenna cluster in the neighboring cells. With BS antenna clusters uniformly distributed in the inscribed circle of each cell, there is a non-zero probability that some antenna cluster falls into the vicinity area of the user if it is located at the cell edge, thus leading to the divergence of inter-cell interference power.

Fig. 5.1 illustrates the normalized inter-cell interference power with the CA layout $P_k^{int,C}$ and the mean normalized inter-cell interference power with the DA layout $\mathbb{E}[P_k^{int,D}]$ of user k given its angular coordinate at $\theta_k=\frac{\pi}{6}$. As we can see from Fig. 5.1, both $P_k^{int,C}$ and $\mathbb{E}[P_k^{int,D}]$ grow monotonically with the radial coordinate ρ_k of user k because of the reduction of the distances from user k to BS antenna clusters in the neighboring Cell 1. With the DA layout, the mean normalized inter-cell interference power $\mathbb{E}[P_k^{int,D}]$ becomes infinite at $\rho_k=1$.

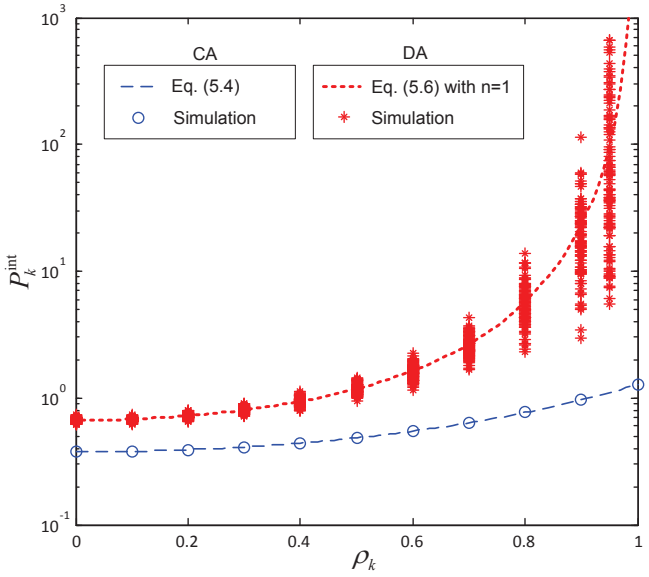

FIGURE 5.1: Normalized inter-cell interference power P_k^{int} of user k versus its radial coordinate ρ_k. $\theta_k = \frac{\pi}{6}$. $K = 50$. $L = 200$. $N = 2$. $M = 400$. $\alpha = 4$. With the DA layout, simulation results are obtained based on 100 realizations of the BS antenna topology.

The analysis is verified by the simulation results presented in Fig. 5.1. It can be observed from Fig. 5.1 that with the DA layout, in addition to the mean, the variance of the normalized inter-cell interference also grows with the radial coordinate ρ_k of user k. It indicates that as the user moves towards the cell edge, the rate performance becomes increasingly sensitive to its position.

In the following section, we will focus on the asymptotic average ergodic rates with SVD and BD as the number of BS antennas M and the number of user antennas N go to infinity with $M/N \to \xi K \gg 1$. With the DA layout, as the BS antennas are grouped into L clusters with N antennas at each cluster, the asymptotic assumption reduces to $N \to \infty$. Similar to Chapter 4, we suppose that equal power allocation is adopted, and study the scaling behavior of the average ergodic rates with SVD and BD.

5.3 Asymptotic Average Ergodic Rate

5.3.1 SVD

With SVD, each user suffers from both intra-cell and inter-cell interference. Similar to (4.3), the ergodic rate with SVD in a multi-user multi-cell MIMO system can be obtained by combining (2.6), (3.19-3.23), (4.2), (4.14) and (5.1) as

$$R_k^{MC-SVD}=\frac{1}{N}\mathbb{E}_{\mathbf{H}_{k,\mathcal{B}_0}}\left[\log_2\det\left(\mathbf{I}_N+\mu_k^{MC-SVD}\mathbf{\Lambda}_{k,\mathcal{B}_0}\mathbf{\Omega}_k\mathbf{\Omega}_k^{\dagger}\mathbf{\Lambda}_{k,\mathcal{B}_0}^{\dagger}\right)\right], \tag{5.11}$$

where the average received SINR μ_k^{MC-SVD} is given by

$$\mu_k^{MC-SVD}=\frac{\|\boldsymbol{\gamma}_{k,\mathcal{B}_0}\|^2}{K\left(\frac{N_0}{P_t}+\frac{1}{M}\sum_{i=1}^{6}\sum_{m\in\mathcal{B}_i}|\gamma_{k,m}|^2\right)+\sum_{j\in\mathcal{K}_0,j\neq k}\sum_{m=1}^{M}|\gamma_{k,m}|^2\sum_{n=1}^{N}\mathbb{E}\left[|w_{m,n}^j|^2\right]}, \tag{5.12}$$

by combining (4.15) and (5.1).

5.3.1.1 CA Layout

With the CA layout, by combining (4.17) and (5.4), the average received SINR with the CA layout $\mu_k^{MC-SVD-C}$ can be written as

$$\begin{aligned}\mu_k^{MC-SVD-C}&=\frac{M\rho_k^{-\alpha}}{K\left(\frac{N_0}{P_t}+\sum_{i=1}^{6}\left(\rho_k^2+4-4\rho_k\cos\left(\theta_k-\left(i\cdot\frac{\pi}{3}-\frac{\pi}{6}\right)\right)\right)^{-\alpha/2}\right)+(K-1)\rho_k^{-\alpha}}\\&\approx\frac{M}{K\left(1+\rho_k^{\alpha}\left(\frac{N_0}{P_t}+\sum_{i=1}^{6}\left(\rho_k^2+4-4\rho_k\cos\left(\theta_k-\left(i\cdot\frac{\pi}{3}-\frac{\pi}{6}\right)\right)\right)^{-\alpha/2}\right)\right)},\end{aligned} \tag{5.13}$$

for large $K\gg 1$.

Similar to Section 4.3.1, the asymptotic ergodic rate with the CA layout as $M,N\to\infty$ and $M/N\to\xi K\geq 1$ can be obtained by combining (4.19), (5.11),

and (5.13) as

$$\mathcal{R}_k^{MC-SVD-C} = \log_2\left(1+\frac{\xi}{1+\rho_k^{\alpha}\left(\frac{N_0}{P_t}+\sum_{i=1}^{6}\left(\rho_k^2+4-4\rho_k\cos\left(\theta_k-\left(i\cdot\frac{\pi}{3}-\frac{\pi}{6}\right)\right)\right)^{-\alpha/2}\right)}\right)$$
$$\approx \log_2\left(1+\frac{\xi}{1+\sum_{i=1}^{6}\left(1+4\rho_k^{-2}-4\rho_k^{-1}\cos\left(\theta_k-\left(i\cdot\frac{\pi}{3}-\frac{\pi}{6}\right)\right)\right)^{-\alpha/2}}\right), \quad (5.14)$$

for large $\frac{P_t}{N_0} \gg 1$.

It is clear from (5.14) that $\mathcal{R}_k^{MC-SVD-C}$ varies with the position of user k. By combining (5.14) and (2.21), the asymptotic average ergodic rate with the CA layout can be obtained as

$$\bar{\mathcal{R}}^{MC-SVD-C} = \int_0^{2\pi}\int_0^1 x\log_2\left(1+\frac{\xi}{1+\sum_{i=1}^{6}\left(1+\frac{4}{x^2}-\frac{4}{x}\cos\left(y-\left(i\cdot\frac{\pi}{3}-\frac{\pi}{6}\right)\right)\right)^{-\alpha/2}}\right)\cdot$$
$$f_{\rho_k}(x)f_{\theta_k}(y)dxdy, \quad (5.15)$$

where $f_{\rho_k}(x) = 2x$ and $f_{\theta_k}(y) = \frac{1}{2\pi}$ denote the pdfs of the radial and angular coordinates of user k, respectively.

5.3.1.2 DA Layout

With the DA layout, as the distances from the user to the interfering BS antennas in its own cell are much smaller than the distances to the BS antennas in the neighboring cells, the average ergodic rate is mainly determined by the intra-cell interference. As we will show in Section 5.3.3, the asymptotic upper-bound of the average ergodic rate developed in the single-cell case in (4.35) also serves as a close upper-bound for the multi-cell case.

5.3.2 BD

When BD is adopted, the intra-cell interference is completely eliminated, and thus each user only suffers from inter-cell interference. Similar to (4.12), the ergodic rate with BD in a multi-user multi-cell MIMO system can be obtained by

combining (2.6), (4.8-4.11), (4.14) and (5.1) as

$$R_k^{MC-BD} = \frac{1}{N}\mathbb{E}_{\mathbf{H}_{k,\mathcal{B}_0}}\left[\log_2 \det\left(\mathbf{I}_N + \mu_k^{MC-BD}\tilde{\mathbf{\Lambda}}_{k,\mathcal{B}_0}\tilde{\mathbf{\Omega}}_k\tilde{\mathbf{\Omega}}_k^{\dagger}\tilde{\mathbf{\Lambda}}_{k,\mathcal{B}_0}^{\dagger}\right)\right], \tag{5.16}$$

where the average received SINR μ_k^{MC-BD} is given by

$$\mu_k^{MC-BD} = \frac{\|\boldsymbol{\gamma}_{k,\mathcal{B}_0}\|^2}{\frac{KN_0}{P_t} + \frac{K}{M}\sum_{i=1}^{6}\sum_{m\in\mathcal{B}_i}|\gamma_{k,m}|^2}, \tag{5.17}$$

by combining (4.16) and (5.1)

5.3.2.1 CA Layout

With the CA layout, by combining (4.36) and (5.4), the average received SINR with the CA layout $\mu_k^{MC-BD-C}$ can be written as

$$\mu_k^{MC-BD-C} = \frac{M\rho_k^{-\alpha}}{\frac{KN_0}{P_t} + K\sum_{i=1}^{6}\left(\rho_k^2 + 4 - 4\rho_k\cos\left(\theta_k - \left(i\cdot\frac{\pi}{3} - \frac{\pi}{6}\right)\right)\right)^{-\alpha/2}}. \tag{5.18}$$

Similar to Section 4.4.1, the asymptotic ergodic rate with the CA layout can be obtained by combining (4.38), (5.16) and (5.18) as

$$\mathcal{R}_k^{MC-BD-C} \approx \log_2\left(1 + \frac{\left(\xi - 1 + \frac{1}{K}\right)\rho_k^{-\alpha}}{\frac{N_0}{P_t} + \sum_{i=1}^{6}\left(\rho_k^2 + 4 - 4\rho_k\cos\left(\theta_k - \left(i\cdot\frac{\pi}{3} - \frac{\pi}{6}\right)\right)\right)^{-\alpha/2}}\right). \tag{5.19}$$

By combining (5.19) and (2.21), the asymptotic average ergodic rate with the CA layout can be obtained as

$$\bar{\mathcal{R}}^{MC-BD-C} \approx \int_0^{2\pi}\int_0^1 \log_2\left(1 + \left(\xi - 1 + \frac{1}{K}\right)\cdot \frac{x^{-\alpha}}{\frac{N_0}{P_t} + \sum_{i=1}^{6}\left(x^2 + 4 - 4x\cos\left(y - \left(i\cdot\frac{\pi}{3} - \frac{\pi}{6}\right)\right)\right)^{-\alpha/2}}\right) f_{\rho_k}(x) f_{\theta_k}(y)\,dx\,dy, \tag{5.20}$$

where $f_{\rho_k}(x) = 2x$ and $f_{\theta_k}(y) = \frac{1}{2\pi}$ denote the pdfs of the radial and angular coordinates of user k, respectively. For $\xi \gg 1$, $K \gg 1$, and $\frac{P_t}{N_0} \gg 1$, we have

$$\bar{R}^{MC-BD-C} \approx \log_2(\xi - 1) + \Psi^C(\alpha), \tag{5.21}$$

where $\Psi^C(\alpha)$ is given by

$$\Psi^C(\alpha) = \frac{\alpha}{\ln 4} - \frac{1}{\pi}\int_0^{2\pi}\int_0^1 x \log_2\left(\sum_{i=1}^{6}\left(x^2+4-4x\cos\left(y-\left(i\cdot\frac{\pi}{3}-\frac{\pi}{6}\right)\right)\right)^{-\alpha/2}\right) dxdy. \tag{5.22}$$

With the path-loss factor $\alpha = 4$, for instance, we have $\Psi^C(4) \approx 3.54$.

5.3.2.2 DA Layout

Similar to Section 4.4.2, with $L \gg K$, Appendix D shows that a lower-bound of the ergodic rate with the DA layout can be obtained as

$$R_{k,lb}^{MC-BD-D} = \frac{1}{N}\mathbb{E}_{\tilde{\mathbf{H}}_{k,0}^{(1)}}\left[\log_2\det\left(\mathbf{I}_N + \frac{\frac{1}{K}\left(\tilde{d}_{k,0}^{(1)}\right)^{-\alpha}}{\frac{N_0}{P_t}+\frac{1}{L}\sum_{i=1}^{6}\sum_{l=1}^{L} d_{k,l,i}^{-\alpha}}\cdot\frac{1}{N}\tilde{\mathbf{H}}_{k,0}^{(1)}\left(\tilde{\mathbf{H}}_{k,0}^{(1)}\right)^{\dagger}\right)\right], \tag{5.23}$$

where $\tilde{d}_{k,0}^{(1)}$ denotes the minimum access distance from user $k \in \mathcal{K}_0$ to $L-K+1$ BS antenna clusters which are uniformly distributed in the inscribed circle of Cell 0. $\tilde{\mathbf{H}}_{k,0}^{(1)} \in \mathbb{C}^{N\times N}$ denotes the corresponding small-scale fading matrix. According to the Marcenko-Pastur law [64], as $N \to \infty$, the empirical eigenvalue distribution of $\frac{1}{N}\tilde{\mathbf{H}}_{k,0}^{(1)}\left(\tilde{\mathbf{H}}_{k,0}^{(1)}\right)^{\dagger} \sim \mathcal{W}_N\left(N, \frac{1}{N}\mathbf{I}_N\right)$ converges almost surely to the distribution given in (4.25). By combining (5.23) and (4.25), the asymptotic lower-bound of the ergodic rate with the DA layout as $N \to \infty$ can be obtained as

$$\mathcal{R}_{k,lb}^{MC-BD-D} = \Phi\left(\frac{\frac{1}{K}\left(\tilde{d}_{k,0}^{(1)}\right)^{-\alpha}}{\frac{N_0}{P_t}+\frac{1}{L}\sum_{i=1}^{6}\sum_{l=1}^{L} d_{k,l,i}^{-\alpha}}\right), \tag{5.24}$$

where $\Phi(x)$ is given in (4.27). With $L \gg K$, $\tilde{d}_{k,0}^{(1)} \ll 1$. According to (4.44), the asymptotic lower-bound $R_{k,lb}^{MC-BD-D}$ can be then approximated by

$$\begin{aligned}\mathcal{R}_{k,lb}^{MC-BD-D} &\approx \log_2\left(\frac{\frac{1}{K}\left(\tilde{d}_{k,0}^{(1)}\right)^{-\alpha}}{\frac{N_0}{P_t}+\frac{1}{L}\sum_{i=1}^{6}\sum_{l=1}^{L} d_{k,l,i}^{-\alpha}}\right) - \log_2 e \\ &\overset{\frac{P_t}{N_0}\gg 1}{\approx} \log_2\left(\frac{\frac{1}{K}\left(\tilde{d}_{k,0}^{(1)}\right)^{-\alpha}}{\frac{1}{L}\sum_{i=1}^{6}\sum_{l=1}^{L} d_{k,l,i}^{-\alpha}}\right) - \log_2 e.\end{aligned} \tag{5.25}$$

By combining (5.25) and (2.20), the asymptotic lower-bound of the average ergodic rate with the DA layout can be written as

$$\begin{aligned}\bar{\mathcal{R}}_{lb}^{MC-BD-D} &= \mathbb{E}_{\rho_k,\tilde{d}_{k,0}^{(1)}}\left[\log_2\left(\frac{1}{K}\left(\tilde{d}_{k,0}^{(1)}\right)^{-\alpha}\right)\right] - \mathbb{E}_{\rho_k,\theta_k}\left[\log_2\left(\sum_{i=1}^{6}\mathbb{E}_{d_{k,l,i}|\rho_k,\theta_k}\left[d_{k,l,i}^{-\alpha}|\rho_k,\theta_k\right]\right)\right] \\ &\quad - \log_2 e \\ &= 2\int_0^1\int_0^{1+y} y\log_2\left(\frac{1}{K}x^{-\alpha}\right) f_{\tilde{d}_{k,0}^{(1)}|\rho_k}(x|y)dxdy + \Psi^D(\alpha), \end{aligned} \tag{5.26}$$

where $f_{\tilde{d}_{k,0}^{(1)}|\rho_k}(x|y)$ is given in (4.47). $\Psi^D(\alpha)$ denotes the sum of the last two items on the right-hand side of (5.26), which can be obtained as

$$\begin{aligned}\Psi^D(\alpha) = &-\frac{1}{\pi}\int_0^{2\pi}\int_0^1 y\log_2\left(\sum_{i=1}^{6}\int_{\sqrt{y^2+4-4y\cos\left(z-\left(i\cdot\frac{\pi}{3}-\frac{\pi}{6}\right)\right)}-1}^{\sqrt{y^2+4-4y\cos\left(z-\left(i\cdot\frac{\pi}{3}-\frac{\pi}{6}\right)\right)}+1} x^{-\alpha} f_{d_{k,l,i}|\rho_k,\theta_k}(x|y,z)dx\right)dydz \\ &- \log_2 e, \end{aligned} \tag{5.27}$$

where $f_{d_{k,l,i}|\rho_k,\theta_k}(x|y,z)$ is given in (2.15). With the path-loss factor $\alpha = 4$, for instance, we have $\Psi^D(4) \approx -3.054$.

5.3.3 Simulation Results and Discussions

In this section, simulation results are presented to verify the analysis. With the CA layout, the average ergodic rate is obtained by averaging over 100 realizations of the positions of the users. With the DA layout, it is further averaged over 100 realizations of BS antenna topologies.

As we can see from Fig. 5.2, with the CA layout, the asymptotic results are accurate even when N is small, i.e., $N = 2$. With the DA layout, the average ergodic rates have the same scaling orders as their asymptotic bounds.

By comparing Fig. 5.2 and Fig. 4.7, we can observe that the average ergodic rates in the multi-cell case scale with the ratio ξ of the number of BS antennas M to the total number of user antennas KN in the same orders as that in the single-cell case. With SVD, the average ergodic rates have the scaling orders of $\Theta\left(\log_2\xi\right)$ and $\Theta\left(\frac{\alpha}{2}\log_2\xi\right)$ for the CA and DA cases, respectively, where $\alpha > 2$ is the path-loss factor. With BD, the scaling orders of the average ergodic rates with the CA and DA layouts are found to be $\Theta\left(\log_2\xi\right)$ and $\Theta\left(\log_2\left(\xi L^{\frac{\alpha}{2}-1}\right)\right)$, respectively.

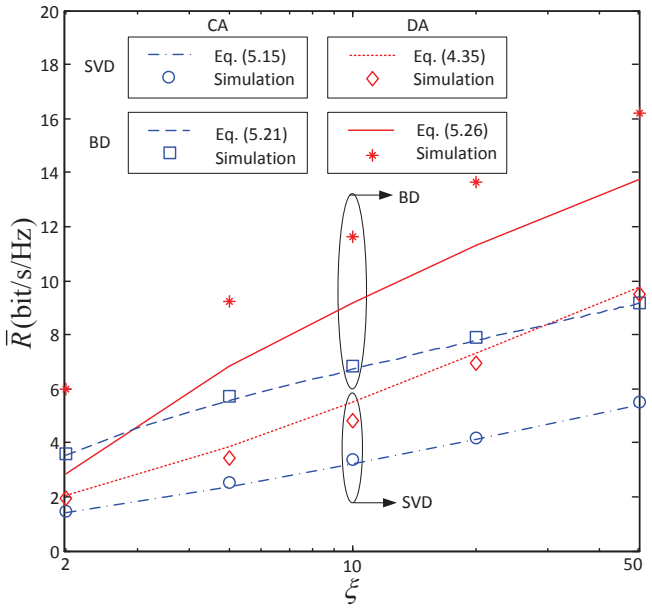

FIGURE 5.2: Average ergodic rates with SVD and BD versus the ratio ξ of the number of BS antennas M to the total number of user antennas KN with the CA and DA layouts in the multi-cell case. $N = 2$. $K = 20$. $P_t/N_0 = 10$dB. $\alpha = 4$.

In fact, we can see from (5.4) and (5.5) that the inter-cell interference does not affect the scaling orders in both CA and DA cases. As the ratio ξ increases, the rate gains with the DA layout become more prominent, indicating that substantial gains can be achieved when the number of BS antennas is large.

5.4 Summary

In this chapter, the asymptotic analysis is further extended to a multi-user multi-cell MIMO system. By assuming that the number of BS antennas M and the number of user antennas N go to infinity with $M/N \to \xi K \gg 1$, the asymptotic average ergodic rates with the CA layout and the asymptotic bounds of the average ergodic rates with the DA layout are developed to characterize the scaling behavior. The analysis reveals that the inter-cell interference does not affect the scaling behavior, and the scaling orders of the average ergodic rates in the multi-cell case are the same as that in the single-cell case with the CA and DA layouts. A higher average ergodic rate can always be achieved in the DA case, and the rate gains become increasingly prominent as the number of BS antennas grows.

Note that it comes with a caveat. Despite the better average rate performance, the inter-cell interference with the DA layout is shown to be sensitive to the user's position at the cell edge, leading to a large rate difference among cell-edge users when equal power allocation is adopted. To achieve a uniform rate across each cell, proper transmit power allocation should be performed at each BS. In the next chapter, we will focus on the effect of power allocation on the ergodic rate.

Chapter 6

Effect of Power Allocation on Ergodic Rate of MIMO Cellular Networks

---

In this chapter, we will discuss the effect of power allocation on the ergodic rates with the CA and DA layouts. This chapter is organized as follows. Section 6.1 presents a literature review on previous related work. The ergodic rates with different power allocation schemes are studied for the CA and DA cases in Section 6.2 and Section 6.3, respectively, and a comparison of the average ergodic rates with equal power allocation and interference-aware power allocation is presented in Section 6.4. Section 6.5 summarizes this chapter.

6.1 Literature Review

In the previous chapters, we assume an equal power allocation and focus on the average rate performance. The cellular system is, nevertheless, essentially an asymmetric one where users in different locations are subject to remarkably distinct large-scale fading effects [77]. As both the desired signal and the interference level are crucially determined by the large-scale fading coefficients from the user to BS antennas, the rate performance of each user could be very sensitive to its position if equal power allocation is adopted. It is, therefore, of paramount importance to study how the rate performance of each user varies with its position under different power allocation strategies.

In an interference-free (or loosely speaking, noise-limited) network, a uniform rate can be achieved by adjusting the transmit power of each user inversely proportional to its large-scale fading coefficient to maintain a constant average received power. For interference-limited MIMO cellular networks, in contrast, the analysis shows that it still leads to a large variance of rate due to a drastic change of the interference level with the user's position. In this case, the key to a uniform rate lies in the SINR.

To equalize the SINR performance, extensive studies have been conducted on the so-called "SINR balancing" or "max-min weighted SINR" problem by using various optimization techniques [34, 36, 78–83]. If multiple antennas are employed at each user, the optimization problem becomes non-convex and cannot be solved efficiently [79, 81]. Various suboptimal algorithms have been proposed in [79, 82, 83]. For downlink multiple-input-single-output (MISO) single-cell systems, iterative algorithms have been developed to find the optimal transmit power and linear transmit beamformer to maximize the minimum weighted SINR based on the instantaneous CSI, which, nevertheless, become computationally intensive when the number of users K or the number of BS antennas M is large [34, 36, 78–81]. As we will show in this chapter, a uniform ergodic rate can be achieved in the CA layout as long as the average received SINR is kept a constant.

Specifically, we focus on the effect of power allocation on the ergodic rate of a multi-user multi-cell MIMO system with 7 cells and K users uniformly distributed in the inscribed circle of each cell. With the CA layout, by assuming that the number of BS antennas M and the number of user antennas N go to infinity with $M/N \to \xi K \gg 1$, the asymptotic ergodic rates with SVD and BD of each user

are derived as explicit functions of the large-scale fading coefficients from the user to the BSs. With equal power allocation, for instance, the analysis reveals that the ergodic rate increases without bound as the user moves toward the BS, and a huge rate gap exists between cell-center and cell-edge users if an orthogonal precoding scheme such as BD is adopted. With SVD, the gap is significantly reduced because all the users suffer from severe intra-cell interference. As the user moves away from the BS, nevertheless, a 50% decrease in the rate can still be observed if the ratio of the number of BS antennas to the total number of user antennas is small. It is further shown that the rate performance of each user is still sensitive to its position even if the average received power is kept constant. To achieve a uniform ergodic rate, an interference-aware power allocation scheme is proposed, with which the transmit power for each user is carefully adjusted to maintain a constant average received SINR based on the large-scale fading coefficients from the users to the BSs. With the DA layout, the ergodic rates with SVD and BD are shown to be even more sensitive to the user's position compared to the CA case if equal power allocation is adopted. To achieve a uniform rate, the instantaneous received SINR, rather than the average received SINR, should be equalized. In this case, the transmit power for each user should be calculated based on its inter-cell interference power and the instantaneous CSI between the user and the BS antennas in its own cell.

6.2 Ergodic Rate with the CA Layout

Let us start from the CA case. As M BS antennas are co-located at the center of each cell, we denote the large-scale coefficient from user k to any antenna of BS i as $\gamma^C_{k,\mathcal{B}_i}$, $i = 0, \cdots, 6$. Appendix F shows that the covariance matrix of the inter-cell interference with the CA layout can be obtained as

$$\mathbf{Q}_k^{inter,C} = \sum_{i=1}^{6} |\gamma^C_{k,\mathcal{B}_i}|^2 P_t \mathbf{I}_N. \tag{6.1}$$

By combining (2.6), (3.19-3.23), (4.2), (4.19), and (6.1), the asymptotic ergodic rate of user k with SVD as $M, N \to \infty$ and $M/N \to \xi K \gg 1$ can be written as

$$\mathcal{R}_k^{MC-SVD-C} = \log_2\left(1 + \bar{\mu}_k^{MC-SVD-C}\right), \tag{6.2}$$

where the normalized average received SINR $\bar{\mu}_k^{MC-SVD-C}$ is given by

$$\bar{\mu}_k^{MC-SVD-C} = \frac{1}{N}\mu_k^{MC-SVD-C} = \frac{\xi K \bar{P}_k |\gamma_{k,\mathcal{B}_0}^C|^2}{N_0 + |\gamma_{k,\mathcal{B}_0}^C|^2(P_t - \bar{P}_k) + \sum_{i=1}^6 |\gamma_{k,\mathcal{B}_0}^C|^2 P_t}. \quad (6.3)$$

Similarly, by combining (2.6), (4.7-4.11), (4.38), and (6.1), the asymptotic ergodic rate of user k with BD as $M, N \to \infty$ and $M/N \to \xi K \gg 1$ can be written as

$$\mathcal{R}_k^{MC-BD-C} = \log_2\left(1 + \left(1 - \frac{K-1}{\xi K}\right)\bar{\mu}_k^{MC-BD-C}\right), \quad (6.4)$$

where the normalized average received SINR $\bar{\mu}_k^{MC-BD-C}$ is given by

$$\bar{\mu}_k^{MC-BD-C} = \frac{1}{N}\mu_k^{MC-BD-C} = \frac{\xi K \bar{P}_k |\gamma_{k,\mathcal{B}_0}^C|^2}{N_0 + \sum_{i=1}^6 |\gamma_{k,\mathcal{B}_0}^C|^2 P_t}. \quad (6.5)$$

In the following of this section, the asymptotic ergodic rates with SVD and BD will be characterized under different power allocation strategies. For illustration, let us start from equal power allocation.

6.2.1 Equal Power Allocation

With equal power allocation, the transmit power P_t is equally divided over K users in each cell, which is given in (4.14). By combining (4.14) and (6.3), the normalized average received SINR with equal power allocation can be obtained as

$$\bar{\mu}_{k,epa}^{MC-SVD-C} = \frac{\xi |\gamma_{k,\mathcal{B}_0}^C|^2}{\frac{N_0}{P_t} + |\gamma_{k,\mathcal{B}_0}^C|^2(1 - \frac{1}{K}) + \sum_{i=1}^6 |\gamma_{k,\mathcal{B}_i}^C|^2} \approx \frac{\xi |\gamma_{k,\mathcal{B}_0}^C|^2}{\sum_{i=0}^6 |\gamma_{k,\mathcal{B}_i}^C|^2}, \quad (6.6)$$

for large $\frac{P_t}{N_0} \gg 1$ and $K \gg 1$. By combining (6.6) and (6.2), the asymptotic ergodic rate of user k with SVD and equal power allocation can be written as

$$\mathcal{R}_{k,epa}^{MC-SVD-C} = \log_2\left(1 + \xi \cdot \frac{|\gamma_{k,\mathcal{B}_0}^C|^2}{\sum_{i=0}^6 |\gamma_{k,\mathcal{B}_i}^C|^2}\right). \quad (6.7)$$

Similarly, with BD, the normalized average received SINR $\bar{\mu}_{k,epa}^{MC-BD-C}$ of user k with equal power allocation can be obtained by combining (4.14) and (6.5) as

$$\bar{\mu}_{k,epa}^{MC-BD-C} = \frac{\xi K P_t |\gamma_{k,\mathcal{B}_0}^C|^2}{K(N_0 + \sum_{i=1}^6 |\gamma_{k,\mathcal{B}_i}^C|^2 P_t)} \approx \frac{\xi K |\gamma_{k,\mathcal{B}_0}^C|^2}{K \sum_{i=1}^6 |\gamma_{k,\mathcal{B}_i}^C|^2}, \quad (6.8)$$

for large $\frac{P_t}{N_0} \gg 1$ and $K \gg 1$. According to (6.4), the asymptotic ergodic rate of user k with BD and equal power allocation can be written as

$$\mathcal{R}_{k,epa}^{MC-BD-C} = \log_2\left(1 + \left(\xi - 1 + \frac{1}{K}\right) \cdot \frac{|\gamma_{k,\mathcal{B}_0}^C|^2}{\sum_{i=1}^6 |\gamma_{k,\mathcal{B}_i}^C|^2}\right). \tag{6.9}$$

We can see from (6.7) and (6.9) that the ergodic rates with SVD and BD are crucially determined by the ratio ξ of the number of BS antennas M to the total number of user antennas KN. Both rates grow unboundedly as $\xi \to \infty$. The rate performance of user k also closely depends on the large-scale fading coefficients $\gamma_{k,\mathcal{B}_i}^C$, $i = 0, \ldots, 6$, which, according to (2.10), are determined by user k's position $\mathbf{r}_k^U = (\rho_k, \theta_k)$. Specifically, we have

$$\begin{aligned}\frac{\sum_{i=1}^6 |\gamma_{k,\mathcal{B}_i}^C|^2}{|\gamma_{k,\mathcal{B}_0}^C|^2} = \sum_{i=1}^6 \rho_k^\alpha \big((\rho_k \cos(\theta_k) - 2\cos(i \cdot \tfrac{\pi}{3} - \tfrac{\pi}{6}))^2 \\ +(\rho_k \sin(\theta_k) - 2\sin(i \cdot \tfrac{\pi}{3} - \tfrac{\pi}{6}))^2\big)^{-\alpha/2}.\end{aligned} \tag{6.10}$$

It is clear from (6.10) that $\frac{\sum_{i=1}^6 |\gamma_{k,\mathcal{B}_i}^C|^2}{|\gamma_{k,\mathcal{B}_0}^C|^2}$ is a periodic function of period $\pi/3$ for any $\rho_k \in [0, 1]$. It is maximized when $\theta_k = i \cdot \frac{\pi}{3} - \frac{\pi}{6}$ and minimized when $\theta_k = i \cdot \frac{\pi}{3}$, $i = 1, \ldots, 6$. Let us focus on the worst case, i.e., $\theta_k = \pi/6$, in the following discussion. By substituting $\theta_k = \pi/6$ into (6.10), we have

$$\begin{aligned}\frac{\sum_{i=1}^6 |\gamma_{k,\mathcal{B}_i}^C|^2|_{\theta_k=\pi/6}}{|\gamma_{k,\mathcal{B}_0}^C|^2} = \rho_k^\alpha \big((2+\rho_k)^{-\alpha} + (2-\rho_k)^{-\alpha} + 2(\rho_k^2 + 4 + 2\rho_k)^{-\alpha/2} \\ +2(\rho_k^2 + 4 - 2\rho_k)^{-\alpha/2}\big).\end{aligned} \tag{6.11}$$

Appendix G shows that (6.11) is a monotonic increasing function of $\rho_k \in [0, 1]$ with

$$\min_{\rho_k} \frac{\sum_{i=1}^6 |\gamma_{k,\mathcal{B}_i}^C|^2|_{\theta_k=\pi/6}}{|\gamma_{k,\mathcal{B}_0}^C|^2} = 0, \tag{6.12}$$

achieved when $\rho_k = 0$, and

$$\max_{\rho_k} \frac{\sum_{i=1}^6 |\gamma_{k,\mathcal{B}_i}^C|^2|_{\theta_k=\pi/6}}{|\gamma_{k,\mathcal{B}_0}^C|^2} = 1 + 3^{-\alpha} + 2 \cdot 7^{-\alpha/2} + 2 \cdot 3^{-\alpha/2}, \tag{6.13}$$

achieved when $\rho_k = 1$. As a result, both $\mathcal{R}_{k,epa}^{SVD}|_{\theta_k=\pi/6}$ and $\mathcal{R}_{k,epa}^{BD}|_{\theta_k=\pi/6}$ decrease as user k moves away from BS 0. If the path-loss factor $\alpha = 4$, for instance, we

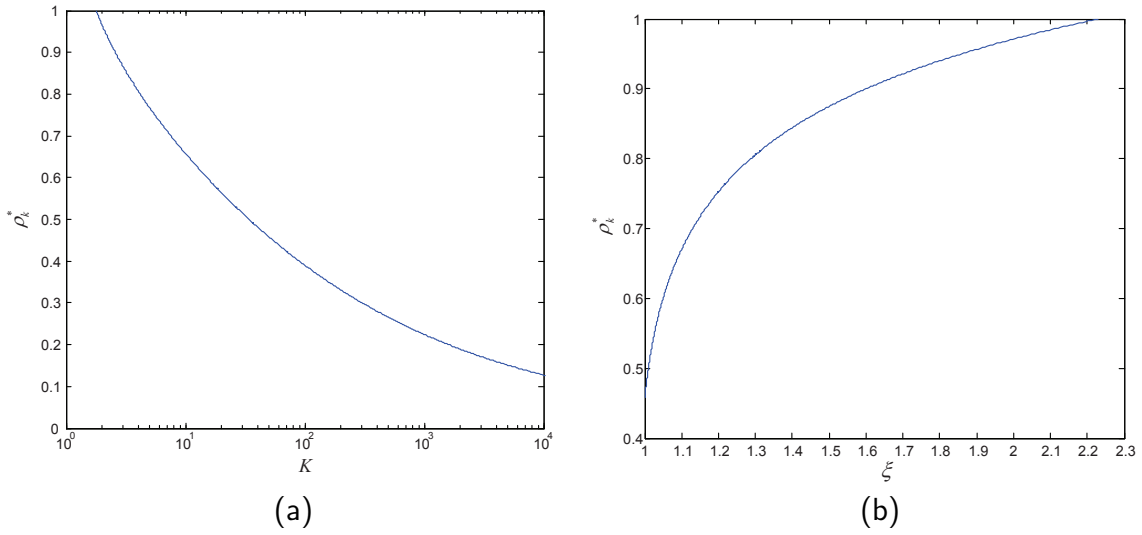

FIGURE 6.1: Crossing point ρ_k^* with path-loss factor $\alpha = 4$. (a) ρ_k^* versus number of users K. $\xi = 1$. (b) ρ_k^* versus ratio ξ. $K = 50$.

have

$$\max_{\rho_k} \mathcal{R}_{k,epa}^{MC-SVD-C}|_{\theta_k=\pi/6}^{\alpha=4} = \log_2(1+\xi), \tag{6.14}$$

$$\max_{\rho_k} \mathcal{R}_{k,epa}^{MC-BD-C}|_{\theta_k=\pi/6}^{\alpha=4} = \infty, \tag{6.15}$$

achieved when $\rho_k = 0$, and

$$\min_{\rho_k} \mathcal{R}_{k,epa}^{MC-SVD-C}|_{\theta_k=\pi/6}^{\alpha=4} = \log_2(1+0.44\xi), \tag{6.16}$$

$$\min_{\rho_k} \mathcal{R}_{k,epa}^{MC-BD-C}|_{\theta_k=\pi/6}^{\alpha=4} = \log_2\left(1+0.78\left(\xi-1+\frac{1}{K}\right)\right), \tag{6.17}$$

achieved when $\rho_k = 1$, by substituting (6.12) and (6.13) into (6.7) and (6.9), respectively.

We can conclude from (6.15) and (6.17) that the rate performance with BD may drastically deteriorate as user k moves away from BS 0. With SVD, the degradation is less significant because users suffer from severe intra-cell interference. For small ξ, nevertheless, a 50% decrease in the rate could still be observed according to (6.14) and (6.16) as ρ_k increases from 0 to 1. We can also see from (6.14-6.17) that although BD leads to a higher rate at the cell center, i.e., $\mathcal{R}_{k,epa}^{BD} \gg \mathcal{R}_{k,epa}^{SVD}$ at $\rho_k = 0$, better rate performance may be achieved with SVD at the cell edge if ξ is small. A closer look at (6.17) indicates that with $\xi = 1$, the rate of user at $\rho_k = 1$ with BD is approximately given by $1.13/K$, which is much lower than that with SVD when the number of users K is large.

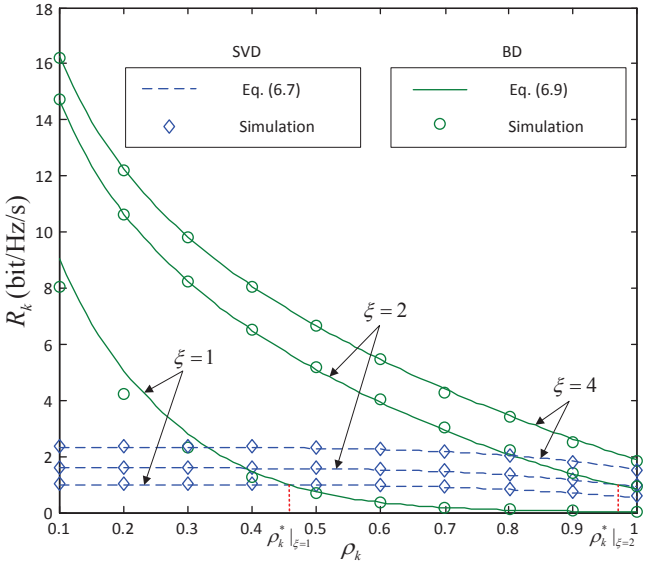

FIGURE 6.2: Ergodic rate versus radial coordinate ρ_k of user $k \in \mathcal{K}_0$ with equal power allocation in the CA layout. $\theta_k = \pi/6$. $\alpha = 4$. $N = 2$. $K = 50$. $P_t/N_0 = 20$dB. $M = 100, 200, 400$.

In particular, according to (6.7), (6.9) and (6.11), $\mathcal{R}_{k,epa}^{BD}|_{\theta_k=\pi/6} > \mathcal{R}_{k,epa}^{SVD}|_{\theta_k=\pi/6}$ if and only if $\rho_k < \rho_k^*$, where ρ_k^* is the root of the following equation:

$$\rho_k^{\alpha}\left((2+\rho_k)^{-\alpha} + (2-\rho_k)^{-\alpha} + 2(\rho_k^2+4+2\rho_k)^{-\alpha/2} + 2(\rho_k^2+4-2\rho_k)^{-\alpha/2}\right) = \frac{\xi - 1 + \frac{1}{K}}{1 - \frac{1}{K}}. \tag{6.18}$$

Fig. 6.1 illustrates how the crossing point ρ_k^* varies with the ratio ξ and the number of users K when the path-loss factor $\alpha = 4$. For instance, when $\xi = 1$, ρ_k^* becomes a monotonic decreasing function of K, which implies that most users with SVD may have better rate performance than that with BD if the number of users K is large. ρ_k^*, however, rapidly increases with ξ. As we can see from Fig. 6.1b, when $\xi > 2.23$, $\rho_k^* > 1$, indicating that a higher rate can be achieved by BD for all the users in the cell. As Fig. 6.2 shows, with $\xi = 4$, $\mathcal{R}_{k,epa}^{BD}$ is larger than $\mathcal{R}_{k,epa}^{SVD}$ for any $\rho_k \in [0, 1]$. With $\xi = 1$ and 2, the two curves cross at $\rho_k^* = 0.46$ and 0.97, respectively. Note that simulation results are also presented in Fig. 6.2 to verify the above analysis. As we can see from Fig. 6.2, the limiting results are accurate even when the number of user antennas N is small, i.e., $N = 2$, as long as the number of BS antennas $M \gg N$.

6.2.2 Channel-Inversion Power Allocation

We have shown that with equal power allocation, the ergodic rates with both SVD and BD drop as user k moves away from BS 0 due to decaying received power. In an interference-free network, the effect of large-scale fading can be compensated by allocating more transmit power to disadvantageous users such that the average received power of each user is a constant regardless of the user's position. As we will demonstrate in this section, the channel-inversion power allocation scheme still leads to serious unfairness for interference-limited MIMO cellular networks. To ensure that every user achieves the same rate, the average received SINR should be adjusted to a constant level. In the following, we will start from the rate analysis with channel-inversion power allocation.

Suppose that the transmit power for each user is properly adjusted such that the average received power of each user is a constant P_0 regardless of the user's position. That is,

$$\bar{P}_k \cdot |\gamma^C_{k,\mathcal{B}_0}|^2 = P_0, \tag{6.19}$$

$k \in \mathcal{K}_0$. Appendix H shows that with a large number of users K, P_0 can be obtained as

$$P_0 = \frac{P_t(1+\alpha/2)}{K}. \tag{6.20}$$

By combining (6.3) and (6.19-6.20), the normalized average received SINR $\bar{\mu}^{SVD}_{k,cpa}$ of user k with SVD in this case can be obtained as

$$\bar{\mu}^{MC-SVD-C}_{k,cpa} = \frac{\xi(1+\alpha/2)}{\frac{N_0}{P_t} + (|\gamma^C_{k,\mathcal{B}_0}|^2 - \frac{1+\alpha/2}{K}) + \sum_{i=1}^{6} |\gamma^C_{k,\mathcal{B}_i}|^2} \approx \frac{\xi\,(1+\alpha/2)}{K\sum_{i=0}^{6} |\gamma^C_{k,\mathcal{B}_i}|^2}, \tag{6.21}$$

for large $\frac{P_t}{N_0} \gg 1$ and $K \gg 1$. According to (6.2), the asymptotic ergodic rate of user k with SVD and channel-inversion power allocation can be written as

$$\mathcal{R}^{MC-SVD-C}_{k,cpa} = \log_2\left(1 + \xi \cdot \frac{1+\alpha/2}{\sum_{i=0}^{6} |\gamma^C_{k,\mathcal{B}_i}|^2}\right). \tag{6.22}$$

With BD, the average received SINR $\mu^{MC-BD-D}_{k,cpa}$ of user k can be obtained by combining (6.5) and (6.19-6.20) as

$$\bar{\mu}^{MC-BD-C}_{k,cpa} = \frac{\xi(1+\alpha/2)}{(\frac{N_0}{P_t} + \sum_{i=1}^{6} |\gamma^C_{k,\mathcal{B}_i}|^2)} \approx \frac{\xi(1+\alpha/2)}{\sum_{i=1}^{6} |\gamma^C_{k,\mathcal{B}_i}|^2}, \tag{6.23}$$

for large $\frac{P_t}{N_0} \gg 1$ and $K \gg 1$. According to (6.4), the asymptotic ergodic rate of user k with BD and channel-inversion power allocation can be written as

$$\mathcal{R}_{k,cpa}^{MC-BD-C} = \log_2\left(1 + \left(\xi - 1 + \frac{1}{K}\right) \cdot \frac{1+\alpha/2}{\sum_{i=1}^{6} |\gamma_{k,\mathcal{B}_i}^{C}|^2}\right). \tag{6.24}$$

As we have shown in (6.10), $\sum_{i=1}^{6} |\gamma_{k,\mathcal{B}_i}^{C}|^2$ is a periodic function of period $\pi/3$ for any $\rho_k \in [0,1]$. In the worst case, i.e., $\theta_k = \pi/6$, $\sum_{i=1}^{6} |\gamma_{k,\mathcal{B}_i}^{C}|^2|_{\theta_k=\pi/6}$ is a monotonic increasing function of $\rho_k \in [0,1]$ according to Appendix G, which is minimized at $6 \cdot 2^{-\alpha}$ when $\rho_k = 0$ and maximized at $1 + 3^{-\alpha} + 2 \cdot 7^{-\alpha/2} + 2 \cdot 3^{-\alpha/2}$ when $\rho_k = 1$. As a result, the corresponding asymptotic ergodic rate of user k with BD, $\mathcal{R}_{k,cpa}^{BD}|_{\theta_k=\pi/6}$, decreases as user k moves away from BS 0 according to (6.24). If the path-loss factor $\alpha = 4$, we have

$$\max_{\rho_k} \mathcal{R}_{k,cpa}^{MC-BD-C}|_{\theta_k=\pi/6}^{\alpha=4} = \log_2\left(1 + 8\left(\xi - 1 + \frac{1}{K}\right)\right), \tag{6.25}$$

achieved when $\rho_k = 0$, and

$$\min_{\rho_k} \mathcal{R}_{k,cpa}^{MC-BD-C}|_{\theta_k=\pi/6}^{\alpha=4} = \log_2\left(1 + 2.35\left(\xi - 1 + \frac{1}{K}\right)\right), \tag{6.26}$$

achieved when $\rho_k = 1$.

In contrast, Appendix G shows that $\sum_{i=0}^{6} |\gamma_{k,\mathcal{B}_i}^{C}|^2|_{\theta_k=\pi/6} = \rho_k^{-\alpha} + \sum_{i=1}^{6} |\gamma_{k,\mathcal{B}_i}^{C}|^2|_{\theta_k=\pi/6}$ is a monotonic decreasing function of $\rho_k \in [0,1]$. It becomes infinite when $\rho_k = 0$ and is minimized at $2 + 3^{-\alpha} + 2 \cdot 7^{-\alpha/2} + 2 \cdot 3^{-\alpha/2}$ when $\rho_k = 1$. Therefore, the ergodic rate of user k with SVD is improved as user k moves away from BS 0 according to (6.22). With $\alpha = 4$, we have

$$\max_{\rho_k} \mathcal{R}_{k,cpa}^{MC-SVD-C}|_{\theta_k=\pi/6}^{\alpha=4} = \log_2\left(1 + 1.32\xi\right), \tag{6.27}$$

achieved when $\rho_k = 1$, and

$$\min_{\rho_k} \mathcal{R}_{k,cpa}^{MC-SVD-C}|_{\theta_k=\pi/6}^{\alpha=4} = 0, \tag{6.28}$$

achieved when $\rho_k = 0$.

Recall that with the channel-inversion power allocation scheme in (6.19), the transmit power allocated to user k is inversely proportional to its large-scale fading

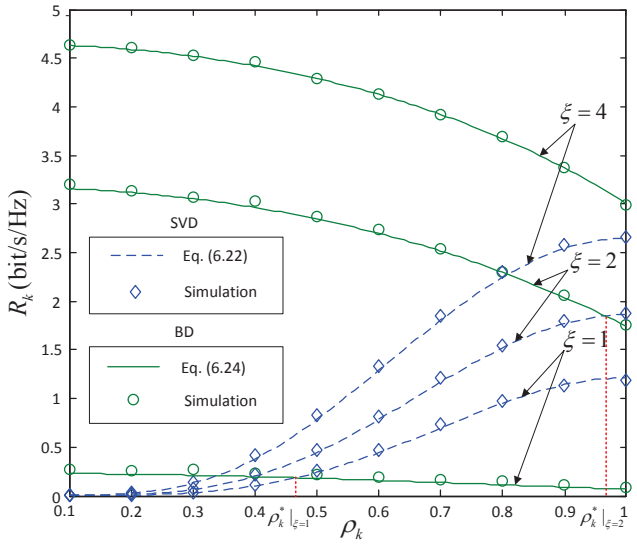

FIGURE 6.3: Ergodic rate versus radial coordinate ρ_k of user $k \in \mathcal{K}_0$ with channel-inversion power allocation in the CA layout. $\theta_k = \pi/6$. $\alpha = 4$. $N = 2$. $K = 50$. $P_t/N_0 = 20$dB. $M = 100, 200, 400$.

gain so as to maintain a constant average received power. If SVD is adopted, users closer to the cell center would suffer from higher intra-cell interference, and thus have even worse performance than those cell-edge users. With BD, on the other hand, users are subject to only inter-cell interference that becomes increasingly stronger as ρ_k grows. Performance degradation is, hence, incurred at the cell edge. It can be easily shown from (6.22) and (6.24) that the two rate curves again cross at ρ_k^*, which is given in (6.18).

Fig. 6.3 illustrates the rate performance with channel-inversion power allocation. We can clearly see from Fig. 6.3 that despite a constant average received power, the rates with both SVD and BD significantly vary with the distance ρ_k from BS 0 to user k, and a large rate gap between cell-center users and cell-edge users is observed in both cases. In fact, (6.2) and (6.4) have revealed that the key to a uniform rate lies in the SINR. If the transmit power for each user is properly adjusted such that the normalized average received SINR becomes a constant independent of the user's position, a uniform rate can be achieved.

6.2.3 Interference-Aware Power Allocation

As SVD and BD lead to distinct SINRs, let us first focus on the SVD case. Suppose that the normalized average received SINR of user k is fixed at a constant

level $\bar{\mu}_0^{MC-SVD-C}$. According to (6.3), the transmit power for user k should be set as

$$\bar{P}_k = \frac{\bar{\mu}_0^{MC-SVD-C}\left(N_0 + \sum_{i=0}^{6}|\gamma_{k,\mathcal{B}_i}^C|^2 P_t\right)}{(\xi K + \bar{\mu}_0^{MC-SVD-C})|\gamma_{k,\mathcal{B}_0}^C|^2}. \tag{6.29}$$

Appendix H shows that for large $\frac{P_t}{N_0} \gg 1$ and $K \gg 1$, $\bar{\mu}_0^{MC-SVD-C}$ is approximately given by

$$\bar{\mu}_0^{MC-SVD-C} \approx \frac{\xi}{\Upsilon(\alpha) + 1 - \frac{1}{K}}, \tag{6.30}$$

where $\Upsilon(\alpha)$ is a monotonic decreasing function of the path-loss factor α:

$$\Upsilon(\alpha) = \frac{6}{\pi}\int_0^{2\pi}\int_0^1 x^{\alpha+1}(x^2 + 4 - 4x\sin y)^{-\alpha/2}dxdy. \tag{6.31}$$

In this case, the asymptotic ergodic rate of user k with SVD can be written as

$$\mathcal{R}_{k,ipa}^{MC-SVD-C} = \log_2\left(1 + \frac{\xi}{\Upsilon(\alpha) + 1 - \frac{1}{K}}\right), \tag{6.32}$$

by combining (6.30) and (6.2).

With BD, according to (6.5), the transmit power for user k should be set as

$$\bar{P}_k = \frac{\bar{\mu}_0^{MC-BD-C}\left(N_0 + \sum_{i=1}^{6}|\gamma_{k,\mathcal{B}_i}^C|^2 P_t\right)}{\xi K|\gamma_{k,\mathcal{B}_0}^C|^2} \tag{6.33}$$

to achieve a constant SINR $\bar{\mu}_0^{MC-BD-C}$. Appendix H shows that for large $\frac{P_t}{N_0} \gg 1$ and $K \gg 1$, $\bar{\mu}_0^{MC-BD-C}$ is approximately given by

$$\bar{\mu}_0^{MC-BD-C} \approx \frac{\xi}{\Upsilon(\alpha)}. \tag{6.34}$$

The corresponding asymptotic ergodic rate of user k can be then written as

$$\mathcal{R}_{k,ipa}^{MC-BD-C} = \log_2\left(1 + \frac{\xi - 1 + \frac{1}{K}}{\Upsilon(\alpha)}\right), \tag{6.35}$$

by combining (6.34) and (6.4).

It is interesting to note from (6.35) that when $\xi = 1$, the sum rate $K\mathcal{R}_{k,ipa}^{MC-BD-C}$ with BD approaches a constant $\frac{\log_2 e}{\Upsilon(\alpha)}$ as the number of users K increases to infinity, which is consistent with [35] where the sum rate with zero-forcing beamforming

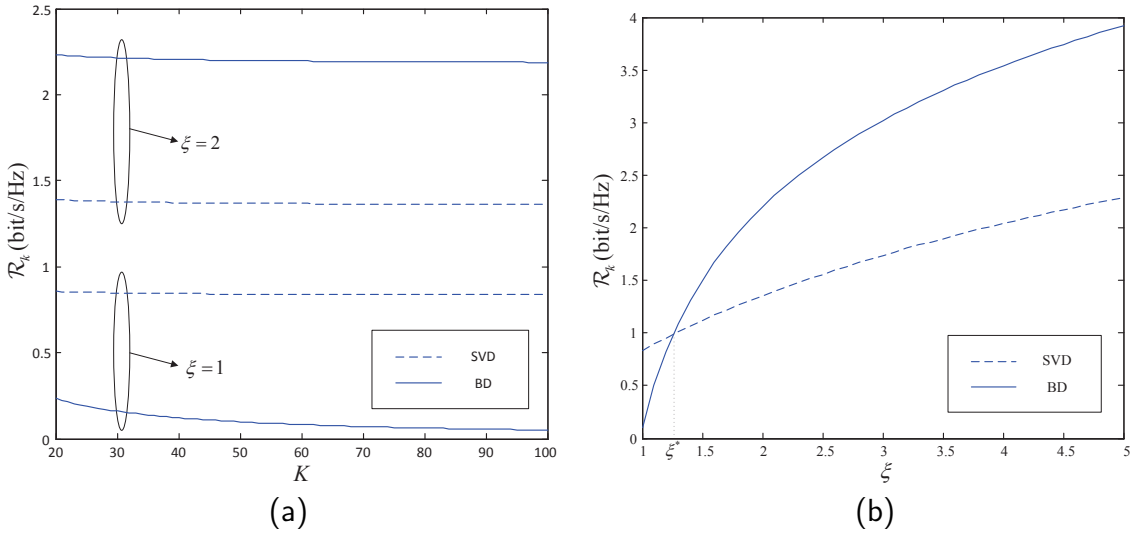

FIGURE 6.4: Asymptotic ergodic rate with interference-aware power allocation in the CA layout. $\alpha = 4$. (a) $\xi = 1$ and 2. (b) $K = 50$.

is shown to be a constant as $K \to \infty$ if $M = K$. In a sharp contrast, a linear growth of the sum rate with K can always be achieved with SVD because $K\mathcal{R}_{k,ipa}^{MC-SVD-C} \approx K \log_2(1 + \frac{\xi}{\Upsilon(\alpha)+1})$ for large K according to (6.32).

We can clearly see from (6.32) and (6.35) that with the proposed interference-aware power allocation scheme, the rate performance becomes independent of user k's position. Both $\mathcal{R}_{k,ipa}^{MC-SVD-C}$ and $\mathcal{R}_{k,ipa}^{MC-BD-C}$ logarithmically increase with the ratio ξ of the number of BS antennas M and the total number of receive antennas KN. A closer look at (6.32) and (6.35) indicates that BD may lead to worse performance than SVD if ξ is small. In particular, $\mathcal{R}_{k,ipa}^{MC-BD-C} > \mathcal{R}_{k,ipa}^{MC-SVD-C}$ if and only if $\xi > \xi^*$, where ξ^* is the root of the following equation:

$$\xi^* = \Upsilon(\alpha) + 1 - \frac{1}{K}. \tag{6.36}$$

Fig. 6.4 illustrates the rate performance when the path-loss factor $\alpha = 4$. In this case, $\Upsilon(4) = 0.284$ and we have

$$\mathcal{R}_{k,ipa}^{MC-SVD-C}|^{\alpha=4} = \log_2\left(1 + \frac{\xi}{1.284 - \frac{1}{K}}\right), \tag{6.37}$$

and

$$\mathcal{R}_{k,ipa}^{MC-BD-C}|^{\alpha=4} = \log_2\left(1 + 3.52\left(\xi - 1 + \frac{1}{K}\right)\right). \tag{6.38}$$

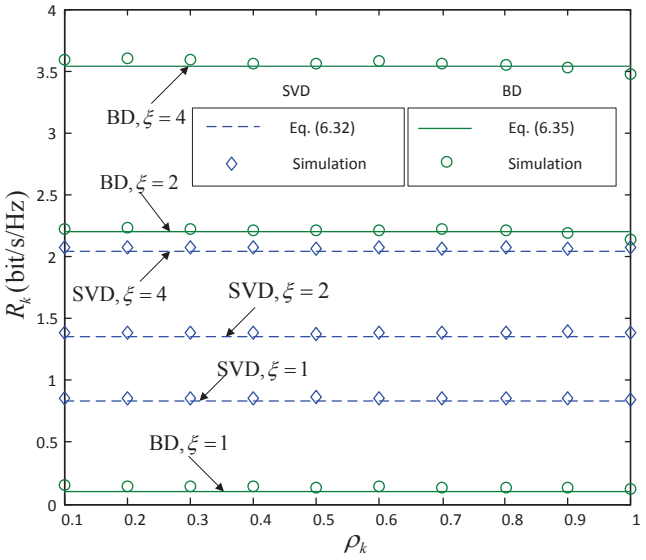

FIGURE 6.5: Ergodic rate versus radial coordinate ρ_k of user $k \in \mathcal{K}_0$ with interference-aware power allocation in the CA layout. $\alpha = 4$. $N = 2$. $K = 50$. $P_t/N_0 = 20$dB. $M = 100, 200, 400$.

With $\xi = 1$, for instance, $\mathcal{R}_{k,ipa}^{MC-SVD-C}|^{\alpha=4}$ and $\mathcal{R}_{k,ipa}^{MC-BD-C}|^{\alpha=4}$ are approximately given by 0.83 and $5/K$, respectively, for a large number of users K. As we can see from Fig. 6.4a, the asymptotic ergodic rate with BD rapidly drops as K grows, and is much lower than that with SVD. It is, nevertheless, significantly improved when ξ increases to 2. As Fig. 6.4b shows, $\mathcal{R}_{k,ipa}^{MC-BD-C}|^{\alpha=4}$ is higher than $\mathcal{R}_{k,ipa}^{MC-SVD-C}|^{\alpha=4}$ if $\xi > \xi^* = 1.26$. The analysis is verified by simulation results presented in Fig. 6.5.

6.3 Ergodic Rate with the DA Layout

So far we have characterized the ergodic rate with the CA layout, which is shown to be crucially determined by the power allocation strategies. With equal power allocation, for instance, the ergodic rate of each user decreases drastically as the user moves towards the cell edge when BD is adopted. With interference-aware power allocation, on the other hand, a uniform ergodic rate can be achieved by equalizing the average received SINR. In this section, we will further focus on the effect of power allocation on the rate performance with the DA layout. For illustration, the ergodic rate with equal power allocation will be first discussed.

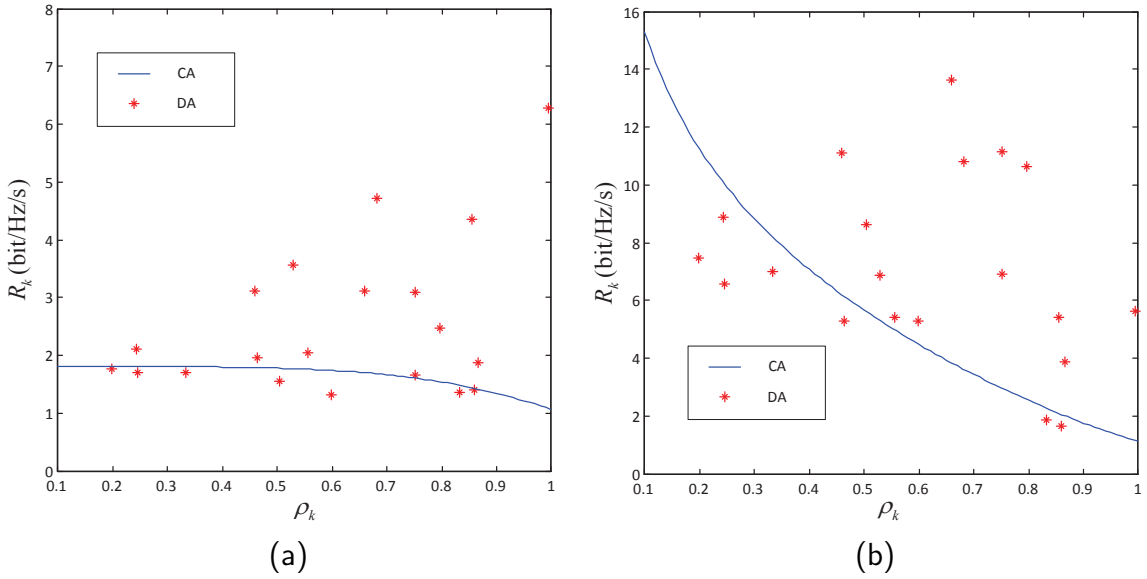

FIGURE 6.6: Simulated ergodic rate versus radial coordinate ρ_k of user $k \in \mathcal{K}_0$ with equal power allocation in the DA layout. $P_t/N_0 = 10$dB. $N = 2$. $L = 50$. $M = 100$. $K = 20$. $\alpha = 4$. (a) SVD. (b) BD.

6.3.1 Equal Power Allocation

In contrast to the CA case where the ergodic rates with SVD and BD can be obtained as explicit functions of the large-scale fading coefficients, with the DA layout, we can only present simulation results. Fig. 6.6 shows the simulated ergodic rates with equal power allocation in the DA layout with SVD and BD. For the sake of comparison, the asymptotic ergodic rates with equal power allocation in the CA layout given in (6.7) and (6.9) are also plotted.

As we can see from Fig. 6.6, although the ergodic rate with the DA layout is better than that with the CA layout on average, it varies significantly with the radial coordinate ρ_k of the user. With SVD, for instance, different from the CA case where the ergodic rate only slightly decreases as ρ_k increases, a large rate variance is observed in the DA case. Moreover, with the CA layout, the ergodic rates with both SVD and BD decrease monotonically as the radial coordinate ρ_k increases. With the DA layout, however, no such monotonicity can be observed. In this case, the ergodic rate is closely dependent on the minimum access distance which could be small even for a cell-edge user as long as it is close to some BS antenna cluster.

Fig. 6.6 indicates that in both the SVD and BD cases, the ergodic rate with the DA layout is more sensitive to the user's position than that with the CA

layout. In the following section, we will further study how to equalize the rate performance with the DA layout.

6.3.2 Interference-Aware Power Allocation

With the CA layout, it has been shown in Section 6.2.3 that a uniform ergodic rate can be achieved by maintaining a constant average received SINR for each user. In that case, the transmit power for each user can be calculated only based on the large-scale fading coefficients from the user to its own and neighboring BSs, i.e., (6.29) with SVD and (6.33) with BD. With the DA layout, in contrast, in addition to the average received SINR, the ergodic rate is further determined by the eigenvalue distribution of normalized channel gain matrix $\tilde{\mathbf{G}}_{k,\mathcal{B}_0}\tilde{\mathbf{G}}_{k,\mathcal{B}_0}^{\dagger}$ which also depends on the positions of distributed BS antenna clusters. Therefore, the ergodic rate of each user could be sensitive to its position even when the average received SINR is kept constant. To achieve a uniform rate, the instantaneous received SINR of each user should be equalized based on the knowledge of instantaneous CSI between the user and its own BS.

For illustration, in this section, we only focus on the single-antenna case, i.e., the number of user antennas $N = 1$. In this case, the channel gain matrix and the precoding matrix reduce to vectors, denoted by $\mathbf{g}_{k,\mathcal{B}_i}$ and $\mathbf{w}_k$, respectively, $i = 1, \cdots, 6$. According to (2.6), the ergodic rate can be written as

$$R_k^{MC-D}|_{N=1} = \mathbb{E}_{\mathbf{h}_{k,\mathcal{B}_0}}\left[\log_2\left(1+\tilde{\mu}_k^{MC-D}\right)\right], \tag{6.39}$$

where $\tilde{\mu}_k^{MC-D}$ denotes the instantaneous received SINR, which is given by

$$\tilde{\mu}_k^{MC-D} = \frac{\bar{P}_k|\mathbf{g}_{k,\mathcal{B}_0}\mathbf{w}_k|^2}{N_0 + \sum_{j\in\mathcal{K}_0, j\neq k}|\mathbf{g}_{k,\mathcal{B}_0}\mathbf{w}_j|^2\bar{P}_j + P_k^{int,D}P_t}, \tag{6.40}$$

where $P_k^{int,D}$ denotes the normalized inter-cell interference power, which can be written as

$$P_k^{int,D} = \frac{1}{P_t}\mathbb{E}\left[\sum_{i=1}^{6}\sum_{j\in\mathcal{K}_i}|\mathbf{g}_{k,\mathcal{B}_i}\mathbf{w}_j|^2\bar{P}_j\right], \tag{6.41}$$

according to (2.1), when $N = 1$.

In contrast to the CA layout where the normalized inter-cell interference power $P_k^{int,C}$ can be obtained as a function of the large-scale fading coefficients from

the user to BSs as shown in (6.1), with the DA layout, $P_k^{int,D}$ further depends on the transmit power $\bar{P}_j$ and the precoding vector $\mathbf{w}_j$ for each user in the neighboring cells, which are unknown without BS cooperation. To obtain the inter-cell interference power level of each user, we assume that each user measures its interference level and feeds back to its BS. With SVD, as the intra-cell interference level of each user can be calculated at the BS, the inter-cell interference $P_k^{int,D}$ can be obtained by subtracting the intra-cell interference from the total feedback interference. With BD, the inter-cell interference $P_k^{int,D}$ equals the feedback interference.

As SVD and BD lead to distinct SINRs, let us first focus on the SVD case.

6.3.2.1 SVD

According to (3.19), the precoding matrix $\mathbf{W}_k^{SVD}$ reduces to

$$\mathbf{w}_k^{SVD} = \frac{\mathbf{g}_{k,\mathcal{B}_0}^{\dagger}}{\|\mathbf{g}_{k,\mathcal{B}_0}\|}, \tag{6.42}$$

$k \in \mathcal{K}_0$, when $N = 1$. The instantaneous received SINR $\tilde{\mu}_k^{MC-SVD-D}$ can be then written as

$$\tilde{\mu}_k^{MC-SVD-D} = \frac{\|\mathbf{g}_{k,\mathcal{B}_0}\|^2 \bar{P}_k}{N_0 + P_k^{int,D} P_t + \sum_{j \in \mathcal{K}_0, j \neq k} \frac{\|\mathbf{g}_{k,\mathcal{B}_0} \mathbf{g}_{j,\mathcal{B}_0}^{\dagger}\|^2}{\|\mathbf{g}_{j,\mathcal{B}_0}\|^2} \bar{P}_j}, \tag{6.43}$$

by combining (6.42) and (6.40).

Suppose that the instantaneous received SINR of each user is kept at a constant level $\tilde{\mu}_0^{MC-SVD-D}$. The transmit power for user k, $\bar{P}_k$, should be then set as

$$\bar{P}_k = \frac{\tilde{\mu}_0^{MC-SVD-D} \left(N_0 + P_k^{int,D} P_t + \sum_{j \in \mathcal{K}_0, j \neq k} \frac{\|\mathbf{g}_{k,\mathcal{B}_0} \mathbf{g}_{j,\mathcal{B}_0}^{\dagger}\|^2}{\|\mathbf{g}_{j,\mathcal{B}_0}\|^2} \bar{P}_j \right)}{\|\mathbf{g}_{k,\mathcal{B}_0}\|^2}, \tag{6.44}$$

according to (6.43), $k = 1, \cdots, K$. As the total transmit power of each cell is P_t, by combining (6.44) and (2.5), we have

$$\tilde{\mu}_0^{MC-SVD-D} = \frac{P_t}{\sum_{k\in\mathcal{K}_0} \frac{N_0 + P_k^{int,D} P_t + \frac{\|\mathbf{g}_{k,\mathcal{B}_0} \mathbf{g}_{j,\mathcal{B}_0}^{\dagger}\|^2}{\|\mathbf{g}_{j,\mathcal{B}_0}\|^2} \bar{P}_j}{\|\mathbf{g}_{k,\mathcal{B}_0}\|^2}}. \tag{6.45}$$

Finally, by combining (6.44-6.45), the constant instantaneous received SINR $\tilde{\mu}_0^{MC-SVD-D}$ and the transmit power for K users, $\{\bar{P}_k\}_{k\in\mathcal{K}_0}$, can be jointly calculated from the $K+1$ equations.

6.3.2.2 BD

According to (4.8), the precoding matrix $\mathbf{W}_k^{BD}$ reduces to

$$\mathbf{w}_k^{BD} = \frac{\mathbf{f}_k}{\|\mathbf{f}_k\|}, \tag{6.46}$$

$k \in \mathcal{K}_0$, when $N = 1$, where $\mathbf{f}_k$ is the k-th column vector of $\mathbf{F}$, which is defined as

$$\mathbf{F} = \mathbf{G}_{\mathcal{B}_0}^{\dagger} \left(\mathbf{G}_{\mathcal{B}_0} \mathbf{G}_{\mathcal{B}_0}^{\dagger} \right)^{-1}, \tag{6.47}$$

with $\mathbf{G}_{\mathcal{B}_0} = \left[\mathbf{g}_{1,\mathcal{B}_0}^T, \mathbf{g}_{2,\mathcal{B}_0}^T, \cdots, \mathbf{g}_{K,\mathcal{B}_0}^T \right]^T$. The instantaneous received SINR $\tilde{\mu}_k^{MC-BD-D}$ can be then written as

$$\tilde{\mu}_k^{MC-BD-D} = \frac{\bar{P}_k}{\|\mathbf{f}_k\|^2 \left(N_0 + P_k^{int,D} P_t \right)}, \tag{6.48}$$

by combining (6.46) and (6.40).

Suppose that the instantaneous received SINR of each user is fixed at a constant level $\tilde{\mu}_0^{MC-BD-D}$. The transmit power for user k should be set as

$$\bar{P}_k = \tilde{\mu}_0^{MC-BD-D} \|\mathbf{f}_k\|^2 \left(N_0 + P_k^{int,D} P_t \right), \tag{6.49}$$

according to (6.48), $k = 1, \cdots, K$. As the total transmit power of each cell is P_t, by combining (6.49) and (2.5), we have

$$\tilde{\mu}_0^{MC-BD-D} = \frac{P_t}{\sum_{k=1}^{K} \|\mathbf{f}_k\|^2 \left(N_0 + P_k^{int,D} P_t \right)}. \tag{6.50}$$

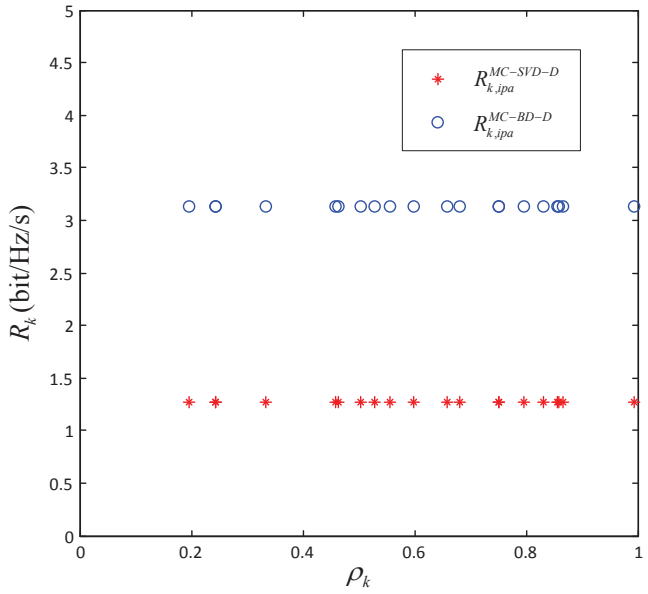

FIGURE 6.7: Simulated ergodic rates with SVD and BD versus radial coordinate ρ_k of user $k \in \mathcal{K}_0$ with interference-aware power allocation in the DA layout. $N = 1$. $L = 50$. $K = 20$. $\alpha = 4$. $P_t/N_0 = 10$dB.

Finally, the transmit power for K users, i.e., $\{\bar{P}_k\}_{k\in\mathcal{K}_0}$, can be obtained by substituting (6.50) into (6.49).

Fig. 6.7 plots the ergodic rate with interference-aware power allocation in the DA layout. Simulation results verify that with the proposed interference-aware power allocation, i.e., (6.44) for SVD and (6.49) for BD, the rate performance is independent of the user's position in both the SVD and BD cases.

6.4 Discussions

To better understand the effect of power allocation, Fig. 6.8 presents the average ergodic rates with equal power allocation and interference-aware power allocation in the DA layout, which are obtained by averaging over 100 realizations of the positions of users and BS antennas. With the CA layout, the asymptotic ergodic rates are obtained in (5.15) and (5.20) for SVD and BD with equal power allocation, and (6.32) and (6.35) for SVD and BD with interference-aware power allocation, respectively.

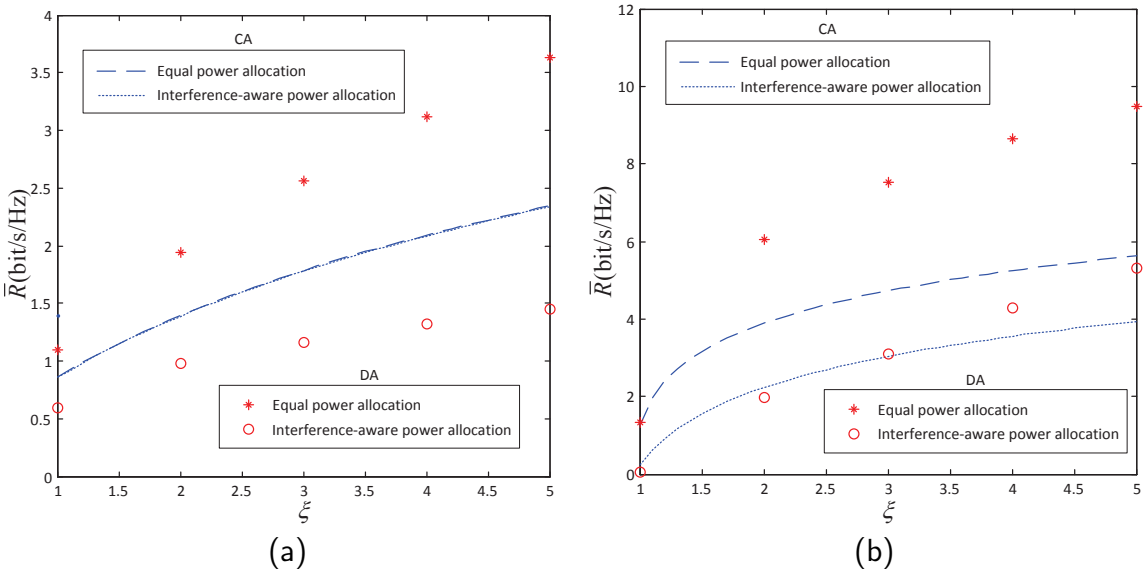

FIGURE 6.8: Simulated average ergodic rates with the DA layout and asymptotic average ergodic rates with the CA layout with equal power allocation and interference-aware power allocation. $P_t/N_0 = 10$dB. $N = 1$. $K = 20$. $\alpha = 4$. (a) SVD. (b) BD.

As we can see from Fig. 6.8, in both the CA and DA cases, the average ergodic rate with equal power allocation is higher than that with interference-aware power allocation, which indicates a fundamental tradeoff between fairness and the average rate performance. More specifically, with BD, for instance, equal power allocation leads to serious unfairness, as the cell-edge users are subject to stronger inter-cell interference and have much worse rate performance than the cell-center users. To achieve a uniform rate, more transmit power has to be allocated to those disadvantageous users, thus dragging down the average rate. With SVD, the tradeoff becomes less significant because the intra-cell interference is so dominant that the SINR does not vary that much with the user's position under equal power allocation.

It can be further observed from Fig. 6.8 that the rate gap between equal power allocation and interference-aware power allocation is much more significant in the DA case. With SVD, for instance, the gap is negligible in the CA case as the ergodic rate barely changes with the radial coordinate ρ_k when equal power allocation is adopted. With the DA layout, recall from Fig. 6.6a that a large rate variance is observed with equal power allocation. To achieve a uniform rate, a significant amount of transmit power has to be allocated to the users with weaker desired signal power and/or stronger interference to overcome the rate difference,

thus leading to a much lower average ergodic rate with interference-aware power allocation. In fact, we can see from Fig. 6.8a that the average ergodic rate with SVD in the DA layout is even inferior to that with the CA layout when interference-aware power allocation is adopted. With BD, the rate gap between equal power allocation and interference-aware power allocation is also more significant with the DA layout due to a larger rate difference with equal power allocation as shown in Fig. 6.6b.

Also note from Fig. 6.8 that with the CA layout, the rate gap between equal power allocation and interference-aware power allocation almost remains constant as the ratio ξ of the number of BS antennas to the total number of user antennas increases. With the DA layout, on the other hand, the gap further increases with the ratio ξ, which indicates a significant tradeoff between fairness and average rate performance when the number of BS antennas is large. It also implies that fairness should be included as an important and indispensable constraint when optimizing the rate performance of MIMO cellular networks if a large number of distributed BS antennas are employed.

6.5 Summary

In this chapter, the effect of power allocation on ergodic rate is studied. As users at different locations have distinct large-scale fading coefficients, the ergodic rate of each user may vary remarkably with its position in both the CA and DA cases if equal power allocation is adopted. To equalize the rate performance, interference-aware power allocation schemes are proposed. It is shown that with the CA layout, a uniform ergodic rate can be achieved as long as the average received SINR is kept constant. With the DA layout, in contrast, the power allocation needs to be performed based on the instantaneous CSI.

Despite the better fairness, the average rate with interference-aware power allocation could be substantially lower than that with equal power allocation. The rate gap between equal power allocation and interference-aware power allocation becomes more significant with the DA layout, and is further enlarged as the ratio ξ of the number of BS antennas to the number of user antennas increases. It highlights the importance of including fairness into system design for MIMO cellular networks with a large number of distributed BS antennas.

Chapter 7

Conclusion and Future Work

7.1 Conclusion

Owing to its great potential for capacity gains, MIMO technology has attracted extensive attention in the past decade, and has been adopted in current cellular systems. To support the massive mobile applications, a large number of BS antennas are expected to be employed in the next-generation cellular systems to provide a high data rate. With the co-located BS antennas, better rate performance can be achieved than the single-antenna system thanks to its diversity and spatial multiplexing gains. If the BS antennas are grouped into geographically distributed clusters, the minimum access distance from each user to BS antennas can be significantly reduced, and thus substantial rate gains can be expected over that with the co-located ones. Nevertheless, the implementation cost of distributed BS antennas is much higher than that of co-located ones as it is incompatible with the current cellular structure. It is, therefore, of great practical importance to compare the rate performance of MIMO cellular networks under different BS antenna layouts to justify the increased cost.

This thesis is devoted to a comparative study of the downlink performance of a 1-tier (7-cell) MIMO cellular network with a massive number of BS antennas which are either co-located at the center of each cell or grouped into L uniformly distributed clusters in the inscribed circle of each cell. The scaling behavior of the average ergodic rate is first studied. In the single-user case, by assuming that the number of BS antennas M and the number of user antennas N go to infinity with $M/N \to \xi \gg 1$, the asymptotic average ergodic capacity with the CA layout and

an asymptotic lower-bound of the average ergodic capacity with the DA layout are developed. The analysis reveals that the average ergodic capacities without and with CSIT in the CA case have the scaling orders of $\Theta(1)$ and $\Theta\left(\log_2 \xi\right)$, respectively. With the DA layout, higher scaling orders can be achieved, which are found to be $\Theta\left(\left(\frac{\alpha}{2}-1\right)\log_2 \xi\right)$ and $\Theta\left(\frac{\alpha}{2}\log_2 \xi\right)$ for the average ergodic capacities without and with CSIT, respectively, where $\alpha > 2$ is the path-loss factor. Substantial gains can be achieved with the DA layout when the number of BS antennas is large thanks to the reduced minimum access distance.

The analysis is further extended to a K-user MIMO cellular system. In the single-cell case, by assuming that the number of BS antennas M and the number of user antennas N go to infinity with $M/N \to \xi K \gg 1$, the asymptotic average ergodic rates with the CA layout are derived in both the SVD and BD cases. With the DA layout, asymptotic bounds are developed to study the scaling behavior. The analysis reveals that the scaling behavior of the average ergodic rate in the multi-user case is crucially determined by the precoding strategies. With SVD, the average ergodic rates with the CA and DA layouts scale with the ratio ξ in the orders of $\Theta\left(\log_2 \xi\right)$ and $\Theta\left(\frac{\alpha}{2}\log_2 \xi\right)$, respectively. With BD, the scaling orders are found to be $\Theta\left(\log_2 \xi\right)$ and $\Theta\left(\log_2\left(\xi L^{\frac{\alpha}{2}-1}\right)\right)$ in the CA and DA cases, respectively. In the multi-cell case, although the rate performance is degraded by the inter-cell interference, the scaling orders are the same as the single-cell case.

The above analysis reveals that the DA layout always achieves better average rate performance, and the rate gain over the CA layout increases as more BS antennas are employed. For the next-generation cellular networks where a large number of BS antennas are expected to be deployed to meet the ever-increasing demand for high data rates, such a prominent rate gain may serve as a strong justification for the high implementation cost of distributed BS antennas.

Despite the better average rate performance with the DA layout, users at different locations have distinct large-scale fading coefficients, leading to a significant rate difference when equal power allocation is adopted. To achieve a uniform rate, the transmit power should be carefully adjusted to maintain a constant received SINR at each user, which, on the other hand, may cause substantial degradation of the average ergodic rate compared to that with equal power allocation in both the CA and DA cases. With the DA layout, the rate gap between equal power allocation and interference-aware power allocation becomes more significant in both

the SVD and BD cases, and further increases as the ratio ξ of the number of BS antennas to the number of user antennas grows.

To conclude, the main contributions of this thesis are summarized as follows:

1. In the single-user case, the effect of CSIT on the scaling behavior of the average ergodic capacities with the CA and DA layouts is studied. The asymptotic average ergodic capacity with the CA layout and an asymptotic lower-bound of the average ergodic capacity with the DA layout are derived for the cases with and without CSIT. The analysis shows that the average ergodic capacity with the DA layout has a higher scaling order than that with the CA layout regardless of whether CSIT is available or not.

2. In the multi-user single-cell case, the effect of precoding schemes on the scaling behavior of the average ergodic rates with the CA and DA layouts is studied. Explicit expressions of the asymptotic average ergodic rates with SVD and BD are derived in the CA case. With the DA layout, an asymptotic upper-bound of the average ergodic rate with SVD and an asymptotic lower-bound of the average ergodic rate with BD are developed to characterize the scaling orders. The analysis reveals that higher scaling orders can be achieved with the DA layout, and the rate gain becomes more prominent when an orthogonal precoding scheme such as BD is adopted.

3. In the multi-user multi-cell case, the inter-cell interference is studied in both the CA and DA cases. It is found that the mean of the inter-cell interference power with the DA layout is higher than that with the CA layout, and its variance increases unboundedly as the user moves towards the cell edge. Yet the scaling orders of the average ergodic rates with the CA and DA layouts in both the SVD and BD cases are not affected by the inter-cell interference in the multi-cell case.

4. The effect of power allocation on the ergodic rates with the CA and DA layouts is studied. With the CA layout, explicit expressions for the asymptotic average ergodic rates with SVD and BD under equal power allocation, channel-inversion power allocation and interference-aware power allocation are derived. It is shown that with the proposed interference-aware power allocation, a uniform ergodic rate can be achieved by adjusting the transmit power for each user only based on the large-scale fading coefficients to its

own and neighboring BSs. With the DA layout, the ergodic rates with SVD and BD are shown to be more sensitive to the user's position than that in the CA case if equal power allocation is adopted. To achieve a uniform rate, the transmit power for each user needs to be adjusted based on the knowledge of its inter-cell interference and instantaneous CSI to maintain a constant instantaneous received SINR.

5. A comparison of the average ergodic rates with equal power allocation and interference-aware power allocation in both the CA and DA cases is presented, which indicates a fundamental tradeoff between fairness and average rate performance in MIMO cellular networks. With the DA layout, the tradeoff is more evident, and becomes more significant as the ratio of the number of BS antennas to the total number of user antennas increases, which highlights the importance of including fairness as an indispensable constraint in the cellular system design when a large number of distributed BS antennas is employed.

7.2 Future Work

The work in this thesis only provides a starting point. In the future, the analysis should be extended to more practical scenarios. Specifically, when modeling the large-scale fading effect, we only consider the path loss and ignore the shadowing effect in this thesis. Although the log-normal shadowing may not change the scaling behavior of the average rate performance, the additional diversity gains could improve the performance with the DA layout. It would be of great practical importance to further incorporate shadowing into the rate analysis.

Moreover, in Chapter 4 and Chapter 5, for analytical tractability, the average rate performance with the DA layout is characterized by assuming an equal number of antennas at each user and each cluster. For a given amount of BS antennas, how many BS antennas should be employed at each cluster is a fundamental issue to be addressed. In the single-user case, we have shown in Chapter 3 that the average ergodic capacity is maximized if each cluster has one single BS antenna. In the multi-user case, how the rate performance varies with the cluster size may depend on the precoding schemes, which needs to be further explored.

In Chapter 6, the proposed interference-aware power allocation scheme for the DA case only focuses on the MISO case where each user is assumed to be equipped with a single antenna, and the rate is equalized by keeping the SINR of each user at the same constant level. In the next-generation cellular systems, multiple antennas are expected to be employed at each user to provide high data rates. In this case, the SINRs of multiple sub-channels of each user should be jointly adjusted to achieve a uniform rate, which is a challenging issue that deserves much attention in future study.

In Chapter 5 and Chapter 6, we assume that no BS cooperation is adopted. In current cellular systems, BS cooperation has been included in the LTE standard to improve the cell-edge performance [2]. The performance with BS cooperation was usually evaluated under simplified models with a small group of users and BS antennas even in the CA case [68–76]. With the DA layout, the analysis becomes much more challenging as the large-scale fading coefficients are further dependent on the positions of BS antenna clusters. For a complete comparison, it would be important to extend the rate analysis in this thesis to the case with BS cooperation in the future, and investigate the effect of different levels of BS cooperation on the rate performance of MIMO cellular networks with massive BS antennas.

Finally, it should be mentioned that although a 1-tier cellular model with regular cell boundaries is assumed in this thesis, such a geographic division of cells becomes less justified with the DA layout. As pointed out in [84], with distributed BS antennas, it would be difficult to determine where to place the cell center and where the cell edge should be. Instead of dividing cells according to the geographic boundaries, the cells could be formed in a user-centric manner, where each user could choose its serving BS antenna set to form a virtual cell. In the future, it would be important to extend the analysis to a large-scale distributed antenna system with virtual cells, and study the how the scaling behavior of the average rate performance varies with the size of virtual cells.

Appendix A

Derivation of (2.15)

In each cell, BS antenna clusters are uniformly distributed over the inscribed circle with radius 1 centered at O_i, where $O_0 = (0, 0)$ and $O_i = (2, i \cdot \frac{\pi}{3} - \frac{\pi}{6})$ for $i = 1, \cdots, 6$. For user $k \in \mathcal{K}_0$ at (ρ_k, θ_k), the conditional pdf of the distance $d_{k,l,i}$ from user k to BS antenna cluster l in Cell i, $l = 1, \cdots, L$, $i = 1, \cdots, 6$, is given by

$$f_{d_{k,l,i}|\rho_k,\theta_k}(x|y, z) = dF_{d_{k,l,i}|\rho_k,\theta_k}(x|y, z)/dx, \tag{A.1}$$

where $F_{d_{k,l,i}|\rho_k,\theta_k}(x|y, z)$ is the conditional cdf of $d_{k,l,i}$ given the position of user k, which is given by

$$F_{d_{k,l,i}|\rho_k,\theta_k}(x|y, z) = \frac{S_{overlap}}{\pi}, \tag{A.2}$$

where $S_{overlap}$ is the intersection area of the circle with center O_i and radius 1 and the circle with center A and radius x, as shown in Fig. A.1. It can be obtained

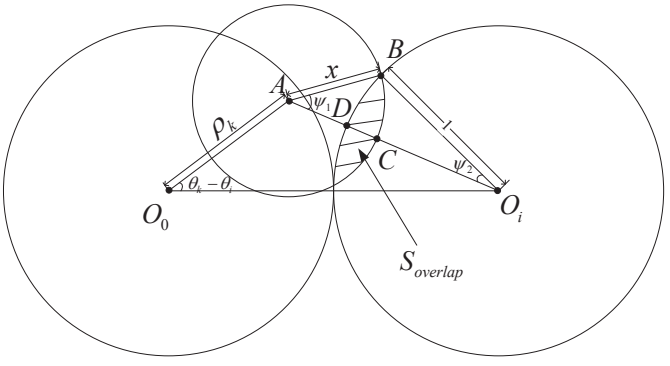

FIGURE A.1: Graphic illustration of $S_{overlap}$.

that

$$S_{overlap} = 2(S_{ABC} + S_{O_iBD} - S_{\triangle ABO_i}), \tag{A.3}$$

where S_{ABC} and S_{O_iBD} denote the areas of circular sectors ABC and O_iBD, respectively, which are given by

$$S_{ABC} = \frac{\psi_1}{2\pi} \cdot \pi x^2, \tag{A.4}$$

and

$$S_{O_iBD} = \frac{\psi_2}{2\pi} \cdot \pi x^2, \tag{A.5}$$

with

$$\psi_1 = \arccos \frac{x^2 + \left(y^2 + 4 - 4y\cos\left(z - \left(i \cdot \frac{\pi}{3} - \frac{\pi}{6}\right)\right)\right) - 1}{2x\sqrt{y^2 + 4 - 4y\cos\left(z - \left(i \cdot \frac{\pi}{3} - \frac{\pi}{6}\right)\right)}}, \tag{A.6}$$

and

$$\psi_2 = \arccos \frac{1 + \left(y^2 + 4 - 4y\cos\left(z - \left(i \cdot \frac{\pi}{3} - \frac{\pi}{6}\right)\right)\right) - x^2}{2\sqrt{y^2 + 4 - 4y\cos\left(z - \left(i \cdot \frac{\pi}{3} - \frac{\pi}{6}\right)\right)}}, \tag{A.7}$$

if

$$\sqrt{y^2 + 4 - 4y\cos\left(z - \left(i \cdot \frac{\pi}{3} - \frac{\pi}{6}\right)\right)} - 1 \leq x \leq \sqrt{y^2 + 4 - 4y\cos\left(z - \left(i \cdot \frac{\pi}{3} - \frac{\pi}{6}\right)\right)} + 1, \tag{A.8}$$

and otherwise $\psi_1 = \psi_2 = 0$. $S_{\triangle ABO_i}$ is the area of $\triangle ABO_i$, which is given by

$$S_{\triangle ABO_i} = \frac{1}{2} x \sqrt{y^2 + 4 - 4y\cos\left(z - \left(i \cdot \frac{\pi}{3} - \frac{\pi}{6}\right)\right)} \sin\psi_1. \tag{A.9}$$

(2.15) can be then obtained by combining (A.1-A.9).

Appendix B

Derivation of (3.39) and (3.40)

With the BS antenna clusters uniformly distributed in the inscribed circle of Cell 0, the pdf of the access distance $d_{k,l,0}$ from the user at $(0,0)$ to BS antenna cluster l in Cell 0 can be obtained as $f_{d_{k,l,0}|\rho_k}(x|0) = 2x$. Define $\delta_l = \ln d_{k,0}^{(l+1)} - \ln d_{k,0}^{(l)}$, $l = 1, \cdots, L-1$ and $\delta_L = -\ln d_{k,0}^{(L)}$. The first term on the right-hand side of (3.36) and (3.37) can be then written as

$$-\frac{\alpha}{\lceil\beta\rceil}\sum_{l=1}^{\lceil\beta\rceil}\int_0^1 \log_2 x \cdot f_{d_{k,0}^{(l)}}(x)dx = \frac{\alpha \log_2 e}{\lceil\beta\rceil}\sum_{i=1}^{\lceil\beta\rceil}\sum_{l=i}^{L}\int_0^\infty x \cdot f_{\delta_l}(x)dx, \tag{B.1}$$

where $f_{\delta_l}(x)$ is the pdf of δ_l, which is given by [85, Theorem 3.3]

$$f_{\delta_l}(x) = 2le^{-2lx}. \tag{B.2}$$

(3.39) and (3.40) can be then obtained by combining (B.1-B.2) into (3.36) and (3.37), respectively.

Appendix C

Derivation of (4.2)

Let $q_{l,t}^{intra}$ denote the entry of $\mathbf{Q}_k^{intra}$ at the l-th row and t-th column. It can be written as

$$q_{l,t}^{intra} = \sum_{j \in \mathcal{K}_0, j \neq k} \bar{P}_j \mathbb{E}\left[\sum_{n=1}^{N} \mathbf{g}_l^{k,\mathcal{B}_0} \mathbf{w}_n^j \left(\mathbf{g}_t^{k,\mathcal{B}_0} \mathbf{w}_n^j \right)^{\dagger} \right], \tag{C.1}$$

where $\mathbf{g}_l^{k,\mathcal{B}_0} \in \mathbb{C}^{1 \times M}$ denotes the l-th row vector of $\mathbf{G}_{k,\mathcal{B}_0}$ and $\mathbf{w}_n^j \in \mathbb{C}^{M \times 1}$ denotes the n-th column vector of $\mathbf{W}_j$. Note that the precoding matrix $\mathbf{W}_j$ of user $j \in \mathcal{K}_0$ is independent of the channel gain matrix $\mathbf{G}_{k,\mathcal{B}_0}$ from BS antennas in Cell 0 to user $k \in \mathcal{K}_0$, $i = 1 \ldots 6$. Therefore we have

$$q_{l,t}^{intra} = \begin{cases} \sum_{m \in \mathcal{B}_0} |\gamma_{k,m}|^2 \sum_{n=1}^{N} \sum_{j \in \mathcal{K}_0, j \neq k} \bar{P}_j \mathbb{E}\left[|w_{m,n}^j|^2 \right] & l = t \\ 0 & l \neq t, \end{cases} \tag{C.2}$$

where $w_{m,n}^j$ denotes the entry of $\mathbf{W}_j$ at the m-th row and n-th column. The covariance $\mathbf{Q}_k^{intra}$ can be then obtained as (4.2).

Appendix D

Derivation of (4.42) and (5.23)

With a large number of BS antenna clusters L, each user $k \in \mathcal{K}_0$ is close to some antenna cluster l_k^*, such that the large-scale fading coefficient $d_{k,l_k^*,0}^{-\alpha} \gg d_{k,l,0}^{-\alpha}$ if $l \neq l_k^*$. The normalized large-scale fading matrix can be then approximated by

$$\mathbf{B}_{k,\mathcal{B}_0} \approx \sqrt{\frac{1}{N}} \left[\mathbf{0}_{N\times N(l_k^*-1)}, \mathbf{1}_{N\times N}, \mathbf{0}_{N\times N(L-l_k^*)}\right], \tag{D.1}$$

according to (2.8). Moreover, with $L \gg K$, the probability that user j_1 and user j_2 are close to the same BS antenna cluster is low, i.e., $\Pr\{l_{j_1}^* = l_{j_2}^* | j_1 \neq j_2\} \approx 0$. Denote $\mathcal{S}_k = \{1, \cdots, L\} - \{l_j^*\}_{j\in\mathcal{K}_0, j\neq k}$. As both L BS antenna clusters and K users are uniformly distributed, we can conclude that $\mathcal{S}_k$ is composed by $L-K+1$ uniformly distributed BS antenna clusters. By combining (2.7), (4.5-4.6) and (D.1), $\hat{\mathbf{V}}_{k,\mathcal{B}_0}^{(0)}$ can be written as

$$\hat{\mathbf{V}}_{k,\mathcal{B}_0}^{(0)} \approx \left[\mathbf{E}_{l_1}, \cdots, \mathbf{E}_{l_{L-K+1}}\right], \tag{D.2}$$

where the t-th sub-matrix $\mathbf{E}_{l_t} \in \mathbb{C}^{M\times N}$ is given by

$$\mathbf{E}_{l_t} = \left[\mathbf{0}_{N\times N(l_t-1)}, \mathbf{I}_N, \mathbf{0}_{N\times N(L-l_t)}\right]^T, \tag{D.3}$$

$l_t \in \mathcal{S}_k$, $t = 1, \cdots, L-K+1$.

According to (D.2), when $L \gg K$, $\mathbf{G}_{k,\mathcal{B}_0}\hat{\mathbf{V}}_{k,\mathcal{B}_0}^{(0)}$ can be approximated by

$$\mathbf{G}_{k,\mathcal{B}_0}\hat{\mathbf{V}}_{k,\mathcal{B}_0}^{(0)} \approx \left[d_{k,l_1,0}^{-\alpha/2}\mathbf{H}_{k,l_1,0}, \cdots, d_{k,l_{L-K+1},0}^{-\alpha/2}\mathbf{H}_{k,l_{L-K+1},0}\right], \tag{D.4}$$

where $d_{k,l_t,0}$ and $\mathbf{H}_{k,l_t,0}$ denote the access distance from user k to BS antenna cluster l_t in Cell 0 and the corresponding small-scale fading matrix, respectively, $l_t \in \mathcal{S}_k$, $t = 1, \cdots, L-K+1$. We can further obtain from (D.4) that

$$\mathbf{G}_{k,\mathcal{B}_0}\hat{\mathbf{V}}_{k,\mathcal{B}_0}^{(0)}\left(\mathbf{G}_{k,\mathcal{B}_0}\hat{\mathbf{V}}_{k,\mathcal{B}_0}^{(0)}\right)^{\dagger} = \sum_{l_t\in\mathcal{S}_k} d_{k,l_t,0}^{-\alpha}\mathbf{H}_{k,l_t,0}\mathbf{H}_{k,l_t,0}^{\dagger} = \sum_{l=1}^{L-K+1}\left(\tilde{d}_{k,0}^{(l)}\right)^{-\alpha}\tilde{\mathbf{H}}_{k,0}^{(l)}\left(\tilde{\mathbf{H}}_{k,0}^{(l)}\right)^{\dagger}, \tag{D.5}$$

where $\tilde{d}_{k,0}^{(l)}$ and $\tilde{\mathbf{H}}_{k,0}^{(l)}$ denote the access distance between user k and the l-th closest BS antenna cluster in $\mathcal{S}_k$ and the corresponding small-scale fading matrix, $l = 1, \cdots, L-K+1$. Note that $\left(\tilde{d}_{k,0}^{(l)}\right)^{-\alpha}\tilde{\mathbf{H}}_{k,0}^{(l)}\left(\tilde{\mathbf{H}}_{k,0}^{(l)}\right)^{\dagger}$ is a positive definite Hermitian matrix.

For $N \times N$ positive semi-definite Hermitian matrices $\mathbf{A}$ and $\mathbf{B}$, we have

$$\det(\mathbf{A}+\mathbf{B})^{\frac{1}{N}} \geq \det(\mathbf{A})^{\frac{1}{N}} + \det(\mathbf{B})^{\frac{1}{N}}, \tag{D.6}$$

according to Minkowski's determinant theorem [86], where the equality holds when $\mathbf{A} = c\mathbf{B}$. For positive definite Hermitian matrices $\mathbf{A}$ and $\mathbf{B}$, we further have

$$\det(\mathbf{A}+\mathbf{B}) > \det(\mathbf{A}) + \det(\mathbf{B}). \tag{D.7}$$

By combining (D.7) and (D.5), we have

$$\det\left(\mathbf{I}_N + c\cdot\mathbf{G}_{k,\mathcal{B}_0}\hat{\mathbf{V}}_{k,\mathcal{B}_0}^{(0)}\left(\mathbf{G}_{k,\mathcal{B}_0}\hat{\mathbf{V}}_{k,\mathcal{B}_0}^{(0)}\right)^{\dagger}\right) > \det\left(\mathbf{I}_N + c\cdot\left(\tilde{d}_{k,0}^{(1)}\right)^{-\alpha}\tilde{\mathbf{H}}_{k,0}^{(1)}\left(\tilde{\mathbf{H}}_{k,0}^{(1)}\right)^{\dagger}\right), \tag{D.8}$$

where $c > 0$ is a positive constant.

D.1 Derivation of (4.42)

According to (4.12), the ergodic rate of user k with BD is lower-bounded by

$$R_k^{MU-BD} > \frac{1}{N}\mathbb{E}_{\mathbf{H}_{k,\mathcal{B}_0}}\left[\log_2\det\left(\mathbf{I}_N + \frac{\mu_k^{MU-BD}}{N}\tilde{\mathbf{X}}_{k,\mathcal{B}_0}\tilde{\mathbf{X}}_{k,\mathcal{B}_0}^{\dagger}\right)\right], \tag{D.9}$$

where the right-hand side of (D.9) is obtained by applying equal power allocation over N sub-channels. Note that $\tilde{\mathbf{X}}_{k,\mathcal{B}_0} = \tilde{\mathbf{G}}_{k,\mathcal{B}_0}\hat{\mathbf{V}}_{k,\mathcal{B}_0}^{(0)}$. By combining (4.13) and

(D.9), the lower-bound can be further written as

$$R_k^{MU-BD-D} > \frac{1}{N}\mathbb{E}_{\mathbf{H}_{k,\mathcal{B}_0}}\left[\log_2 \det\left(\mathbf{I}_N + \frac{1}{N}\frac{\bar{P}_k}{N_0}\mathbf{G}_{k,\mathcal{B}_0}\hat{\mathbf{V}}_{k,\mathcal{B}_0}^{(0)}\left(\mathbf{G}_{k,\mathcal{B}_0}\hat{\mathbf{V}}_{k,\mathcal{B}_0}^{(0)}\right)^{\dagger}\right)\right]. \tag{D.10}$$

(4.42) can be then obtained by combining (D.10) and (D.8).

D.2 Derivation of (5.23)

Similar to the multi-user single-cell case, we obtain an lower-bound of the ergodic rate from (5.16) as

$$R_k^{MC-BD} > \frac{1}{N}\mathbb{E}_{\mathbf{H}_{k,\mathcal{B}_0}}\left[\log_2 \det\left(\mathbf{I}_N + \frac{\mu_k^{MC-BD}}{N}\tilde{\mathbf{X}}_{k,\mathcal{B}_0}\tilde{\mathbf{X}}_{k,\mathcal{B}_0}^{\dagger}\right)\right], \tag{D.11}$$

where the right-hand side of (D.11) is obtained by applying equal power allocation over N sub-channels. As $\tilde{\mathbf{X}}_{k,\mathcal{B}_0} = \tilde{\mathbf{G}}_{k,\mathcal{B}_0}\hat{\mathbf{V}}_{k,\mathcal{B}_0}^{(0)}$, by combining (2.11), (5.17) and (D.11), the lower-bound can be further written as

$$\begin{aligned} R_k^{MC-BD-D} > \frac{1}{N}\mathbb{E}_{\mathbf{H}_{k,\mathcal{B}_0}}\Bigg[\log_2 \det\Bigg(\mathbf{I}_N + \frac{1}{N}\frac{1}{\frac{KN_0}{P_t} + \frac{K}{L}\sum_{i=1}^{6}\sum_{l=1}^{L} d_{k,l,i}^{-\alpha}} \cdot \\ \mathbf{G}_{k,\mathcal{B}_0}\hat{\mathbf{V}}_{k,\mathcal{B}_0}^{(0)}\left(\mathbf{G}_{k,\mathcal{B}_0}\hat{\mathbf{V}}_{k,\mathcal{B}_0}^{(0)}\right)^{\dagger}\Bigg)\Bigg]. \end{aligned} \tag{D.12}$$

(5.23) can be then obtained by combining (D.12) and (D.8).

Appendix E

Derivation of (5.1)

Let $q_{l,t}^{inter}$ denote the entry of $\mathbf{Q}_k^{inter}$ at the l-th row and t-th column. It can be written as

$$q_{l,t}^{inter} = \sum_{i=1}^{6} \sum_{j \in \mathcal{K}_i} \bar{P}_j \mathbb{E}\left[\sum_{n=1}^{N} \mathbf{g}_l^{k,\mathcal{B}_i} \mathbf{w}_n^j \left(\mathbf{g}_t^{k,\mathcal{B}_i} \mathbf{w}_n^j \right)^{\dagger} \right], \tag{E.1}$$

where $\mathbf{g}_l^{k,\mathcal{B}_i} \in \mathbb{C}^{1\times M}$ denotes the l-th row vector of $\mathbf{G}_{k,\mathcal{B}_i}$ and $\mathbf{w}_n^j \in \mathbb{C}^{M\times 1}$ denotes the n-th column vector of $\mathbf{W}_j$. Note that the precoding matrix $\mathbf{W}_j$ of user $j \in \mathcal{K}_i$ is independent of the channel gain matrix $\mathbf{G}_{k,\mathcal{B}_i}$ from BS antennas in Cell i to user $k \in \mathcal{K}_0$, $i = 1 \ldots 6$. With equal power allocation, by combining (4.14) and (E.1), we have

$$q_{l,t}^{inter} = \begin{cases} P_t \sum_{i=1}^{6} \sum_{m \in \mathcal{B}_i} |\gamma_{k,m}|^2 \sum_{n=1}^{N} \frac{1}{K} \sum_{j \in \mathcal{K}_i} \mathbb{E}\left[|w_{m,n}^j|^2 \right] & l = t \\ 0 & l \neq t, \end{cases} \tag{E.2}$$

where $w_{m,n}^j$ denotes the entry of $\mathbf{W}_j$ at the m-th row and n-th column. As the number of users $K \to \infty$, we have $\frac{1}{K} \sum_{j \in \mathcal{K}_i} \mathbb{E}\left[|w_{m,n}^j|^2 \right] \to \frac{1}{MN}$. The covariance $\mathbf{Q}_k^{inter}$ can be then obtained as (5.1).

Appendix F

Derivation of (6.1)

Let $q_{l,t}^{inter}$ denote the entry of $\mathbf{Q}_k^{inter}$ at the l-th row and t-th column. It can be written as

$$q_{l,t}^{inter}=\sum_{i=1}^{6}\sum_{j\in\mathcal{K}_i}\bar{P}_j\mathbb{E}\left[\sum_{n=1}^{N}\mathbf{g}_l^{k,\mathcal{B}_i}\mathbf{w}_n^j\left(\mathbf{g}_t^{k,\mathcal{B}_i}\mathbf{w}_n^j\right)^{\dagger}\right], \tag{F.1}$$

where $\mathbf{g}_l^{k,\mathcal{B}_i}\in\mathbb{C}^{1\times M}$ denotes the l-th row vector of $\mathbf{G}_{k,\mathcal{B}_i}$ and $\mathbf{w}_n^j\in\mathbb{C}^{M\times 1}$ denotes the n-th column vector of $\mathbf{W}_j$. Note that the precoding matrix $\mathbf{W}_j$ of user $j\in\mathcal{K}_i$ is independent of the channel gain matrix $\mathbf{G}_{k,\mathcal{B}_i}$ from BS antennas in Cell i to user $k\in\mathcal{K}_0$, $i=1\dots 6$. Therefore, we have

$$q_{l,t}^{inter}=\begin{cases}\sum_{i=1}^{6}\sum_{j\in\mathcal{K}_i}\bar{P}_j\sum_{m\in\mathcal{B}_i}|\gamma_{k,m}|^2\sum_{n=1}^{N}\mathbb{E}\left[|w_{m,n}^j|^2\right] & l=t\\ 0 & l\neq t,\end{cases} \tag{F.2}$$

where $w_{m,n}^j$ denotes the entry of $\mathbf{W}_j$ at the m-th row and n-th column. With the CA layout, as $\gamma_{k,m}^C=\gamma_{k,\mathcal{B}_i}^C$ for $m\in\mathcal{B}_i$, $i=1,\cdots,6$, (F.2) can be further written as

$$q_{l,t}^{inter,C}=\begin{cases}\sum_{i=1}^{6}|\gamma_{k,\mathcal{B}_i}^C|^2\sum_{j\in\mathcal{K}_i}\bar{P}_j\sum_{m\in\mathcal{B}_i}\sum_{n=1}^{N}\mathbb{E}\left[|w_{m,n}^j|^2\right] & l=t\\ 0 & l\neq t.\end{cases} \tag{F.3}$$

As $\sum_{m\in\mathcal{B}_i}\sum_{n=1}^{N}|w_{m,n}^j|^2=1$, by combining (F.3) and (2.5), the covariance matrix $\mathbf{Q}_k^{inter,C}$ can be obtained as (6.1).

Appendix G

Monotonicity Properties of $\sum_{i=1}^{6} |\gamma_{k,\mathcal{B}_i}^{C}|^2|_{\theta_k=\pi/6}$, $\sum_{i=0}^{6} |\gamma_{k,\mathcal{B}_i}^{C}|^2|_{\theta_k=\pi/6}$ and $\frac{\sum_{i=1}^{6} |\gamma_{k,\mathcal{B}_i}^{C}|^2|_{\theta_k=\pi/6}}{|\gamma_{k,\mathcal{B}_0}^{C}|^2}$ with respect to $\rho_k \in [0,1]$

G.1 $\sum_{i=1}^{6} |\gamma_{k,\mathcal{B}_i}^{C}|^2|_{\theta_k=\pi/6}$

Denote $S_1 = \sum_{i=1}^{6} |\gamma_{k,\mathcal{B}_i}^{C}|^2|_{\theta_k=\pi/6}$. According to (6.11), S_1 can be written as

$$S_1 = (2+\rho_k)^{-\alpha} + (2-\rho_k)^{-\alpha} + 2(\rho_k^2+4+2\rho_k)^{-\alpha/2} + 2(\rho_k^2+4-2\rho_k)^{-\alpha/2}. \quad \text{(G.1)}$$

It can be obtained from (G.1) that

$$\begin{aligned}\frac{dS_1}{d\rho_k} &= -\alpha(2+\rho_k)^{-1-\alpha} + \alpha(2-\rho_k)^{-1-\alpha} - 2\alpha(1+\rho_k)((1+\rho_k)^2+3)^{-1-\alpha/2} \\ &\quad + 2\alpha(1-\rho_k)((1-\rho_k)^2+3)^{-1-\alpha/2}, \end{aligned} \quad \text{(G.2)}$$

and

$$\begin{aligned}\frac{d^2S_1}{d^2\rho_k} &= \alpha(1+\alpha)(2+\rho_k)^{-2-\alpha} + 2\alpha\left((1+\alpha)(1+\rho_k)^2-3\right)\cdot\left((1+\rho_k)^2+3\right)^{-2-\alpha/2} \\ &\quad + 2\alpha(2+\alpha)(1-\rho_k)^2\left((1-\rho_k)^2+3\right)^{-2-\alpha/2} + \alpha(1+\alpha)(2-\rho_k)^{-2-\alpha} \\ &\quad - 2\left((1-\rho_k)^2+3\right)^{-1-\alpha/2}. \end{aligned} \tag{G.3}$$

For $\alpha > 2$ and $\rho_k \in [0,1]$, it can be easily seen from (G.3) that the first three items on the right-hand side are all positive. Moreover, according to $(2-\rho_k)^2 \leq (1+\rho_k)^2+3$, we have $(2-\rho_k)^{-2-\alpha} \geq ((1-\rho_k)^2+3)^{-1-\alpha/2}$. As a result,

$$\alpha(1+\alpha)(2-\rho_k)^{-2-\alpha} - 2\alpha\left((1-\rho_k)^2+3\right)^{-1-\alpha/2} > 0, \tag{G.4}$$

for $\alpha > 2$ and $\rho_k \in [0,1]$. We can then conclude from (G.3) that $\frac{d^2S_1}{d^2\rho_k} > 0$, which indicates that $\frac{dS_1}{d\rho_k}$ is a monotonic increasing function of $\rho_k \in [0,1]$. According to (G.2), $\frac{dS_1}{d\rho_k}|_{\rho_k=0} = 0$. Therefore, $\frac{dS_1}{d\rho_k} \geq \frac{dS_1}{d\rho_k}|_{\rho_k=0} = 0$, indicating that S_1 is a monotonic increasing function of $\rho_k \in [0,1]$.

G.2 $\sum_{i=0}^{6} \left|\gamma_{k,\mathcal{B}_i}^{C}\right|^2|_{\theta_k=\pi/6}$

Denote $S_2 = \sum_{i=0}^{6} |\gamma_{k,\mathcal{B}_i}^{C}|^2|_{\theta_k=\pi/6} = S_1 + {\rho_k}^{-\alpha}$. We have

$$\frac{dS_2}{d\rho_k} = \frac{dS_1}{d\rho_k} - \alpha\rho_k^{-1-\alpha}. \tag{G.5}$$

It has been shown in Appendix G.1 that $\frac{dS_1}{d\rho_k}$ is a monotonic increasing function of $\rho_k \in [0,1]$ for $\alpha > 2$. As a result,

$$\frac{dS_1}{d\rho_k} \leq \frac{dS_1}{d\rho_k}|_{\rho_k=1} = \alpha - \alpha\cdot 3^{-1-\alpha} - \alpha\cdot 4\cdot 7^{-1-\alpha/2}. \tag{G.6}$$

Note that $-\alpha\rho_k^{-1-\alpha}$ is also a monotonic increasing function of $\rho_k \in [0,1]$ for $\alpha > 2$. We then have

$$-\alpha\rho_k^{-1-\alpha} < -\alpha. \tag{G.7}$$

By combining (G.5-G.7), we can conclude that $\frac{dS_2}{d\rho_k} < 0$, indicating that S_2 is a monotonic decreasing function of $\rho_k \in [0,1]$.

G.3 $\frac{\sum_{i=1}^{6} |\gamma_{k,\mathcal{B}_i}^{C}|^2|_{\theta_k=\pi/6}}{|\gamma_{k,\mathcal{B}_0}^{C}|^2}$

Denote $S_3 = \frac{\sum_{i=1}^{6} |\gamma_{k,\mathcal{B}_i}^{C}|^2|_{\theta_k=\pi/6}}{|\gamma_{k,\mathcal{B}_0}^{C}|^2} = \rho_k^{\alpha} S_1$. As both ρ_k^{α} and S_1 are monotonic increasing functions of $\rho_k \in [0,1]$ for $\alpha > 2$, we can conclude that S_3 is a monotonic increasing function of $\rho_k \in [0,1]$.

Appendix H

Derivation of (6.20), (6.30) and (6.34)

H.1 Average Received Power P_0 with Channel-Inversion Power Allocation

By combining (2.5) and (6.19), we have

$$P_0 = \frac{P_t}{\sum_{k\in\mathcal{K}_0} |\gamma^C_{k,\mathcal{B}_0}|^{-2}}. \tag{H.1}$$

With K users uniformly distributed in the inscribed circle of each cell, we have

$$\frac{1}{K}\sum_{k\in\mathcal{K}_0} |\gamma^C_{k,\mathcal{B}_0}|^{-2} \overset{K\to\infty}{\to} \int_0^1 x^\alpha \cdot f_{\rho_k}(x)dx = \frac{2}{2+\alpha}, \tag{H.2}$$

where $f_{\rho_k}(x) = 2x$ is the pdf of the radial coordinate ρ_k of user k. (6.20) can be then obtained by combining (H.1) and (H.2).

H.2 Normalized Average Received SINRs $\bar{\mu}_0^{MC-SVD-C}$ and $\bar{\mu}_0^{MC-BD-C}$ with Interference-Aware Power Allocation

By combining (2.5) with (6.29) and (6.33), we can obtain that

$$\bar{\mu}_0^{MC-SVD-C} = \frac{\xi}{\frac{1}{K}\sum_{k\in\mathcal{K}_0} \frac{\frac{N_0}{P_t}+\sum_{i=0}^{6}|\gamma_{k,\mathcal{B}_i}^{C}|^2}{|\gamma_{k,\mathcal{B}_0}^{C}|^2} - 1} \approx \frac{\xi}{\frac{1}{K}\sum_{k\in\mathcal{K}_0} \frac{\sum_{i=0}^{6}|\gamma_{k,\mathcal{B}_i}^{C}|^2}{|\gamma_{k,\mathcal{B}_0}^{C}|^2} - 1}, \quad \text{(H.3)}$$

and

$$\mu_0^{MC-BD-C} = \frac{\xi}{\frac{1}{K}\sum_{k\in\mathcal{K}_0} \frac{\frac{N_0}{P_t}+\sum_{i=1}^{6}|\gamma_{k,\mathcal{B}_i}^{C}|^2}{|\gamma_{k,\mathcal{B}_0}^{C}|^2}} \approx \frac{\xi}{\frac{1}{K}\sum_{k\in\mathcal{K}_0} \frac{\sum_{i=1}^{6}|\gamma_{k,\mathcal{B}_i}^{C}|^2}{|\gamma_{k,\mathcal{B}_0}^{C}|^2}}, \quad \text{(H.4)}$$

respectively, for large total transmit power P_t. Moreover, with K users uniformly distributed in the inscribed circle of each cell, we can obtain

$$\begin{aligned}
&\frac{1}{K}\sum_{k\in\mathcal{K}_0} \frac{\sum_{i=1}^{6}|\gamma_{k,\mathcal{B}_i}^{C}|^2}{|\gamma_{k,\mathcal{B}_0}^{C}|^2} \overset{K\to\infty}{\to} \sum_{i=1}^{6}\int_0^{2\pi}\int_0^1 x^{\alpha}\left((x\cos y - 2\cos(i\cdot\tfrac{\pi}{3}-\tfrac{\pi}{6}))^2\right.\\
&\left.+(x\sin y - 2\sin(i\cdot\tfrac{\pi}{3}-\tfrac{\pi}{6}))^2\right)^{-\alpha/2} f_{\rho_k}(x) f_{\theta_k}(y) dxdy\\
&= \frac{6}{\pi}\int_0^{2\pi}\int_0^1 x^{\alpha+1}(x^2+4-4x\sin y)^{-\alpha/2} dxdy, \quad \text{(H.5)}
\end{aligned}$$

where $f_{\rho_k}(x) = 2x$ and $f_{\theta_k}(y) = \frac{1}{2\pi}$ are the pdfs of the radial and angular coordinates of user k, respectively. (6.30) and (6.34) can be then obtained by combining (H.5) with (H.3) and (H.4), respectively.

Bibliography

[1] *Ericsson Mobility Report*, Ericsson, Jun. 2013.

[2] J. Korhonen, *Introduction to 4G Mobile Communications.* Artech House, 2014.

[3] R. Frenkiel, "Cellular radiotelephone system structured for flexible use of different cell sizes," Mar. 13, 1979, US Patent 4,144,411.

[4] S. Redl, M. Weber, and M. Oliphant, *An Introduction to GSM.* Artech House, 1995.

[5] M. Saily, G. Sebire, and E. Riddington, Eds., *GSM/EDGE Evolution and Performance.* John Wiley & Sons, Ltd., 2011.

[6] J. Korhonen, *Introduction to 3G Mobile Communications.* Artech House, 2003.

[7] *Looking ahead to 5G*, Nokia Solutions and Networks, Dec. 2013.

[8] C. Shepard, H. Yu, and L. Zhong, "ArgosV2: A flexible many-antenna research platform," in *Proc. ACM MobiCom*, 2013, pp. 163–166.

[9] G. Foschini and M. Gans, "On limits of wireless communications in a fading environment when using multiple antennas," *Wireless Personal Commun.*, vol. 6, pp. 311–335, 1998.

[10] E. Telatar, "Capacity of multi-antenna Gaussian channels," *Euro. Trans. Telecommun.*, vol. 10, no. 6, pp. 585–595, Nov. 1999.

[11] A. Tulino and S. Verdu, *Random Matrix Theory and Wireless Communications.* Now Publisher Inc., 2004.

[12] R. Couillet and M. Debbah, *Random Matrix Methods for Wireless Communications.* Cambridge University Press, 2011.

[13] A. Lozano and A. Tulino, "Capacity of multiple-transmit multiple-receive antenna architectures," *IEEE Transactions on Information Theory*, vol. 48, no. 12, pp. 3117–3128, Dec. 2002.

[14] A. Tulino, A. Lozano, and S. Verdu, "Impact of antenna correlation on the capacity of multiantenna channels," *IEEE Transactions on Information Theory*, vol. 51, no. 7, pp. 2491–2509, Jul. 2005.

[15] W. Roh and A. Paulraj, "MIMO channel capacity for the distributed antenna," in *Proc. IEEE VTC*, vol. 2, Sep. 2002, pp. 706–709.

[16] H. Zhuang, L. Dai, L. Xiao, and Y. Yao, "Spectral efficiency of distributed antenna system with random antenna layout," *Electronics Letters*, vol. 39, no. 6, pp. 495–496, Mar. 2003.

[17] H. Zhang and H. Dai, "On the capacity of distributed MIMO systems," in *Proc. IEEE CISS*, Mar. 2004, pp. 1–5.

[18] W. Feng, Y. Li, S. Zhou, J. Wang, and M. Xia, "Downlink capacity of distributed antenna systems in a multi-cell environment," in *Proc. IEEE WCNC*, Apr. 2009, pp. 1–5.

[19] D. Aktas, M. Bacha, J. Evans, and S. Hanly, "Scaling results on the sum capacity of cellular networks with MIMO links," *IEEE Transactions on Information Theory*, vol. 52, no. 7, pp. 3264–3274, Jul. 2006.

[20] F. Heliot, R. Hoshyar, and R. Tafazolli, "An accurate closed-form approximation of the distributed MIMO outage probability," *IEEE Transactions on Wireless Communications*, vol. 10, no. 1, pp. 5–11, Jan. 2011.

[21] J. Zhang, C.-K. Wen, S. Jin, X. Gao, and K.-K. Wong, "On capacity of large-scale MIMO multiple access channels with distributed sets of correlated antennas," *IEEE Journal on Selected Areas in Communications*, vol. 31, no. 2, pp. 133–148, Feb. 2013.

[22] W. Choi and J. Andrews, "Downlink performance and capacity of distributed antenna systems in a multicell environment," *IEEE Transactions on Wireless Communications*, vol. 6, no. 1, pp. 69–73, Jan. 2007.

[23] S.-R. Lee, S.-H. Moon, J.-S. Kim, and I. Lee, "Capacity analysis of distributed antenna systems in a composite fading channel," *IEEE Transactions on Wireless Communications*, vol. 11, no. 3, pp. 1076–1086, Mar. 2012.

[24] D. Wang, J. Wang, X. You, Y. Wang, M. Chen, and X. Hou, "Spectral efficiency of distributed MIMO systems," *IEEE Journal on Selected Areas in Communications*, vol. 31, no. 10, pp. 2112–2127, Oct. 2013.

[25] P. Viswanath, D. Tse, and V. Anantharam, "Asymptotically optimal water-filling in vector multiple-access channels," *IEEE Transactions on Information Theory*, vol. 47, no. 1, pp. 241–267, Jan. 2001.

[26] W. Yu, W. Rhee, S. Boyd, and J. Cioffi, "Iterative water-filling for Gaussian vector multiple-access channels," *IEEE Transactions on Information Theory*, vol. 50, no. 1, pp. 145–152, Jan. 2004.

[27] P. Viswanath and D. Tse, "Sum capacity of the vector Gaussian broadcast channel and uplink-downlink duality," *IEEE Transactions on Information Theory*, vol. 49, no. 8, pp. 1912–1921, Aug. 2003.

[28] S. Viswanath, N. Jindal, and A. Goldsmith, "Duality, achievable rates, and sum-rate capacity of Gaussian MIMO broadcast channels," *IEEE Transactions on Information Theory*, vol. 49, no. 10, pp. 2658–2668, Oct. 2003.

[29] L. Dai, "A comparative study on uplink sum capacity with co-located and distributed antennas," *IEEE Journal on Selected Areas in Communications*, vol. 29, no. 6, pp. 1200 –1213, Jun. 2011.

[30] G. Caire and S. Shamai, "On the achievable throughput of a multiantenna Gaussian broadcast channel," *IEEE Transactions on Information Theory*, vol. 49, no. 7, pp. 1691–1706, Jul. 2003.

[31] W. Yu and J. Cioffi, "Sum capacity of Gaussian vector broadcast channels," *IEEE Transactions on Information Theory*, vol. 50, no. 9, pp. 1875–1892, Sep. 2004.

[32] H. Weingarten, Y. Steinberg, and S. Shamai, "The capacity region of the Gaussian multiple-input multiple-output broadcast channel," *IEEE Transactions on Information Theory*, vol. 52, no. 9, pp. 3936–3964, Sep. 2006.

[33] M. Costa, "Writing on dirty paper," *IEEE Transactions on Information Theory*, vol. 29, no. 3, pp. 439–441, May 1983.

[34] M. Schubert and H. Boche, "Solution of the multiuser downlink beamforming problem with individual SINR constraints," *IEEE Transactions on Vehicular Technology*, vol. 53, no. 1, pp. 18–28, Jan. 2004.

[35] C. Peel, B. Hochwald, and A. Swindlehurst, "A vector-perturbation technique for near-capacity multiantenna multiuser communication-part I: channel inversion and regularization," *IEEE Transactions on Communications*, vol. 53, no. 1, pp. 195–202, Jan. 2005.

[36] A. Wiesel, Y. Eldar, and S. Shamai, "Linear precoding via conic optimization for fixed MIMO receivers," *IEEE Transactions on Signal Processing*, vol. 54, no. 1, pp. 161–176, Jan. 2006.

[37] M. Stojnic, H. Vikalo, and B. Hassibi, "Rate maximization in multi-antenna broadcast channels with linear preprocessing," in *Proc. IEEE GLOBECOM*, 2004, pp. 3957–3961.

[38] W. Yu and T. Lan, "Transmitter optimization for the multi-antenna downlink with per-antenna power constraints," *IEEE Transactions on Signal Processing*, vol. 55, no. 6, pp. 2646–2660, Jun. 2007.

[39] K.-K. Wong, R. Murch, and K. Letaief, "A joint-channel diagonalization for multiuser MIMO antenna systems," *IEEE Transactions on Wireless Communications*, vol. 2, no. 4, pp. 773–786, Apr. 2003.

[40] L.-U. Choi and R. Murch, "A transmit preprocessing technique for multiuser MIMO systems using a decomposition approach," *IEEE Transactions on Wireless Communications*, vol. 3, no. 1, pp. 20–24, Jan. 2004.

[41] Q. Spencer, A. Swindlehurst, and M. Haardt, "Zero-forcing methods for downlink spatial multiplexing in multiuser MIMO channels," *IEEE Transactions on Signal Processing*, vol. 52, no. 2, pp. 461–471, Feb. 2004.

[42] Z. Pan, K.-K. Wong, and T.-S. Ng, "Generalized multiuser orthogonal space-division multiplexing," *IEEE Transactions on Wireless Communications*, vol. 3, no. 6, pp. 1969–1973, Jun. 2004.

[43] J. Joung and Y. H. Lee, "Regularized channel diagonalization for multiuser MIMO downlink using a modified mmse criterion," *IEEE Transactions on Signal Processing*, vol. 55, no. 4, pp. 1573–1579, Apr. 2007.

[44] V. Stankovic and M. Haardt, "Generalized design of multi-user MIMO precoding matrices," *IEEE Transactions on Wireless Communications*, vol. 7, no. 3, pp. 953–961, Mar. 2008.

[45] A. Tenenbaum and R. Adve, "Linear processing and sum throughput in the multiuser MIMO downlink," *IEEE Transactions on Wireless Communications*, vol. 8, no. 5, pp. 2652–2661, May 2009.

[46] H. Sung, S.-R. Lee, and I. Lee, "Generalized channel inversion methods for multiuser MIMO systems," *IEEE Transactions on Communications*, vol. 57, no. 11, pp. 3489–3499, Nov. 2009.

[47] R. Zamir, S. Shamai, and U. Erez, "Nested linear/lattice codes for structured multiterminal binning," *IEEE Transactions on Information Theory*, vol. 48, no. 6, pp. 1250–1276, Jun. 2002.

[48] C. Windpassinger, R. F. H. Fischer, and J. B. Huber, "Lattice-reduction-aided broadcast precoding," *IEEE Transactions on Communications*, vol. 52, no. 12, pp. 2057–2060, Dec. 2004.

[49] B. Hochwald, C. Peel, and A. Swindlehurst, "A vector-perturbation technique for near-capacity multiantenna multiuser communication-part II: perturbation," *IEEE Transactions on Communications*, vol. 53, no. 3, pp. 537–544, Mar. 2005.

[50] D. Gesbert, M. Kountouris, R. Heath, C.-B. Chae, and T. Salzer, "From single user to multiuser communications: Shifting the MIMO paradigm," *IEEE Signal Processing Magazine*, vol. 24, no. 5, pp. 36–46, Sep. 2007.

[51] Z. Shen, R. Chen, J. Andrews, R. Heath, and B. Evans, "Sum capacity of multiuser MIMO broadcast channels with block diagonalization," *IEEE Transactions on Wireless Communications*, vol. 6, no. 6, pp. 2040–2045, Jun. 2007.

[52] J. Park, E. Song, and W. Sung, "Capacity analysis for distributed antenna systems using cooperative transmission schemes in fading channels," *IEEE Transactions on Wireless Communications*, vol. 8, no. 2, pp. 586–592, Feb. 2009.

[53] X. Li, M. Luo, M. Zhao, L. Huang, and Y. Yao, "Downlink performance and capacity of distributed antenna system in multi-user scenario," in *Proc. IEEE WiCOM*, Sep. 2009, pp. 1–4.

[54] T. Wang, Y. Wang, K. Sun, and Z. Chen, "On the performance of downlink transmission for distributed antenna systems with multi-antenna arrays," in *Proc. IEEE VTC*, Sep. 2009, pp. 1 –5.

[55] T. Ahmad, S. Al-Ahmadi, H. Yanikomeroglu, and G. Boudreau, "Downlink linear transmission schemes in a single-cell distributed antenna system with port selection," in *Proc. IEEE VTC*, May 2011, pp. 1–5.

[56] H. Kim, S.-R. Lee, K.-J. Lee, and I. Lee, "Transmission schemes based on sum rate analysis in distributed antenna systems," *IEEE Transactions on Wireless Communications*, vol. 11, no. 3, pp. 1201–1209, Mar. 2012.

[57] H. Zhu, "Performance comparison between distributed antenna and microcellular systems," *IEEE Journal on Selected Areas in Communications*, vol. 29, no. 6, pp. 1151–1163, Jun. 2011.

[58] ——, "On frequency reuse in cooperative distributed antenna systems," *IEEE Communications Magazine*, vol. 50, no. 4, pp. 85–89, Apr. 2012.

[59] R. Heath, T. Wu, Y. H. Kwon, and A. Soong, "Multiuser MIMO in distributed antenna systems with out-of-cell interference," *IEEE Transactions on Signal Processing*, vol. 59, no. 10, pp. 4885–4899, Oct. 2011.

[60] T. Marzetta, "Noncooperative cellular wireless with unlimited numbers of base station antennas," *IEEE Transactions on Wireless Communications*, vol. 9, no. 11, pp. 3590–3600, Nov. 2010.

[61] H. Q. Ngo, E. Larsson, and T. Marzetta, "Energy and spectral efficiency of very large multiuser mimo systems," *IEEE Transactions on Communications*, vol. 61, no. 4, pp. 1436–1449, Apr. 2013.

[62] F. Rusek, D. Persson, B. K. Lau, E. Larsson, T. Marzetta, O. Edfors, and F. Tufvesson, "Scaling up MIMO: Opportunities and challenges with very large arrays," *IEEE Signal Processing Magazine*, vol. 30, no. 1, pp. 40–60, Jan. 2013.

[63] *Special Issue: Large-scale Multiple Antenna Wireless Systems, IEEE Journal on Selected Areas in Communications*, vol. 31, no. 2, Feb. 2013.

[64] V. A. Marcenko and L. A. Pastur, "Distribution of eigenvalues for some sets of random matrices," *Mathematics of the USSR-Sbornik*, vol. 1, no. 4, pp. 457–483, 1967.

[65] J. Wang and L. Dai, "Asymptotic rate analysis for non-orthogonal downlink multi-user systems with co-located and distributed antennas," in *Proc. IEEE WCNC*, April 2013, pp. 3219–3224.

[66] D. Tse and P. Viswanath, *Fundamental of Wireless Communications*. Cambridge Press, 2005.

[67] D. Gesbert, S. V. Hanly, H. Huang, S. Shamai, O. Simeone, and W. Yu, "Multi-cell MIMO cooperative networks: A new look at interference," *IEEE Journal on Selected Areas in Communications*, no. 12, pp. 1380–1408, Dec. 2010.

[68] O. Somekh, B. Zaidel, and S. Shamai, "Sum rate characterization of joint multiple cell-site processing," *IEEE Transactions on Information Theory*, vol. 53, no. 12, pp. 4473–4497, Dec. 2007.

[69] O. Somekh, O. Simeone, Y. Bar-Ness, A. Haimovich, and S. Shamai, "Cooperative multicell zero-forcing beamforming in cellular downlink channels," *IEEE Transactions on Information Theory*, vol. 55, no. 7, pp. 3206–3219, Jul. 2009.

[70] X. Ge, K. Huang, C.-X. Wang, X. Hong, and X. Yang, "Capacity analysis of a multi-cell multi-antenna cooperative cellular network with co-channel interference," *IEEE Transactions on Wireless Communications*, vol. 10, no. 10, pp. 3298–3309, Oct. 2011.

[71] R. Zakhour and S. Hanly, "Base station cooperation on the downlink: Large system analysis," *IEEE Transactions on Information Theory*, vol. 58, no. 4, pp. 2079–2106, Apr. 2012.

[72] B. L. Ng, J. Evans, S. Hanly, and D. Aktas, "Distributed downlink beamforming with cooperative base stations," *IEEE Transactions on Information Theory*, vol. 54, no. 12, pp. 5491–5499, Dec. 2008.

[73] L. Venturino, N. Prasad, and X. Wang, "Coordinated linear beamforming in downlink multi-cell wireless networks," *IEEE Transactions on Wireless Communications*, vol. 9, no. 4, pp. 1451–1461, Apr. 2010.

[74] H. Dahrouj and W. Yu, "Coordinated beamforming for the multicell multi-antenna wireless system," *IEEE Transactions on Wireless Communications*, vol. 9, no. 5, pp. 1748–1759, May 2010.

[75] R. Zhang, "Cooperative multi-cell block diagonalization with per-base-station power constraints," *IEEE Journal on Selected Areas in Communications*, vol. 28, no. 9, pp. 1435–1445, Sep. 2010.

[76] J. Zhang and J. Andrews, "Adaptive spatial intercell interference cancellation in multicell wireless networks," *IEEE Journal on Selected Areas in Communications*, vol. 28, no. 9, pp. 1455–1468, Sep. 2010.

[77] H. Huh, S.-H. Moon, Y.-T. Kim, I. Lee, and G. Caire, "Multi-cell MIMO downlink with cell cooperation and fair scheduling: A large-system limit analysis," *IEEE Transactions on Information Theory*, vol. 57, no. 12, pp. 7771–7786, Dec. 2011.

[78] A. Fehske, F. Richter, and G. Fettweis, "SINR balancing for the multi-user downlink under general power constraints," in *Proc. IEEE GLOBECOM*, 2008, pp. 1–6.

[79] D. Cai, T. Quek, and C.-W. Tan, "A unified analysis of max-min weighted SINR for MIMO downlink system," *IEEE Transactions on Signal Processing*, vol. 59, no. 8, pp. 3850–3862, Aug. 2011.

[80] C.-W. Tan, M. Chiang, and R. Srikant, "Maximizing sum rate and minimizing MSE on multiuser downlink: Optimality, fast algorithms and equivalence via max-min SIR," in *Proc. IEEE ISIT*, 2009, pp. 2669–2673.

[81] L. Zhang, R. Zhang, Y.-C. Liang, Y. Xin, and H. Poor, "On Gaussian MIMO BC-MAC duality with multiple transmit covariance constraints," *IEEE Transactions on Information Theory*, vol. 58, no. 4, pp. 2064–2078, Apr. 2012.

[82] B. Song, R. Cruz, and B. Rao, "Network duality for multiuser MIMO beamforming networks and applications," *IEEE Transactions on Communications*, vol. 55, no. 3, pp. 618–630, Mar. 2007.

[83] A. Tolli, H. Pennanen, and P. Komulainen, "SINR balancing with coordinated multi-cell transmission," in *Proc. IEEE WCNC*, 2009, pp. 1–6.

[84] L. Dai, "An uplink capacity analysis of the distributed antenna system (DAS): From cellular DAS to DAS with virtual cells," *IEEE Transactions on Wireless Communications*, vol. 13, no. 5, pp. 2717–2731, May 2014.

[85] H.-C. Yang and M.-S. Alouini, *Order Statistics in Wireless Communications*. Cambridge University Press, 2011.

[86] M. Marcus and H. Minc, *Survey of Matrix Theory and Matrix Inequalities*. Allyn and Bacon, Inc., 1964.

List of Publications

Journal Papers

1. Zhiyang Liu and Lin Dai, "A Comparative Study of Downlink MIMO Cellular Networks with Co-located and Distributed Base-Station Antennas," *IEEE Transactions on Wireless Communications*, vol. 13, no. 11, pp. 6259-6274, Nov. 2014.

2. Zhiyang Liu and Lin Dai, "Asymptotic Per-User Rate Analysis of Downlink MIMO Cellular Networks with Linear Precoding", *IEEE Transactions on Wireless Communications*, vol. 11, no. 12, pp. 4536-4548, Dec. 2012.

Conference Papers

1. Zhiyang Liu and Lin Dai, "Asymptotic Capacity Analysis of Downlink MIMO Systems with Co-located and Distributed Antennas," in *Proc. IEEE PIMRC*, London, UK, Sep. 2013.

2. Zhiyang Liu and Lin Dai, "On the Scaling Behavior of Average Ergodic Capacity of Distributed MIMO Systems," to appear in *Proc. IEEE GLOBECOM*, San Diego, CA, USA, Dec. 2015.